Univerzita Karlova v Praze
Přírodovědecká fakulta

Studijní obor: Fyzikální chemie

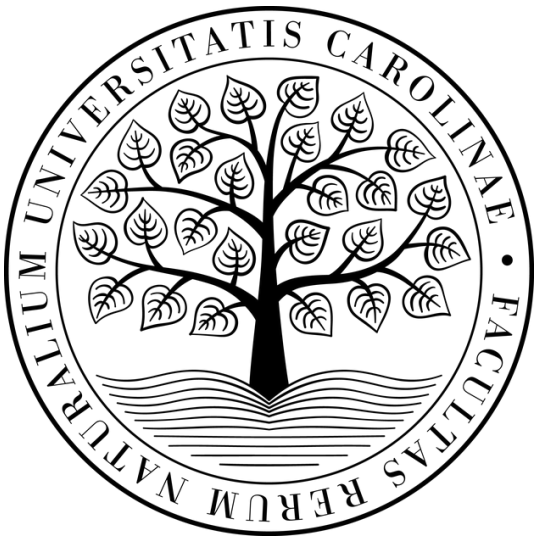

Mgr. Kateřina Krejčová

Biofyzikální a strukturní studie virových polymeráz a methyltransferáz

Biophysical and structural characterization of viral polymerases and methyltransferases

Disertační práce

Školitel: Mgr. et Mgr. Evžen Bouřa, Ph.D.

Praha 2024

PROHLÁŠENÍ

Prohlašuji, že jsem tuto závěrečnou práci vypracovala samostatně a že jsem řádně uvedla všechny použité informační zdroje a literaturu. Současně prohlašuji, že jsem tuto práci nepředložila k získání jiného nebo stejného akademického titulu.

V Praze dne 3.10.2024 Mgr. Kateřina Krejčová

PODĚKOVÁNÍ

V první řadě bych ráda poděkovala mému školiteli panu doktoru Evženovi Bouřovi za jeho vědecké vedení, cenné rady a trpělivost po celou dobu mého doktorského studia. Rovněž bych chtěla poděkovat celému kolektivu Laboratoře strukturní biologie membrán ÚOCHB za skvělou přátelskou atmosféru, díky které byla radost do práce chodit, i když mi zrovna nevycházely experimenty. Dále bych chtěla poděkovat mé rodině, především mamce a přátelům, kteří mě během celého studia podporovali a neustále naslouchali mým historkám, že mi zase něco nevyšlo. Speciální poděkování patří mojí kočce Hyjušce, která vždy měla co přidat do diskuze a nebála se mi vysvětlit, že moje problémy jsou ve srovnání s těmi jejími naprosto nepodstatné. Poslední poděkování bych ráda věnovala mému příteli a naší zatím ještě nenarozené dceři, kteří mě (někteří i doslova) dokopali k tomu, abych disertační práci dopsala co nejrychleji.

Tato práce byla podpořena projektem Národní institut virologie a bakteriologie (Program EXCELES, ID LX22NPO5103)–Financováno Evropskou unií-Next Generation EU.

OBSAH

ABSTRAKT

Flaviviry, stejně jako koronaviry, patří mezi +RNA viry schopné způsobit celou řadu onemocnění, která mohou mít až fatální následky. Teprve nedávná pandemie COVID-19 nám ukázala pravý potenciál těchto virů. I z tohoto důvodu je v současné době snaha vyvinout látky, které budou aktivní vůči co největší skupině +RNA virů. Jedněmi z hlavních cílů antivirové terapie jsou enzymy hrající klíčovou roli v replikaci virů jako jsou RNA-dependentní RNA polymerázy a methyltransferázy. V případě flavivirů má obě tyto funkce nestrukturní protein NS5. Skládá se z N-koncové domény mající methyltransferázovou aktivitu a C-koncové RNA-dependentní RNA polymerázové domény. Tento protein je tedy zodpovědný jak za replikaci RNA, tak za připojení čepičky na 5′ konec RNA. U koronavirů zastává funkci polymerázy protein NSP12 a jeho dva kofaktory NSP7 a NSP8, methyltransferázovou funkci komplex dvou proteinů NSP10 a NSP16.

Tato disertační práce se v první řadě zaměřuje na strukturní a funkční charakterizaci vybraných virových methyltransferáz a polymeráz, a to zejména z důvodu porovnání co největšího množství těchto enzymů mezi sebou. Další snahou bylo nalezení případných odlišností, které by mohly být zásadní ve vývoji nových antivirotik. V neposlední řadě je v této práci představeno několik látek, které jsou slibným výchozím bodem pro vývoj širokospektrálních antivirotik.

ABSTRACT

Flaviviruses and coronaviruses are +RNA viruses capable of causing a wide range of diseases, which can be fatal. The true potential of these viruses was revealed by recent COVID-19 pandemic. Currently, there is an effort to develop compounds that will be active against most or many +RNA viruses. One of the main targets of antiviral therapy are enzymes that play a key role in virus replication, such as RNA-dependent RNA polymerases and methyltransferases. In the case of flaviviruses, the enzyme that is responsible for both these functions is the non-structural protein NS5. It consists of an N-terminal polymerase domain and a C-terminal methyltransferase domain. Therefore, this protein is responsible for both, RNA replication and the addition of the 5´ RNA cap. In coronaviruses, the polymerase function is carried out by the NSP12 protein and its two cofactors NSP7 and NSP8, while the methyltransferase function is performed by a complex of two proteins, NSP10 and NSP16.

This dissertation thesis primarily focuses on the structural and functional characterization of selected viral methyltransferases and polymerases, particularly for the purpose of comparing as many of these enzymes as possible to identify potential differences that could be crucial in the development of new antivirals. Furthermore, several compounds are presented in this work as promising starting points for the development of broad-spectrum antivirals.

1 TEORETICKÝ ÚVOD

1.1 Flaviviry

Flaviviry jsou obalené viry s jednovláknovou RNA s pozitivní polaritou (+RNA). Jsou řazeny do rodiny *Flaviviridae*, pod kterou spadají čtyři rody: hepaciviry, pegiviry, pestiviry a již zmíněné flaviviry[1]. Většina flavivirů je přenášena zejména klíšťaty či komáry a řadí se tak mezi arboviry, jejichž název je odvozen z anglického arthropod-borne virus, tedy viry přenášené členovci. Do této rodiny spadá celá řada známých virů jako je Zika virus[2], Dengue virus[3], virus žluté zimnice[4], virus klíšťové encefalitidy[5] a virus japonské encefalitidy[6], stejně jako méně známé viry jako například Ntaya virus[7], Langat virus[8] a mnoho dalších. Tyto viry jsou schopny způsobit celou řadu onemocnění jako je encefalitida, hemoragická horečka a další a mohou v nejvážnějších případech skončit smrtí[9].

Genom flavivirů se skládá z jediného otevřeného čtecího rámce (ORF, z angl. open reading frame), který je na 5´ a 3´ konci ohraničen takzvanými nepřekládanými oblastmi (UTR, z angl. untranslated region), které jsou důležité při replikaci, translaci a během regulace vrozené imunitní odpovědi[10]. ORF kóduje jeden polyprotein, který je ukotven v membráně endoplasmatického retikula (ER) a je během virové replikace ko- a post-translačně štěpen hostitelskými a virovými proteázami na tři strukturní a sedm nestrukturních proteinů[11] (obrázek 1).

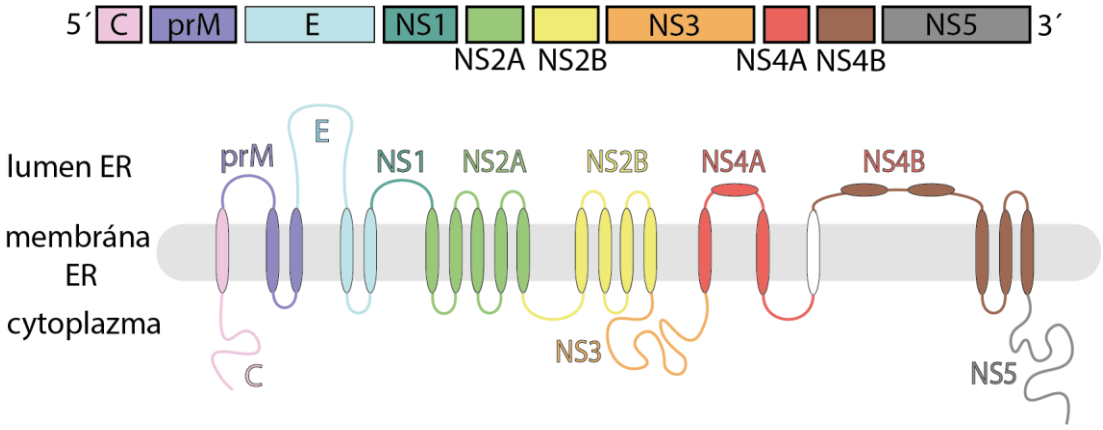

Obrázek 1: **Schéma flavivirového polyproteinu**. Nahoře je znázorněn polyprotein a jednotlivé proteiny, na které je štěpen: 3 struktrurní proteiny: kapsidový (C), premembránový (prM), obalový (E), a 7 nestrukturních proteinů (NS). Dole je znázorněna integrace proteinů do membrány endoplazmatického retikula (ER).

1.1.1 Vstup flavivirů do buňky

Flaviviry využívají pro vstup do buňky klathrinem zprostředkovanou endocytózu, po které následuje konformační změna obalu, fúze membrán a konečně uvolnění virového genomu dovnitř buňky (obrázek 2). Klathrinem zprostředkovaná endocytóza je proces vezikulárního transportu, při kterém dochází k přenosu molekul z povrchu buňky do jejího nitra. Na začátku virové infekce virové částice difundují podél povrchu buňky směrem k již předem vytvořeným klathrinem potaženým jamkám, dokud se nepřipojí na receptor pro vstup (obrázek 2, krok 1). Případně může být nejprve vytvořen komplex virus-receptor a ten je transportován k již existující, klathrinem potažené jamce. Zde vzniká klathrinem opláštěný měchýřek, který je dále transportován z plazmatické membrány do cytosolu a dochází k uvolnění klathrinového pláště[12] (obrázek 2, krok 2). Z měchýřku, nesoucí virovou RNA, vzniká endozom, uvnitř kterého je kyselé prostředí, což způsobí fúzi virové membrány s membránou endozomu a virová genomová RNA je uvolněna do cytoplazmy[13] (obrázek 2, krok 3). Dalším krokem je translace za vzniku polyproteinu (obrázek 2, krok 4), který je následně na ER štěpen proteázami na jednotlivé strukturní a nestrukturní proteiny. Nestrukturní proteiny se účastní replikace RNA, kdy z původního +ssRNA vlákna vzniká -ssRNA (jednovláknová RNA s negativní polaritou, z angl. single-stranded -RNA) vlákno, které následně slouží jako templát pro vznik dalších +ssRNA (obrázek 2, krok 5). V ER dochází ke skládání virové částice (obrázek 2, krok 6) a nezralé viriony jsou přeneseny na Golgiho aparát, kde dochází ke štěpení prM na M (obrázek 2, krok 7) za vzniku zralého virionu. Ten je na závěr uvolněn z buňky pomocí exocytózy[14] (obrázek 2, krok 8 a 9).

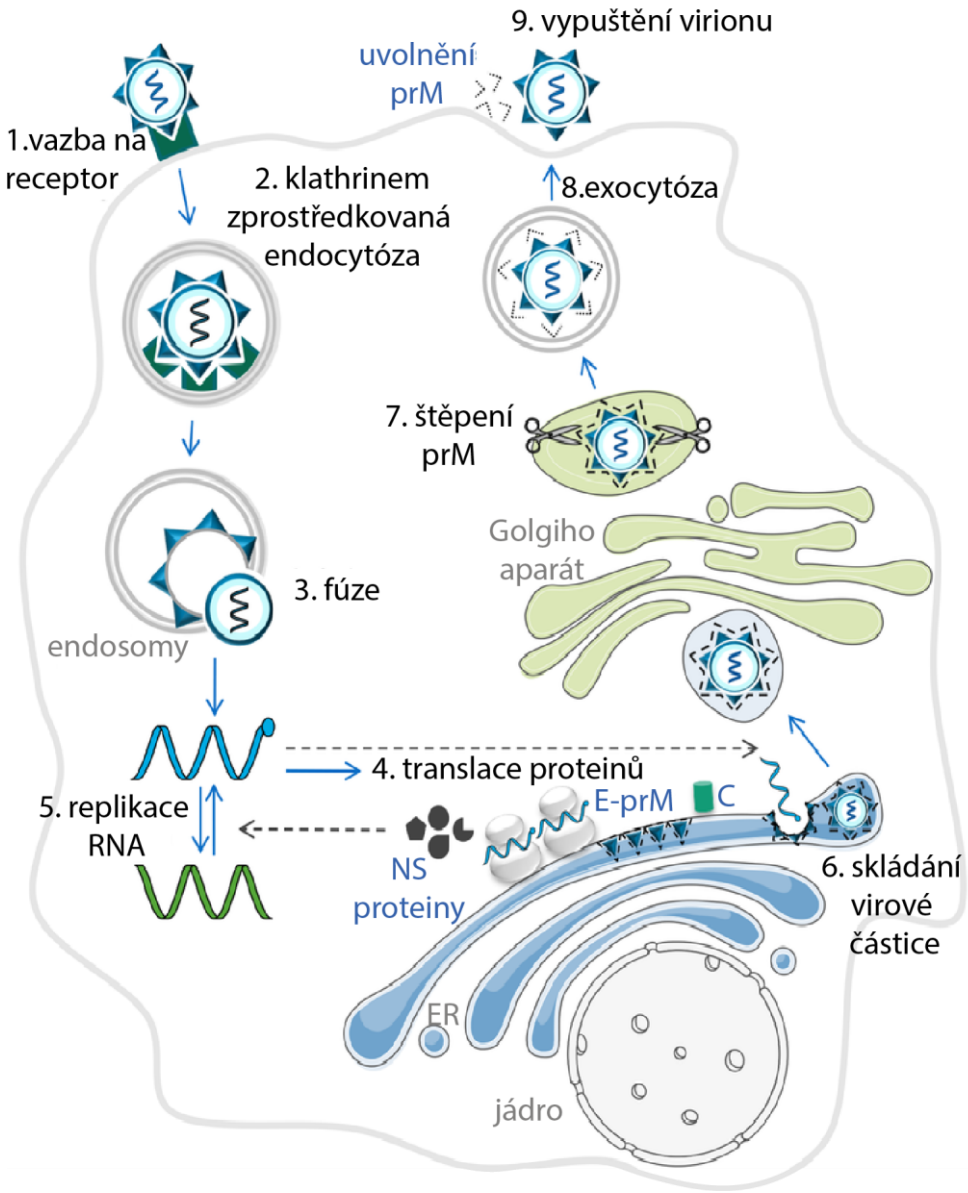

Obrázek 2: **Životní cyklus flavivirů**. Infekce flaviviry začíná vazbou virionu na receptory na povrchu buňky (krok 1). Následuje klathrinem zprostředkovaná endocytóza (2). Kyselé prostředí v endozomech způsobí fúzi virionu s membránou endozomu (3). V cytoplazmě poté dochází k uvolnění genomové RNA, translace polyproteinu (4), který je proteolyticky štěpen na strutruní (E, prM, C) a nestruktuní (NS) proteiny. NS proteiny se účastní replikace RNA (5), za vzniku -ssRNA (zelená) a ta slouží jako templát pro tvorbu dalších +ssRNA (modrá). +ssRNA je dále sbalena pomocí C proteinu za vzniku nukleokapsidy. Skládání virové částice probíhá v ER (6) a nezralé viriony jsou přeneseny přes Golgiho aparát, kde dochází ke štěpení prM na M a vzniká tak zralá virová částice (7). Ta poté opouští buňku pomocí exocytózy (8, 9). Převzato a upraveno[15].

1.1.2 Strukturní proteiny flavivirů

Jak již bylo zmíněno výše, genom flavivirů se skládá z jednoho ORF, který je během a po translaci štěpen na tři strukturní a sedm nestrukturních proteinů[11]. Mezi tři strukturní proteiny patří: kapsidový (C, z angl. capsid) protein, prekurzor membrány (prM) a obalový (E, z angl. enveloped) protein. Schéma virové částice s vyobrazenými strukturními proteiny je na obrázku 3.

Kapsidový protein je klíčovou strukturní složkou flavivirů a nachází se na N-konci virového polyproteinu, ze kterého je vyštěpen pomocí virové proteázy NS2B/NS3. Tento protein, jak již název napovídá, se podílí na tvorbě nukleokapsidy, která je složena z jedné kopie RNA a několika kopií kapsidových proteinů[16]. Mimo této funkce má i další jako například napomáhá intermolekulárním interakcím, jako je vazba na lipidovou membránu hostitelské buňky za účelem podpory replikace viru. Dále se také účastní sestavení virionu a jeho zrání[17,18].

Na C-konci polyproteinu se nachází obalový protein (E), který zprostředkovává vstup viru do hostitelské buňky[19]. Je zodpovědný za vazbu na receptor hostitelské buňky a usnadňuje fúzi virové a hostitelské buněčné membrány, což umožňuje vstup virového genomu do hostitelské buňky. Tento protein prochází významnými strukturními změnami. Během vstupu do buňky dochází ke změně z homodimeru na homotrimer, což vede k fúzi membrány, vypuštění genetické informace a k následné replikaci a translaci[20]. Během sestavování virové částice v ER dochází ke spojení proteinu E s třetím strukturním proteinem prM a tento vzniklý heterodimer prM-E zabraňuje nově vznikajícím virionům splynout s membránou hostitelské buňky dříve než je virus plně připraven k infekci[21]. Při zrání viru je prM štěpen hostitelskou proteázou furinového typu na konečný membránový (M) protein, což je nezbytný krok pro tvorbu infekčních virionů schopných vstoupit do hostitelské buňky[22].

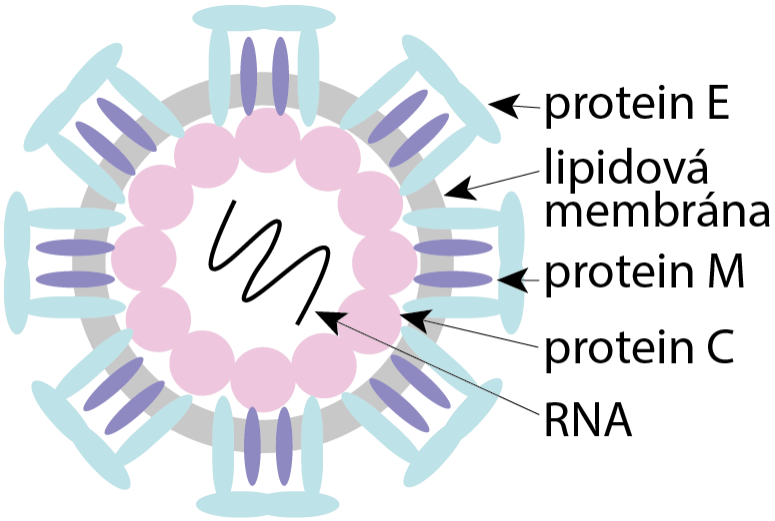

Obrázek 3: **Flavivirová částice**. RNA genom flavivirů je sbalen uvnitř nukleokapsidy složené z C proteinů. Strukturní proteiny prM a E a lipidová vrstva nukleokapsidu zavírají.

1.1.3 Nestrukturní proteiny flavivirů

Nestrukturní proteiny flavivirů hrají zásadní roli ve virové replikaci[11]. Mezi sedm nestrukturních proteinů je řazeno NS1, NS2A, NS2B, NS3, NS4A, NS4B a NS5.

NS1 je multifunkční glykoprotein[23]. Ihned po jeho syntéze dochází k translokaci do lumen ER, kde je dále glykosylován a kde dimerizuje. Následně pomáhá vzniku replikačního komplexu nezbytného pro replikaci virové RNA[24].

NS2A je transmembránový helikální protein. Jeho N-konec se nachází v lumen ER, kdežto C-konec se nachází v cytoplazmě a je štěpen virovou proteázou NS2B-3[25] (obrázek 1, dole). Tento protein se účastní jak syntézy flavivirové RNA, tak sestavování virionu. NS2B je klíčový kofaktor pro proteázovou doménu NS3 proteinu.

NS3 je multifunkční enzym, která má hned několik funkcí. Slouží jako serinová proteáza (NS2B funguje jako kofaktor), 5´-RNA trifosfatáza, nukleosid trifosfatáza a helikáza[26]. Proteázová doména hraje důležitou roli při štěpení polyproteinu, zatímco helikázová doména se účastní replikace, při které rozmotává sekundární strukturu dvojvlákna RNA. To je nezbytný krok pro syntézu nového vlákna RNA[27,28].

Dalšími z nestrukturních proteinů jsou NS4A a NS4B. Zatímco NS4A funguje jako jakési lešení pro replikační komplex, NS4B inhibuje interferonový signál, čímž brání

hostitelské imunitní odpovědi na infekci virem[29,30]. Spolu s NS4A napomáhá disociaci helikázové domény NS3 od RNA[31].

Největším z nestrukturních proteinů je NS5, kterému bude věnována následující kapitola.

1.1.3.1 NS5 protein

Tento nestrukturní protein je složen z N-koncové methyltransferázové domény (MTázy) a C-koncové RNA dependentní RNA polymerázové (RdRp) domény (obrázek 4). Má tedy jak methyltransferázovou, tak polymerázovou aktivitu[32]. MTázová doména je klíčová pro stabilitu nově vzniklé mRNA, jelikož přidává takzvanou čepičku, která ochraňuje virovou RNA před rozpoznáním hostitelským imunitním systémem a zajišťuje její stabilitu[33]. RdRp doména katalyzuje samotnou syntézu virové RNA[34]. Obě tyto domény jsou slibným cílem antivirové léčby, jelikož jak MTázová, tak RdRp doména jsou zásadní pro virovou replikaci a jsou přítomny pouze v infikovaných buňkách.

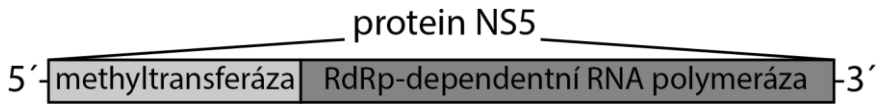

Obrázek 4: **Schéma proteinu NS5**. NS5 protein se skládá z 5´- koncové MTázové a 3´- koncové RdRp domény.

1.1.3.1.1 MTázová doména

Jedná se o globulární protein složený ze tří poddomén: vazebná doména pro GTP, S-adenosyl-L-methionin vazebná doména a vazebné místo pro RNA[35]. Přidání čepičky na virovou mRNA probíhá ve třech následných enzymatických reakcích, jejichž schéma je zobrazeno na obrázku X[36]. Nejprve je pomocí trifosfatázy (RTPázy, z angl. RNA triphosphatase) odštěpen γ-fosfát z 5´ konce RNA (obrázek 5, krok 1). U flavivirů roli RTPázy zastává NS3. Následně je guanylyltransferázou přenesen guanosinmonofosfát (GMP, z angl. guanosine monophosphate) z guanosintrifosfátu (GTP, z angl. guanosine triphosphate) na ppA-RNA (p označuje fosfát a A adenosin), čímž vznikne základ čepičky (obrázek 5, krok 2). Poté N-7-MTáza methyluje guanin na pozici N-7 za vzniku čepičky 0 (m7GpppA-RNA, obrázek 5, krok 3). Vyšší eukaryota dále methylují čepičku 0 na 2´-O pozici ribózy pomocí 2´-O-MTázy za vzniku čepičky 1 (m7GpppAm,

obrázek 5, krok 4) a následně ještě za vzniku čepičky 2 (m7GpppAmNm), kdy dochází k methylaci na 2´-O pozici ribózy následujícího nukleotidu. Donor methylu pro všechny reakce je S-adenosyl-L-methionin (SAM), který se přeměňuje na S-adenosyl-L-homocystein (SAH)[36,37].

Již známé krystalové struktury z různých MTáz odhalují, že katalytická tetráda složená z aminokyselin K-D-K-E (lysin-aspartát-lysin-glutamát) je konzervována mezi 2´-O-MTázami z různých organismů[38–42]. Zatímco celý motiv K-D-K-E je zásadní pro 2´-O-methylaci, pro N-7 methylaci je nezbytný pouze aspartát (D)[43].

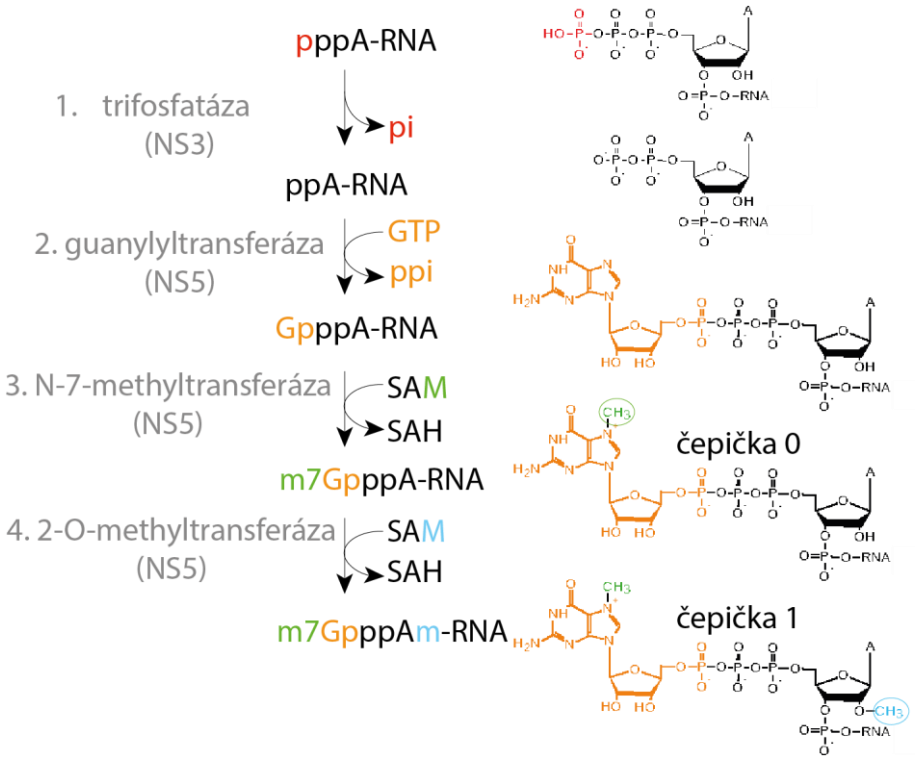

Obrázek 5: **Schéma přidávání čepičky na RNA**. V prvním kroku dochází k odštěpení γ-fosfátu pomocí trifosfatázy, což zastává NS3. Dále dochází k přenosu GMP na 5´ konec pomocí guanylyltransferázy (NS5). NS5 následně přenáší methyl z S-adenosyl-L-methioninu (SAM) na guanin na pozici N-7 za vzniku čepičky 0. Posledním krokem je 2´-O-methylace nukleotidu za vzniku čepičky 1.

1.1.3.1.2 RdRp doména

Polymerázová doména proteinu NS5 katalyzuje *de novo* syntézu RNA. Genomové +RNA vlákno je použito jako templát, ze kterého RdRp nejprve syntetizuje komplementární vlákno s negativní polaritou (-RNA) a vzniká replikační meziprodukt dvojvláknové RNA. Z nově vzniklé -RNA jsou následně syntetizovány další +RNA

vlákna. Na dvojvláknovou RNA se váže NS3 helikáza, a to specificky na 5′-UTR sekvenci 5′-AGUUGUUAGUCU-3′ a dochází k rozdělení replikačního meziproduktu na jednotlivá vlákna ve směru 3′-5′. Nová genomová RNA je uvolněna stejně jako -RNA vlákno, které může znovu sloužit jako templát pro další kolo replikace[28]. Pro elongaci RNA je důležitá změna konformace aktivního centra RdRp z uzavřené na otevřenou[44]. Nově vytvořená virová RNA je dále sbalena a nezralý virion je přenesen sekreční dráhou, kde je prM štěpen a zralý virion je uvolněn z infikované buňky pomocí exocytózy.

Všechny flaviviry mají obdobnou strukturu RdRp, jak je možné vidět z porovnání již známých struktur[41,45–47]. Podobá se sevřené pravé ruce, kterou lze rozdělit na subdomény dlaně, prstů a palce, které obklopují aktivní místo. Rovněž je možno pozorovat sedm strukturních motivů (A-G), které jsou zodpovědné za vazbu NTP a katalýzu a také tři tunely: tunel pro vstup templátu, NTP a tunel pro výstup dsRNA[48]. Na motivech A a C se nachází dva konzervované aspartátové zbytky (D533 a D665), které jsou zodpovědné za vazbu dvoumocných iontů potřebných při polymerizační reakci. Motiv B umožňuje pohyb templátového vlákna během pozdní fáze transkripce[49]. K359, nacházející se na motivu D, hraje důležitou roli při změně struktury probíhající během tvorby RNA-NTP-UTP komplexu[50]. Motivy E a C interagují s RNA produktem. Motiv F je složen z několika podmotivů a nejspíše pomáhá stabilizovat přicházející nukleotid[51]. Posledním motivem je motiv G, který reguluje vstup jednovláknové RNA do vstupního tunelu pro RNA templát a translokaci RdRp[32]. Již zmíněný tunel se spolu s tzv. N kapsou nachází na spojení subdomén place a dlaně a jedná se o dvě místa vázající inhibitory[41].

1.2 Koronaviry

Koronaviry jsou obalené +ssRNA viry s nesegmentovaným genomem, největším mezi RNA viry. Patří do řádu *Nidovirales*, čeledi *Coronaviridae*, podčeledi *Orthocoronavirinae* a dále se dělí do čtyř rodů: alfa-, beta-, gamma-, deltakoronaviry. Zatímco gammakoronaviry a deltakoronaviry napadají výhradně zvířata (především pak ptáky), alfa a betakoronaviry jsou široce rozšířené mezi savci (včetně lidí) a způsobují především respirační či střevní onemocnění[52,53]. Mezi alfakoronaviry se řadí lidský koronavirus (HCoV, z angl, human coronavirus) 229E, HCoV-NL63, virus infekční

peritonitidy u koček (FIPV, z angl. feline infectious peritonitis virus) a virus prasečího epidemického průjmu (PEDV, z angl. porcine epidemic diarrhea virus). Betakoronaviry zahrnují zbývající lidské koronaviry jako je HCoV-OC43, HCoV-HKU1, těžký akutní respirační syndrom způsobený koronavirem SARS-CoV (z angl, severe accute respiratory syndrome coronavirus), SARS-CoV-2 a MERS (z angl. Middle East respiratory syndrome)[53].

RNA genom koronavirů se skládá nejméně z šesti otevřených čtecích rámců. Čtecí rámce ORF1a a ORF1b, které zaujímají dvě třetiny genomu, kódují dva polypeptidy pp1a a pp1ab. Ty jsou následně ko- a posttranslačně štěpeny proteázami na 16 nestrukturních proteinů (NSP1-16), s výjimkou gammakoronavirů, které nemají NSP1[54] (obrázek 6, šedě a modře). Čtecí rámce na 3´ konci genomu kódují čtyři strukturní proteiny: povrchový nebo také spike (S), membránový (M), obalový (E) a nukleokapsidový (N) protein (obrázek 6, zeleně) a dále také pomocné proteiny (obrázek 6, žlutě). Pomocné proteiny jsou vysoce variabilní skupinou proteinů, které přispívají k přizpůsobení hostitelské buňky na infekci a jsou určujícími faktory virové patogenity[55]. Většina nestrukturních proteinů se účastní replikačního cyklu, zatímco strukturní proteiny se podílejí na skládání virionu a infekci hostitelské buňky.

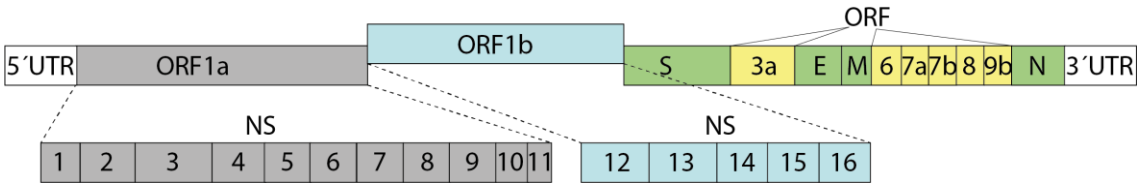

Obrázek 6: **Schematické znázornění genomu SARS-CoV-2**. Jsou znázorněny ORF1a (šedě) a ORF1b (modře), které kódují 16 nestrukturních proteinů (NSP). 4 strukturní proteiny (S, E, M a N) jsou vyobrazeny zeleně a pomocné proteiny kódované ORF 3a, 6, 7a, 7b, 8 a 9b žlutě.

1.2.1 Lidské koronaviry

Lidské koronaviry obsahují nejdelší nesegmentovaný virový genom, který je ohraničen 5´ a 3´ UTR, které jsou důležité při inter- a intramolekulárních interakcích.

První lidské koronaviry byly objeveny v 60. letech 20. století a jednalo se o respirační onemocnění označené jako HCoV-229E a HCoV-OC43[56]. V listopadu 2002 byla ve Foshanu v Číně zaznamenána rychle se šířící nákaza koronaviru. Ta nakonec propukla v epidemii SARS-CoV[57]. O deset let později, v roce 2012, se ze Saudské

Arábie rozšířil další koronavirus způsobující respirační syndrom nazývaný MERS[58]. Poslední epidemie vypukla v prosinci 2019 v provincii Wuhan v Číně a byla klasifikována jako SARS-CoV-2[59]. Na rozdíl od SARS-CoV, který cílí primárně na pneumocyty a makrofágy v plicních tkáních dolních cest dýchacích, SARS-CoV-2 se replikuje v epitelu horních cest dýchacích.

Přenos koronavirů na člověka ještě není plně objasněn, jedná se pravděpodobně o přenos z netopýra prostřednictvím mezihostitele. Po infekci člověka koronavirem je virus následně přenášen mezi lidmi přímým kontaktem[60].

1.2.1.1 SARS-CoV-2

SARS-CoV-2 je hlavním původcem onemocnění COVID-19, který v roce 2020 propukl ve světovou pandemii. Klinické projevy této nemoci se pohybují od asymptomatické infekce až po onemocnění s fatálními následky. Těžký projev mají většinou imunokopromitovaní a starší pacienti. Významnými rizikovými faktory jsou věk, vysoký krevní tlak, cukrovka, imunodeficience, chronická kardiovaskulární a plicní onemocnění, a v neposlední řadě nádorová onemocnění[61].

Vstup HCoV do buňky je zprostředkován glykoproteinem S. Dochází při něm k přichycení k membráně hostitelské buňky a k následné fúzi membrán. Během biosyntézy se v infikovaných buňkách štěpí protein S na dvě podjednotky S1 a S2. Podjednotka S1 váže angiotenzin-konvertující enzym 2, zatímco podjednotka S2 zprostředkovává fúzi virové a hostitelské buněčné membrány[62]. Jakmile dojde k přiblížení virové a buněčné membrány, vznikne fúzní pór, který umožňuje průnik virového genomu do cytoplazmy hostitelské buňky[63]. Samotné uvolnění genomu do cytoplazmy hostitelské buňky zahrnuje komplexní mašinerii exprese virových genů[64].

1.2.1.2 Strukturní proteiny

Schéma koronavirové částice složené ze strukturních proteinů a genomové RNA je znázorněno na obrázku 7.

S protein je glykoprotein složený ze dvou domén, ekto- a endodomény. Formuje se do homotrimerů nazvaných „spiky“. Ty se nachází na povrchu virů a jsou zodpovědné

za uchycení virové částice k receptorům hostitelských buněk a následnou fúzi virové a buněčné membrány, čímž napomáhají rané fázi infekce[65].

Třídoménový transmembránový glykoprotein M se účastní skládání virových částic a spojuje se s dalšími strukturními proteiny, jako například s nukleokapsidou[66].

E protein je nejmenším ze strukturních proteinů a hraje klíčovou roli při skládání virové částice a jejím následném uvolnění.

Posledním ze strukturních proteinů je nukleokapsidový protein N, který, jak název napovídá, formuje nukleokapsidu a skládá se ze dvou domén. Jeho primární funkcí je vazba na RNA a také hraje roli v replikaci virové RNA a v reakci hostitelské buňky na virovou infekci[67].

U některých betakoronavirů, jako například HCoV-OC43 či HCoV-HKU1, byl přítomen ještě pátý strukturní protein, kterým je hemaglutinin-esteráza. Ta váže sialové kyseliny na povrchu glykoproteinů a má acetyl esterázovou aktivitu[68].

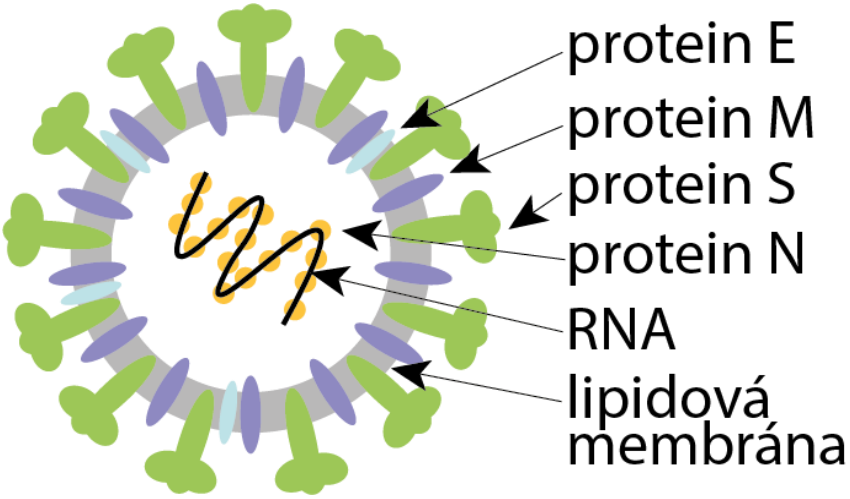

Obrázek 7: **Koronavirová částice**. Virová částice je tvořena čtyřmi strukturními proteiny: obalový (E, světle modře), membránový (M, fialově), spike (S, zeleně) a nukleokapsidový (N, žlutě). N protein interaguje s genomovou RNA. Proteiny S, E a M jsou ukotveny v lipidové membráně (šedě).

1.2.1.3 Nestrukturní proteiny

Jak již bylo zmíněno výše, genom koronavirů (s výjimkou gamakoronavirů) obsahuje 16 nestrukturních proteinů.

NSP1 se v hostitelské buňce váže na kapsu pro vazbu mRNA, čímž brání translaci hostitelských proteinů. To brání syntéze důležitých proteinů zapojených do vrozené imunitní odpovědi. Rovněž zvyšuje translaci virových mRNA[69].

Proteiny NSP2-16 utváří replikačně-transkripční komplex (RTC, z angl. replication-transcription complex), konkrétně NSP2-11 modulují intracelulárních membrány, pomáhají při úniku před imunitní odpovědí hostitele a poskytují kofaktory potřebné pro replikaci[70].

NSP3 má proteázovou aktivitu a podílí se na štěpení posttranslačních modifikací hostitelských proteinů zapojených do vrozené imunitní odpovědi[71].

NSP4 je transmembránový protein podílející se především na modifikaci membrán ER za účelem vytvoření váčků s dvojitou membránou. V tom mu pomáhá NSP6. Tyto váčky slouží k oddělení virové replikace od skládaní virové částice a je to další ochrana před protivirovou odpovědí buňky[72].

Hlavní proteázou je NSP5, ta uvolňuje NSP4-16 z polyproteinu pp1a a pp1ab[73].

NSP7 je spolu s NSP8 kofaktorem NSP12, který zajišťuje samotnou syntézu RNA[74].

NSP9 se váže na NSP8 a aktivuje ho. Působí jako primer pro NSP12 a hraje tak významnou roli při syntéze RNA[75].

NSP10 je kofaktorem NSP16 a napomáhá tak nasazování čepičky na virový mRNA transkript. Rovněž zvyšuje aktivitu NSP14 jakožto exonukleázy při odstraňování nesprávně spárovaných bazí[76].

NSP11 reguluje aktivitu endoribonukleázy a je nezbytný pro virovou replikaci[77].

Již výše zmíněný NSP12 je RdRp. Váže jednu molekulu NSP7 a dvě molekuly NSP8 a tím stabilizuje oblast pro vazbu RNA při virové replikaci[78]. Jeho N-terminální NiRAN doména (z angl. N-terminal nidovirus RdRp-associated nucleotidyltransferase) přenáší GMP na 5´pp-RNA a vzniká tak 5´Gppp-RNA čepička, která je následně methylovaná NSP14 v druhé fázi nasazování čepičky na mRNA[79].

NSP13 působí jako helikáza při rozmotávání RNA, rovněž váže ATP a působí jako RTPáza, tedy odstraňuje 5′ γ-fosfát z mRNA za účelem tvorby 5′ pp-RNA při nasazování čepičky[80].

Jak již bylo zmíněno výše, NSP14 je exoribonukleáza, která kontroluje a odstraňuje nesprávně spárované nukleotidy ve směru 3′-5′, které byly nesprávně přidány RNA polymerázou během replikace genomu[79]. Také funguje jako N-7 MTáza, kdy předává methylovou skupinu ze SAMu na N-7 pozici Gppp-RNA během druhého kroku nasazování čepičky na mRNA[81].

NSP15 je nidovirová RNA uridylyl-specifická endoribonukleáza NendoU (z angl. nidoviral RNA uridylate-specific endoribonuclease). Katalytická doména štěpí poly-U sekvenci na 3′ konci RNA, aby nedošlo k detekci imunitním systémem hostitele[82].

Posledním nestrukturním proteinem je NSP16. Jedná se o 2′-O-MTázu, která přidává v posledním kroku nasazování čepičky methylovou skupinu ze SAMu na 2′-O-ribózu. Jejím kofaktorem je NSP10[83].

1.2.2 Replikace koronavirové RNA

Samotná replikace RNA je zahájena stejně jako u flavivirů syntézou -RNA vlákna z +RNA vlákna, které následně slouží jako templát pro vznik nových genomových +RNA. Ty jsou během translace překládány na nestrukturní proteiny, RTC, případně jsou sbaleny do nově vznikajícího virionu. Koronaviry mají diskontinuální proces virové transkripce, který vede ke vzniku subgenomické RNA (sgRNA)[84]. Během syntézy negativního vlákna dochází k přerušení transkripce replikačně-trankripčním komplexem ve chvíli, kdy narazí na transkripčně regulační sekvenci TRS, nacházející se před většinou ORF. Transkripce je následně znovu zahájena v TRS sousedící s vedoucí sekvencí TRS-L (z angl. TRS leading). V tomto diskontinuálním kroku tedy dochází k interakci mezi komplementárními TRS nově vznikajícího vlákna (-ssRNA) a genomovou +ssRNA. Takto vzniklá sgRNA vlákna s negativní polaritou následně slouží k syntéze sgRNA s pozitivní polaritou, které jsou následně přeloženy do strukturních a pomocných proteinů[85].

1.3 Antivirová terapie

Nukleotidové a nukleosidové analogy jsou slibnými látkami při vývoji nových antivirotik. Nukleosidové analogy jsou chemicky modifikované syntetické nukleosidy, které napodobují ty endogenní a které mohou inhibovat buněčné a virové enzymy, účastnící se jejich metabolismu. Obvykle jsou pojmenovány podle cíle, který inhibují v životním cyklu viru[86,87]. Jsou tedy známy inhibitory RdRp, MTáz, helikáz a inhibitory, které potlačují biosyntetické dráhy nukleosidů v hostitelské buňce. U flavivirů je slibným cílem pro vývoj antivirotik zejména RdRp doména proteinu NS5, jelikož její polymerázová aktivita je unikátní pro viry, a tedy u lidských replikačních enzymů se nevyskytuje[88]. U koronavirů tuto úlohu zastává protein NSP12.

Jednou z nejslibnějších látek, která cílí na NSP12 je remdesivir (obrázek 8), který v organismu podléhá přeměně a ve své trifosfátové podobě se chová jako ATP a působí tedy jako substrát pro virovou RdRp. Po začlenění remdesiviru do vlákna RNA nedochází k okamžitému ukončení syntézy, ale dochází k začlenění dalších tří nukleotidů a až poté je syntéza ukončena. Tento jev je mezi nukleosidovými analogy výjimečný a může souviset s jeho zvýšenou účinností. Opožděné ukončení syntézy vlákna RNA by mohlo vést k maskování remdesiviru před NSP14, která má exonukleázovou opravnou funkci[89]. Jedná se rovněž o první malou molekulu schválenou pro použití proti COVID-19[90]. Následně pak byly schváleny léky molnupiravir a Paxlovid. Zatímco molnupiravir cílí na RdRp, Paxlovid cílí na hlavní proteázu SARS-CoV-2[91,92]. Příkladem inhibitoru MTáz je sinefungin, jehož schéma je na obrázku 9. Jedná se o derivát adenosinu, který soutěží se SAMem (přirozeným substrátem)[93].

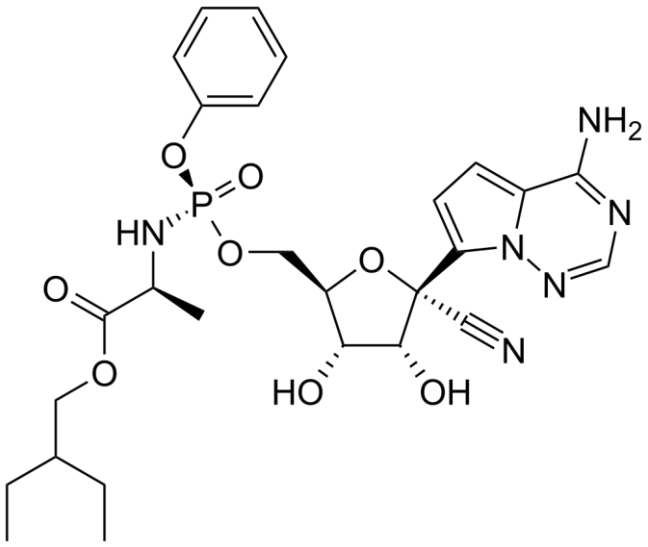

Obrázek 8: **Chemická struktura remdesiviru.**

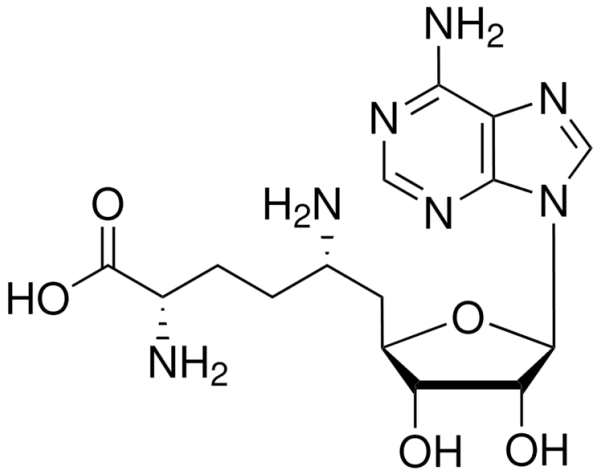

Obrázek 9: **Chemická struktura sinefunginu.**

2 CÍLE PRÁCE

V průběhu doktorského studia byly mým hlavním zaměřením RdRp z flavivirů a koronavirů a také MTázové domény proteinu NS5 z různých flavivirů, a to i z těch méně známých, jako je například Ntaya. Hlavním cílem byla jejich strukturní a funkční charakterizace. Jedná se o nezbytný krok při návrhu antivirotik účinných proti širokému spektru flavivirů, a koronavirů.

Konkrétní cíle byly:

1. Připravit a objasnit strukturu MTázové a RdRp domény proteinu NS5 z Ntaya viru.
2. Porovnat zejména jejich aktivní centra se stejnými enzymy z jiných flavivirů a rovněž porovnat vazebné stavy sinefunginu a GTP se zmíněnými enzymy.
3. Získat a porovnat struktury různých flavivirových MTáz (konkrétně z viru Zika a Ntaya) s navázaným AT-9010. Jedná se o analog GTP, jehož proléčivo AT-752 je považováno za lék proti různým flavivirům.

V další části mého studia jsem testovala aktivitu potenciálních inhibitorů na polymerázách z flavivirů a koronavirů.

Konkrétní cíle byly:

4. *In vitro* testování inhibičního efektu sloučeniny PR673, jakožto nenukleosidového analogu na RdRp z různých flavivirů a ze SARS-CoV-2.
5. *In vitro* testování inhibičního efektu sloučeniny HeE1-2Tyr a jejích derivátů na RdRp ze SARS-CoV-2.

3 PUBLIKACE

Publikace zahrnuté v této dizertační práci:

1. **Structural and functional insights in flavivirus NS5 proteins gained by the structure of Ntaya virus polymerase and methyltransferase**, Krejčová K, Krafcikova P, Klima M, Chalupska D, Chalupsky K, Zilecka E, Boura E., Structure. 2024 Aug 8;32(8):1099-1109.e3

2. **Structural basis for broad spectrum binding of AT-9010 to flaviviral methyltransferases**, Krejčová K**,** Bouřa E, Archives of Virology, bude publikováno

3. **A helquat-like compound as a potent inhibitor of flaviviral and coronaviral polymerases**, Konkolova E*, Krejčová K*, Eyer L*, Hodek J, Zgarbová M, Fořtová A, Jirasek M, Teply F, Reyes-Gutierrez PE, Růžek D, Weber J, Boura E., Molecules. 2022 Mar 15;27(6):1894

4. **Non-nucleotide RNA-dependent RNA polymerase inhibitor that blocks SARS-CoV-2 replication,** Dejmek M*, Konkoľová E*, Eyer L, Straková P, Svoboda P, Šála M, Krejčová K, Růžek D, Boura E, Nencka R., Viruses. 2021 Aug 11;13(8):1585

Publikace nezahrnuté v této dizertační prácí:

1. **Novel analogues of a nonnucleoside SARS-CoV-2 RdRp inhibitor as a potential antivirotics,** Tóth LJ, Krejčová K, Dejmek M, Žilecká E, Klepetářová B, Poštová Slavětínská L, Bouřa E, Nencka R., Beilstein J Org Chem. 2024 May 6;20:1029-1036

* Tito autoři přispěli stejnou měrou

4 VÝSLEDKY

4.1 Structural and functional insights in flavivirus NS5 proteins gained by the structure of Ntaya virus polymerase and methyltransferase

4.1.1 Úvod

Flaviviry jsou viry s jednovláknovou RNA s pozitivní polaritou (+RNA), které jsou zodpovědné za řadu onemocnění, jako jsou žlutá zimnice, horečka dengue, zika, západonilská horečka a další[1]. Epidemie viru Zika zdůraznila jejich nebezpečnost, když se relativně neškodný virus známý již z 50. let minulého století změnil ve smrtící patogen[94]. Klíčovým proteinem v replikaci flavivirů je NS5, který se skládá z N-koncové MTázy a C-koncové RdRp domény. Je zodpovědný za replikaci RNA a rovněž za připojení 5´ RNA čepičky[32]. Přestože flaviviry zapříčinily nejvíce úmrtí již v 19. století, do dnešní doby byla objasněna struktura pouze malého množství RdRp domén[32,34,47,48,95]. Pro vývoj antivirotik účinných proti celé této skupině virů je ale zásadní znát a porovnat struktury co nejvíce z nich, zejména jejich aktivních center, a to i z méně známých virů. Jedním z nich je například Ntaya virus. Naše studie tedy poskytuje komplexní analýzu proteinu NS5 z Ntaya viru, přičemž se zaměřuje na obě jeho domény MTázovou i RdRp. Zároveň zdůrazňuje strukturní konzervaci enzymatických center, což může být slibným výchozím bodem pro návrh antivirotik účinných proti všem flavivirům.

4.1.2 Souhrn

Strukturní analýza MTázové i RdRp domény ukazuje na vysoký stupeň konzervace enzymatických center napříč celou rodinou *Flaviviridae*[40,41,47,48,93]. To naznačuje, že je možný vývoj léků cílených na celou rodinu flavivirů. Byly nicméně zaznamenány rozdíly v enzymových aktivitách MTázových domén různých flavivirových proteinů.

Byla vyřešena struktura Ntaya RdRp domény. Jedná se o převážně alfa-helikální protein se strukturou připomínající tvar lidské pravé ruky, kde jsou rozlišitelné prsty, dlaň a palec, což je typické pro virové polymerázy (obrázek 10, A). Tato doména rovněž obsahuje 2 zinkové prsty důležité pro celkovou stabilitu struktury. Podél kanálu pro vstup templátu, aktivního místa a kanálu pro výstup dsRNA byly pozorovány

konzervované motivy A-G, ve kterých se nalézá většina katalyticky důležitých aminokyselinových zbytků (obrázek 10, D). Celková struktura RdRp domény je v souladu s předchozími popisy flavivirových RdRp. Nejvyšší podobnost pozorujeme s RdRp doménou z viru Zika a naopak nejméně s RdRp ze západonilského viru (WNV, z angl. West Nile virus).

Podrobně jsme rovněž zkoumali konformaci tzv. primovací smyčky (z angl. priming loop) a porovnali ji se smyčkou ze Ziky a západonilské horečky (obrázek 10, B-C). Tato smyčka částečně plní funkci primeru v průběhu syntézy RNA, jelikož flavivirové RdRp patří mezi polymerázy nezávislé na primeru. Uzavřená konformace totiž umožňuje pouze vstup ssRNA. Aminokyselinové zbytky na začátku a na konci smyčky byly vždy ve stejné konformaci, zatímco rozdíl byl pozorován v konformaci postranních řetězců Trp800 a His803. V porovnání Trp800 se Zikou se jednalo pouze o jiný rotamer. U WNV byl Trp800 oproti ostatním dvěma posunut. Zajímavé je, že pozice Trp808 je zcela konzervovaná mezi analyzovanými flavivirovými polymerázami, což naznačuje její důležitost v rámci primovací smyčky.

Nedávno bylo popsáno další místo v blízkosti aktivního místa RdRp, takzvaná N kapsa[96]. Sloučeniny cílené na tuto kapsu jsou účinnými inhibitory replikace viru Dengue a ze sekvenčního porovnání s WNV a JEV bylo předpokládáno, že by se mohlo jednat o vhodné místo pro návrh inhibitorů cílících na celou rodinu flavivirů. Z tohoto důvodu jsme se rozhodli porovnat objem a tvar těchto kapes mezi zkoumanými flaviviry (obrázek 10, E-F). Naše výsledky ukázaly, že N kapsa z Ntaya viru má největší objem, a to téměř dvakrát větší něž kapsa viru Zika. Tvar je rovněž rozdílný, což je ale patrně způsobeno tak značnými rozdíly ve velikostech.

Rovněž jsme objasnili strukturu MTázové domény, a to jak s navázaným sinefunginem, tak s GTP (obrázek 10, G-I). Tato doména má rovněž guanylyltransferázovou aktivitu, která je důležitá při přenosu GMP na RNA v průběhu nasazení čepičky na mRNA. Bylo pozorováno složení z alfa helixů a beta listů, typické pro flavivirové MTázy. Byly popsány vazebné módy pro navázaný sinefungin a GTP, a ty byly následně porovnány s těmi pro Ziku. Sinefungin se váže do SAM vazebného místa, a to především pomocí vodíkových vazeb. Rozdíl byl zaznamenán v orientaci postranního řetězce Glu111. GTP je navázáno v GTP vazebné kapse. Rozdíl v případě vazby GTP byl pozorován v různých konformacích trifosfátu.

V neposlední řadě jsme porovnali enzymatické aktivity MTáz a RdRp z různých flavivirů. Je zajímavé, že ačkoliv enzymatické vlastnosti zkoumaných rekombinantních MTáz byly velmi různorodé, všechny rekombinantní RdRp vykazovaly podobné chování. Nejaktivnější MTázou byla ta ze Ziky a ostatní vykazovaly maximálně 47% aktivitu v porovnání se Zikou. MTáza z YFV vykazovala dokonce pouze 3% aktivitu.

4.1.3 Můj příspěvek

Připravila jsem expresní konstrukt pro Ntaya RdRp, následně jsem provedla rekombinantní expresi a purifikaci jak RdRp, tak MTázové domény NS5 proteinu. Provedla jsem veškeré krystalizační pokusy a nasbírala jsem data. Vyřešila jsem model struktury RdRp a MTázy v komplexu se sinefunginem. Připravila jsem rovněž obrázky do článku a podílela se na jeho přípravě.

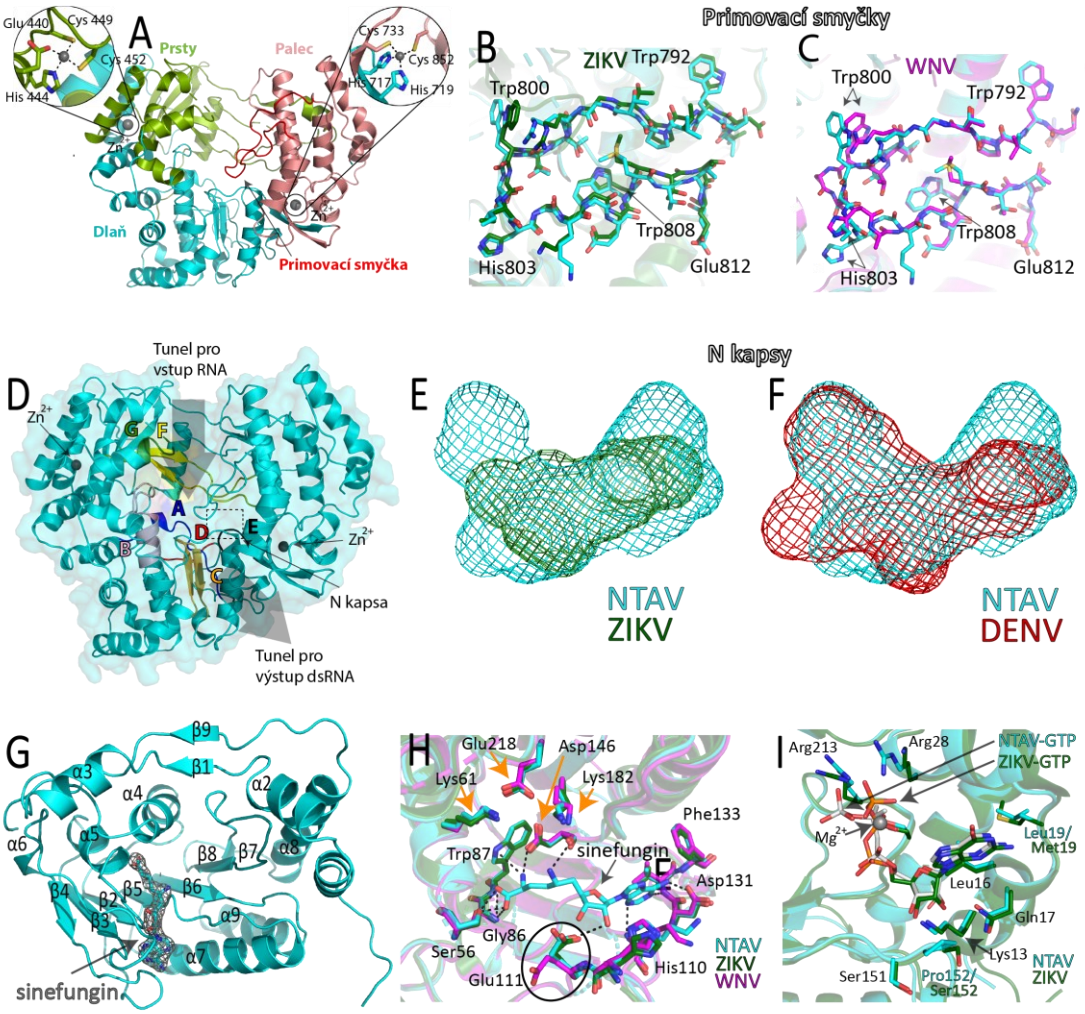

Obrázek 10: Krystalová struktura jednotlivých domén proteinu NS5 viru Ntaya. A) Celková struktura NTAV RdRp domény s vyznačenými subdoménami různými barvami: prsty (zelená), dlaň (modrá), palec (růžová) a červeně je zobrazena primovací smyčka. Zaostřeno je na dva zinkové prsty. B,C) Strukturní porovnání primovacích smyček NTAV (modrá), ZIKV (zelená, PDB: 5M2Z) a WNV (růžová, PDB: 2HZF). D) Struktura NTAV RdRp, s vyznačenými tunely pro vstup RNA a výstup dsRNA, motivy A-G, a polohou N kapsy. E,F) Porovnání velikosti a tvaru N kapes z NTAV (modrá, 349Å^3), ZIKV (zelená, 186Å^3) a DENV (červená, 303Å^3). G) Celková struktura MTázové domény proteinu NS5 viru Ntaya s navázaným sinefunginem (SFG). Je znázorněna Fo-Fc mapa, vykreslená na 2σ kolem SFG. H) Strukturní porovnání vazebných módů sinefunginu pro NTAV, ZIKV (PDB: 5MRK), WNV (PDB: 4R8S). Katalytická tetráda je vyznačena žlutými šipkami. I) Strukturní porovnání vazby GTP mezi NTAV a ZIKV (zelená, PDB: 5GOZ).

4.2 Structural basis for broad spectrum binding of AT-9010 to flaviviral methyltransferases

4.2.1 Úvod

V posledních letech vzrostl vědecký zájem o vývoj inhibitorů MTáz napříč různými virovými rodinami, včetně *Flaviviridae*[97]. 2′-methyl-2′-fluoro guanosin trifosfát označovaný jako AT-9010 je analog GTP. Jeho proléčivo označované AT-752 je považováno za lék proti několika flavivirům. AT-9010 byl identifikován jako duální inhibitor jak RdRp, tak i MTázové domény, přičemž jeho primárním cílem je vazebné místo pro GTP na MTázové doméně proteinu NS5 z orthoflavivirů. Zabraňuje správnému nasazení čepičky na mRNA. Přítomnost fluoru namísto hydroxylové skupiny na 2′ pozici ribózového kruhu zase vede k ukončení replikace RNA, když RdRp zařadí tuto látku místo GTP do nově vznikajícího vlákna. Jelikož ovšem AT-9010 ve formě trifosfátu není schopno proniknout plazmatickou membránou, byla navržena proléčiva AT-752 a AT-281, která se uvnitř buněk přeměňují na aktivní trifosfátovou formu. Obě tyto látky mají nízkou cytotoxicitu[98,99]. V této studii jsme zkoumali vazbu AT-9010 na MTázy z virů Ntaya a Zika a naše publikace tak poskytuje strukturní základ pro vysvětlení účinnosti AT-9010 proti několika flavivirovým MTázám.

4.2.2 Souhrn

Cílem této studie bylo prozkoumat interakci AT-9010, fluorovaného nukleotidového analogu, s MTázovými doménami vybraných orthoflavivirů, a to se zaměřením na pochopení jeho vazebných mechanismů a potenciálu jako širokospektrálního antivirotika. Vybrali jsme viry Ntaya a Zika. Krystaly MTáz těchto virů byly inkubovány s AT-9010, byly vyřešeny krystalové struktury těchto komplexů s cílem porovnání jejich vazebných módů s již vyřešenou strukturou komplexu inhibitoru s MTázou z viru Dengue. Získali jsme struktury s vysokým rozlišením (2Å pro Ziku, obrázek 11, B a 1,8 Å pro Ntayu, obrázek 11, A). Molekula AT-9010 byla u obou proteinů umístěna v GTP vazebném místě, stejně jako v případě Dengue. Byly ovšem pozorovány rozdíly ve vazebných interakcích (obrázek 11, E-F). Nebyla pozorována elektronová hustota v místě γ-fosfátu u Zika MTázy, což naznačuje, že γ-fosfát je v tomto případě velmi flexibilní.

Byly rovněž pozorovány rozdíly ve vazbě molekuly AT-9010 s klíčovými aminokyselinovými zbytky, zejména v interakcích s ribózou a guaninovým kruhem AT-9010, což zdůrazňuje jemné strukturní rozdíly mezi MTázami. V případě Ntaya MTázy, aminokyseliny Leu16 a Leu19 vytváří vodíkové vazby s guaninovým kruhem GTP, zatímco v případě Ziky byla pozorována ještě další interakce, konkrétně s Asn17. Rozdíl v konformaci postranního řetězce byl pozorován v případě aminokyseliny Lys13. Dalším rozdílem byl aminokyselinový zbytek 152. U Ntaya MTázy se na tomto místě nachází prolin, který tvoří vodíkovou vazbu s ribózovým kruhem GTP. Zika má na této pozici serin, který tuto vazbu netvoří.

Srovnání vazby AT-9010 a GTP u MTáz z obou virů ukázalo konzervované pozice báze, cukru a α-fosfátu, zatímco β- a γ- fosfáty se ukázaly jako flexibilní (obrázek 11, C-D). Strukturní rozdíly, jako je přítomnost Lys28 u Ziky a Arg28 u Ntayi, přispívají k rozdílné tvorbě vodíkových vazeb s α-fosfátovou skupinou. I přes tyto rozdíly byl celkový vazebný mód AT-9010 obdobný napříč flavivirovými MTázami, což podporuje jeho potenciál jako širokospektrálního antivirotika.

Tato studie přispívá k pochopení strukturních interakcí AT-9010 s flavivirovými MTázami a zdůrazňuje jeho potenciál jako širokospektrálního inhibitoru proti orthoflavivirům. Výsledky poskytují základ pro vývoj antivirových strategií zaměřených na konzervovanou oblast MTáz.

4.2.3 Můj příspěvek

Provedla jsem rekombinantní expresi a purifikaci MTázové domény NS5 proteinu Ntaya i Zika viru. Provedla jsem veškeré krystalizační pokusy a nasbírala jsem krystalografická data. Vyřešila jsem strukturu Zika MTázy v komplexu s AT-9010. Připravila jsem rovněž obrázky do článku a podílela se na jeho přípravě.

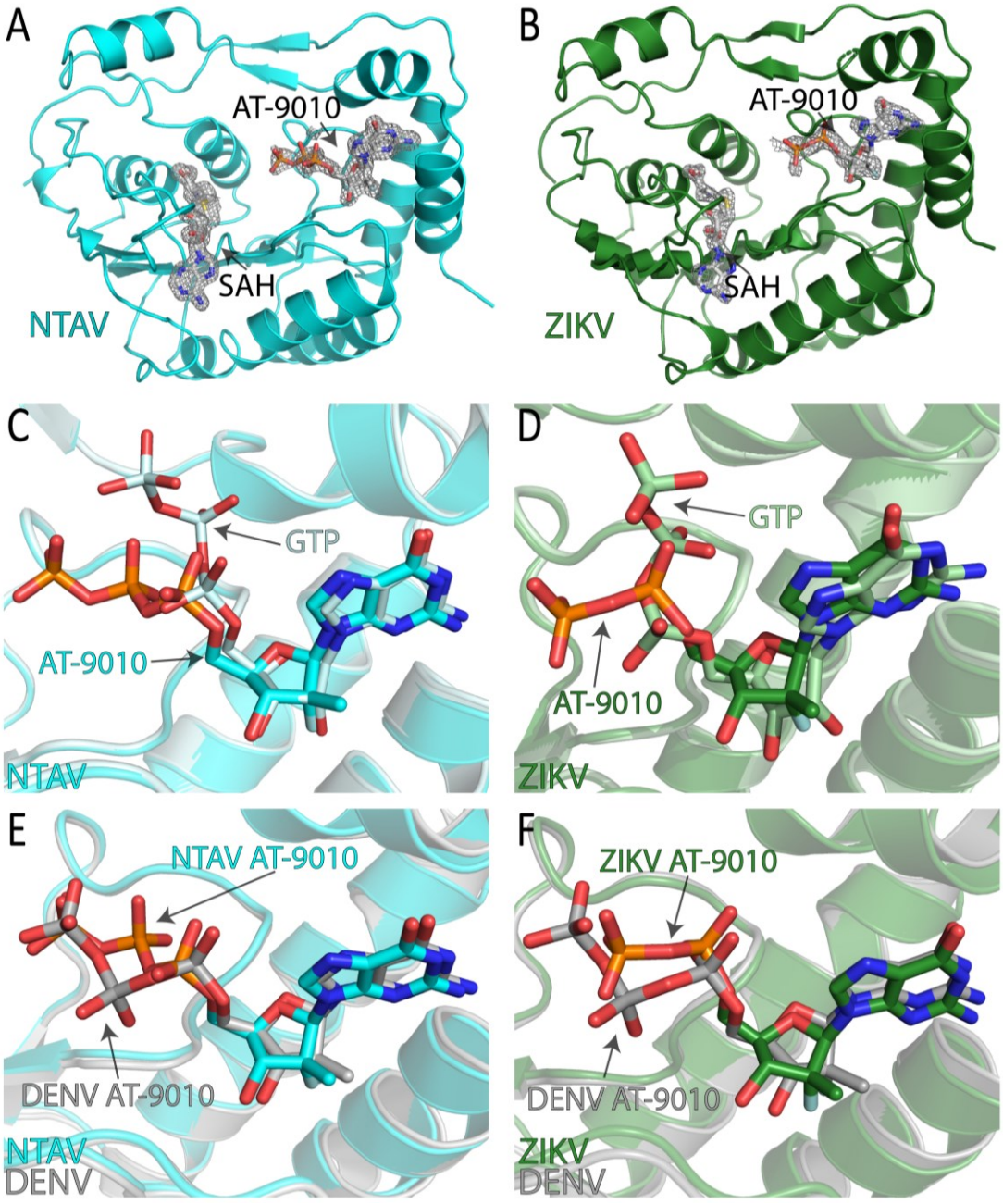

Obrázek 11: **Krystalové struktury Ntaya a Zika MTáz s navazaným AT-9010**. A) Celková struktura Ntaya MTázy s navázaným AT-9010 a SAHem. Je zobrazena Fo-Fc mapa elektronové hustoty vykreslená na 3σ pro obě látky. B) Celková struktura Zika MTázy s navázaným AT-9010 a SAHem. Je zobrazena Fo-Fc mapa elektronové hustoty vykreslená na 3σ pro SAH a na 2σ pro AT-9010. C, D) Strukturní porovnání vazby AT-9010 a GTP pro NTAV (modrá, panel C, PDB kód struktury s GTP: 8CQH) a Ziku (zelená, panel D, PDB kód struktury s GTP: 5GOZ). E, F) Strukturní porovnání mezi Ntaya (modrá, panel E) Zika (zelená, panel F) a Dengue (šedá, PDB kód: 8BCR) MTázovými doménami s navázaným AT-9010.

4.3 A helquat-like compound as a potent inhibitor of flaviviral and coronaviral polymerases

4.3.1 Úvod

RNA viry s pozitivní polaritou (+RNA), jako jsou flaviviry a koronaviry, ukázaly svůj potenciál jakožto patogeny schopné ohrozit společnost. Již dříve tuto schopnost prokázaly viry Zika, MERS-CoV a SARS-CoV[100,101]. Ovšem až SARS-CoV-2 ukázal jejich plný potenciál, když v roce 2019 propukl v pandemii COVID-19[61]. Návrh sloučenin účinných proti většině +RNA virů je tedy v tuto chvíli zásadní. V naší studii byla představena sloučenina PR673, která se svou strukturou podobá helquatu a která je schopna inhibovat replikaci viru SARS-CoV-2 a viru klíšťové encefalitidy (TBEV) v tkáňových kulturách. Pomocí *in vitro* testování RdRp z různých flavivirů a ze SARS-CoV-2 bylo ukázáno, že PR673 zastavuje syntézu RNA. Výsledky naší práce naznačují, že vývoj širokospektrálních nenukleosidových inhibitorů RdRp je možný.

4.3.2 Souhrn

Nejprve byla pomocí screeningu knihovny sloučenin ÚOCHB vybrána molekula PR673 jakožto potenciální inhibitor replikace viru SARS-CoV-2 v buňkách. Hodnoty EC50 se pohybovaly v rozmezí od 17 μM do 29 μM v buňkách Vero-E6, Calu-3 a Caco-2.

Dalším krokem bylo objasnění molekulárního cíle této sloučeniny. Na základě chemické struktury se dalo předpokládat, že by jím mohla být koronavirová RdRp. V případě SARS-CoV-2 se jedná o heterotrimer složený z proteinu NSP12 a jeho dvou kofaktorů NSP7 a NSP8. Pro ověření naší hypotézy byla zjišťována inhibiční aktivita PR673 na tomto proteinovém komplexu. Měření bylo provedeno sledováním ubývání produktu reakce, ve které dochází k prodlužování RNA primeru podle templátu pomocí RdRp. Sekvence použitého primeru a templátu je znázorněna na obrázku 12, A. Tyto reakce jsou následně vizualizovány na polyakrylamidových denaturujících gelech. Jakmile dojde k inhibici, produkt reakce není pozorován. Syntéza RNA byla zcela zastavena při koncentraci inhibitoru vyšší něž 12,5 μM, což dokazuje, že cílem PR673 je skutečně RdRp (Obrázek 12, B).

Dále byla analyzována inhibiční aktivita a stanovena IC50 naší sloučeniny i na flavivirových RdRp (Obrázek 12, B-C). Byly vybrány virus japonské encefalitidy (JEV), Ntaya (NTAV), virus klíšťové encefalitidy (TBEV), virus žluté zimnice (YFV) a virus Zika (ZIKV). Byla pozorována inhibiční aktivita všech testovaných polymeráz s hodnotami IC50 od 3,0 ± 0,1 μM do 4,9 ± 0,5 μM (obrázek 12, C).

Jelikož byla pozorována silná inhibice všech testovaných flavivirových RdRP *in vitro*, rozhodli jsme se zjistit, zda PR673 inhibuje flaviviry i v buňkách. Zvoleným virem byl TBEV. Byla měřena cytotoxicita na buňkách prasečích ledvin a porovnána se zvolenou pozitivní kontrolou, kterou byl 7-deaza-2′-C-methyladenosin (7-deaza-2′-CMA) a která je prokázaným inhibitorem TBEV RdRp. Látka PR673 se ukázala jako netoxická s hodnotou CC50 přes 50 μM. Dále byla pozorována kompletní inhibice replikace TBEV při koncentraci 0,4 μM a PR673 vykazoval hodnotu EC50 0,11 μM.

4.3.3 Můj příspěvek

Podílela jsem se na expresi a purifikaci proteinů NS5 vybraných flavivirů a rovněž RdRp ze SARS-CoV-2. Následně jsem se podílela na *in vitro* testování inhibičního efektu PR673 na všechny připravené enzymy. Vyhodnotila jsem získaná data pro učení IC50. Následně jsem se podílela na přípravě obrázků do článku.

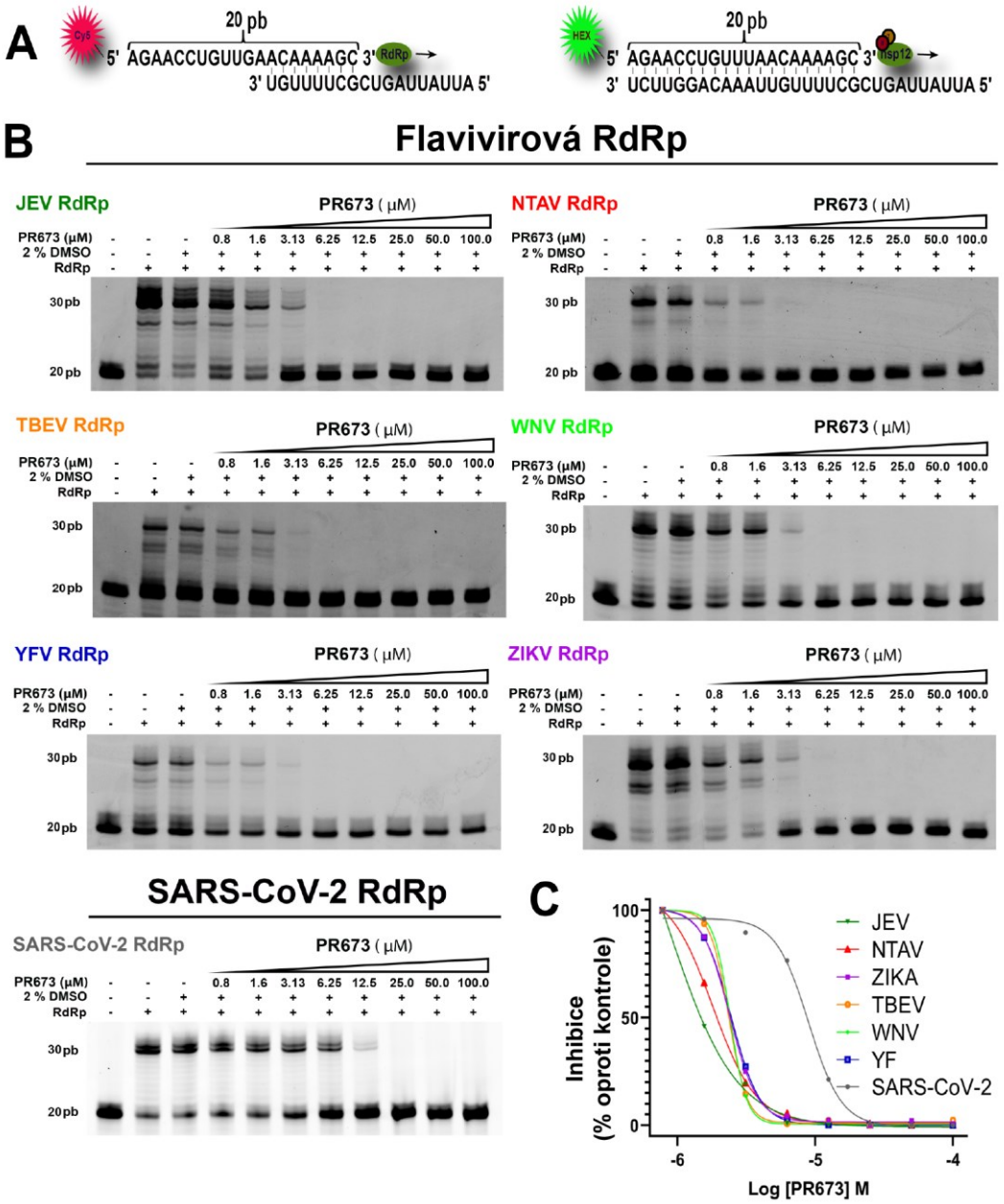

Obrázek 12: **Porovnání inhibiční aktivity látky PR673 vůči různým RdRp.** A) RNA primer a templát použité při tomto měření. RNA primer nese na 5´ konci fluorescenční značku (Cy5 v případě flavivirů a HEX u SARS-CoV-2). Šipky označují směr prodlužování vlákna RNA. B) Inhibice prodlužování vlákna pomocí RdRp látkou PR673. Ředící řada látky PR673 (v μM), za stejné koncentrace polymerázy (20 nM) a templátu/primeru (10 nM). Reakce byly zahájeny přídavkem 10 μM NTP a inkubovány při teplotě 33°C 1 hodinu. Následně byly zastaveny přidáním denaturujícího pufru a získané produkty byly rozděleny pomocí denaturačních polyakrylamidových gelů. C) Procenta inhibice (oproti kontrole) jsou vynesena proti logaritmu koncentrace PR673. Výsledky byly proloženy sigmoidální křivkou závislosti účinku na dávce.

4.4 Non-nucleotide RNA-dependent RNA polymerase inhibitor that blocks SARS-CoV-2 replication

4.4.1 Úvod

SARS-CoV-2 způsobil rozsáhlou pandemii onemocnění COVID-19 po celém světě[52]. Hlavními cíli vývoje nových antivirotik proti tomuto viru se staly klíčové virové enzymy. Jedním z nich je RdRp, jelikož hraje zásadní roli v replikaci virové RNA[102]. V této studii byla použita sloučenina HeE1-2Tyr, již dříve představená v práci Tarantina a kol.[103], a její dva deriváty. Tyto látky byly původně objeveny jako inhibitory RdRp flavivirů. V našem článku ukazujeme, že tyto deriváty pyridobenzothiazolu rovněž významně inhibují RdRp SARS-CoV-2.

4.4.2 Souhrn

V této studii jsme se zaměřili na vývoj nových nenukleosidových inhibitorů RdRp viru SARS-CoV-2. Konkrétně jsme se soustředili na sloučeninu HeE1-2Tyr, která byla již dříve zveřejněna v práci Tarantina a kol.[103], a její další dva nové deriváty. Z důvodu snadnějšího zavedení širšího spektra substituentů do benzothiazolopyridinového jádra byl modifikován způsob syntézy. Tímto způsobem byla připravená molekula HeE1-2Tyr (označovaná číslem 16) a dva nové analogy (17 a 18) a následně byl testován jejich inhibiční účinek na RdRp ze SARS-CoV-2 v *in vitro* měřeních a rovněž byly provedeny experimenty ve tkáňových kulturách.

Byly připraveny proteiny NSP7, NSP8 a NSP12, které dohromady utváří RdRp SARS-CoV-2. S nimi byly následně provedeny *in vitro* experimenty zaměřující se na inhibiční aktivitu připravených látek.

Provedené *in vitro* experimenty potvrdily, že všechny sloučeniny vykazují inhibiční aktivitu, i když s různými IC50. Nejlepším inhibitorem se ukázala původní sloučenina, tedy HeE1-2Tyr, a to s hodnotou IC50 27,6 ± 2,1 μM. Inhibiční účinek sloučeniny 18 byl nejslabší s hodnotou IC50 85,5 ± 2,0 μM (obrázek 13).

Následně byla testována cytotoxicita a antivirová aktivita všech sloučenin v tkáňových kulturách. Tato měření ukázala, že sloučeniny HeE1-2Tyr a 17 účinně inhibují replikaci viru v buňkách Vero a CaCo-2, a to v submikromolárních

koncentracích. Tyto sloučeniny rovněž vykazovaly antivirovou aktivitu s hodnotami EC50 kolem 653,5 nM, resp. 527,3 nM. Tyto hodnoty jsou srovnatelné s remdesivirem, známým inhibitorem RdRp schváleným americkým úřadem pro kontrolu potravin a léčiv (FDA, z angl. Food and Drug Administration).

Dále bylo prokázáno, že výše zmíněné sloučeniny nejsou cytotoxické s hodnotami CC50>50 μM. Rovněž vykazují vysoké selektivní indexy, což prokazuje, že selektivně cílí na virovou replikaci, aniž by významně ovlivnily životaschopnost buněk. Obdobných výsledků získaných z měření na tkáňových kulturách bylo získáno i pro kočičí koronavirus (FIPV), tedy potlačení replikace tohoto viru a nízké hodnoty EC50. Na druhou stranu sloučenina 18 byla méně účinná jak v polymerázových *in vitro* testech, tak v buňkách.

Z této studie tedy vyplývá, že látka HeE1-2Tyr a její analog 17 představují nadějné nenukleosidové inhibitory RdRp mající potenciál pro další vývoj antivirotik proti SARS-CoV-2. Získané výsledky poskytují základ pro další optimalizaci a klinické využití.

4.4.3 Můj příspěvek

Podílela jsem se na expresi a purifikaci proteinů NSP7, NSP8 a NSP12 ze SARS-CoV-2. Následně jsem se podílela na *in vitro* testování inhibičního efektu látek 16, 17 a 18 a vyhodnocení dat pro získání IC50.

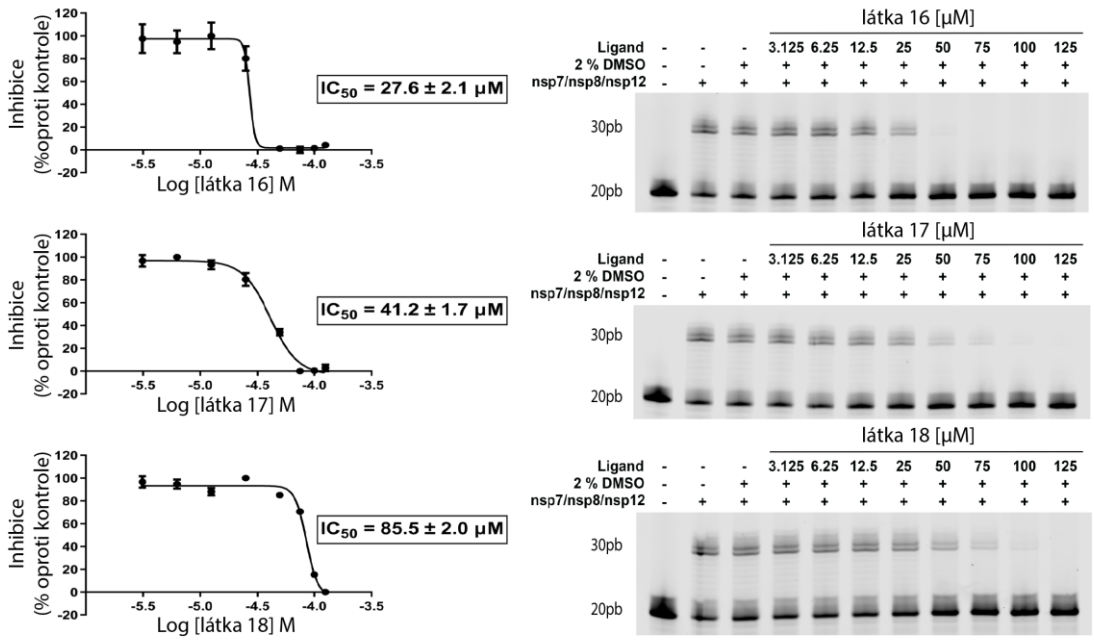

Obrázek 13**: Inhibice RdRp ze SARS-CoV-2 látkami 16, 17 a 18**. Vlevo) Hodnoty IC50 byly stanoveny pomocí radioaktivního měření sledování prodlužování primeru. Odchylka je vypočítána z průměru tří měření. Vpravo) Výsledky měření s použitím fluorescenčně značeného primeru. Se zvyšující se koncentrací látky ubývá produkt.

5 DISKUZE

5.1 Structural and functional insights in flavivirus NS5 proteins gained by the structure of Ntaya virus polymerase and methyltransferase

Tato studie je zaměřena na komplexní analýzu MTázové a RdRp domény proteinu NS5 z viru Ntaya. Již dříve byly zveřejněny struktury daných domén z různých jiných flavivirů[32,39,40,47,48,93]. Pro vývoj antivirotik účinných proti všem flavivirovým MTázám a polymerázám je zásadní objasnit jejich strukturu a odhalit tak jejich strukturní a funkční podobnosti a rozdíly. Naše studie odhaluje strukturní konzervaci enzymatických center, což naznačuje možný vývoj takových antivirotik. Vazbu látky, která by mohla být účinná proti celé rodině flavivirů, jsme následně zkoumali ze strukturního hlediska a výsledku jsou shrnuty v dalším článku, který je rovněž součástí této disertační práce (kapitola 4.2, strany 29-31).

Naše strukturní analýza odhalila určité rozdíly v konformacích několika důležitých oblastí jako je primovací smyčka v RdRp či různé konformace Glu111 ve vazebné kapse pro S-adenosyl-L-methionin (SAM). Glu111 vytváří vodíkovou vazbu s 2′-hydroxylovou skupinou ribózového kruhu ve většině flavivirových MTáz, ale schopnost tohoto aminokyselinového zbytku změnit konformaci na nevazebnou, by mohla vysvětlit mechanismus uvolňování SAHu z aktivního místa, jelikož SAH i SAM jsou vázány stejným způsobem[41].

Z porovnání různých flavivirových MTáz a RdRp je patrné, že aktivní místa těchto enzymů jsou konzervována, což naznačuje, že terapeutické látky vyvinuté proti jednomu flavivirovému enzymu by mohly být účinné proti všem členům této rodiny virů. Bylo nicméně pozorováno, že N kapsa, již dříve navrhovaná jako potenciální vazebné místo pro pan-flavivirové inhibitory[96], není ve skutečnosti stejná mezi medicínsky významnými flaviviry. Důsledkem toho je, že inhibitory cílené na tuto kapsu by byly pravděpodobně účinné pouze proti specifické podskupině flavivirů a ne proti všem.

Naše enzymová analýza byla v souladu s již dříve získanými výsledky[104–106]. Nejaktivnější rekombinantní polymerázou byla Zika a to asi 4× více než nejméně aktivní YFV. Podobná situace byla pozorována u methyltránsferáz. Opět byla

nejaktivnější ta ze Ziky, ale tentokrát o více než o řád, konkrétně 30× více než nejméně aktivní YFV. Tyto výsledky je složité vysvětlit ze strukturního hlediska. Vysvětlení bychom mohli hledat v absenci evolučního tlaku na rychlost MTázy. Je třeba si uvědomit, že RdRp musí syntetizovat celý genom, což zahrnuje přes 10 000 katalytických kroků. Za tu stejnou dobu musí MTázová doména převést jeden guanylylový zbytek, provést jednu N-7 a jednu 2´-O methylaci. Pomalá MTáza může být tedy stejně účinná jako ta rychlá.

5.2 Structural basis for broad spectrum binding of AT-9010 to flaviviral methyltransferases

Tato studie se zaměřuje na porovnání vazebných módů látky AT-9010, inhibitoru RdRp orthoflavivirů, s různými virovými MTázovými doménami. Tato látka, respektive její proléčivo AT-752 je považováno za lék proti určitým flavivirům[98,99]. Náš výzkum odhaluje klíčové podobnosti a rozdíly ve vazbě AT-9010 s MTázami z virů Zika a Ntaya.

AT-9010 se váže do GTP vazebného místa MTázových domén, což bylo očekávané, jelikož se jedná o GTP analog, konkrétně 2′-methyl-2′-fluoro guanosin trifosfát. V naší práci byly popsány interakce mezi guaninovým kruhem AT-9010 a jednotlivými aminokyselinovými zbytky MTáz. Byly pozorovány jisté rozdíly ve vazebném módu pro Ntayu a Ziku. Například u Ntaya MTázy tvoří Leu16 a Leu19 vodíkové vazby s guaninovým kruhem AT-9010, zatímco u Ziky byla pozorována ještě další vazba s aminokyselinovým zbytkem Asn17. Rozdíl v tvorbě vodíkové vazby aminokyselinového zbytku Lys13 můžeme přičítat odlišné konformaci tohoto lysinu. V případě Ziky je amino skupina vzdálena 4,5 Å daleko od 3′-hydroxylové skupiny ribózy, což znemožňuje tvorbu vodíkové vazby. Tyto nepatrné rozdíly zdůrazňují variabilitu ve struktuře MTáz různých flavivirů.

Byly rovněž pozorovány rozdíly ve trifosfátové části molekuly AT-9010. Ve struktuře se Zikou nebyla pozorována elektronová hustota v místě γ-fosfátu, což ukazuje na vysokou flexibilitu této části. Významnou roli ve vazbě trifosfátu hraje aminokyselinový zbytek 28. Zatímco v případě Ziky je na této pozici lysin a tvoří vodíkovou vazbu s α-fosfátem, u Ntayi se na tomto místě vyskytuje arginin, který tuto vodíkovou vazbu netvoří.

Z celkového porovnání vazebných módů AT-9010 s našimi dvěma MTázami a ještě s již dříve publikovanou strukturou Dengue[99] lze shrnout, že i přes několik rozdílů je vazba této látky dostatečně konzervovaná. To ze strukturního hlediska podporuje použití AT-9010 jako širokospektrálního antivirotika. Strukturní analýza dále naznačuje, že flexibilita trifosfátové části nemá zásadní vliv na celkovou vazbu této látky. Drobné strukturní rozdíly, které by mohly ovlivnit afinitu vazby, otevírají cestu k dalším

optimalizacím AT-9010 a podobných sloučenin s cílem zlepšit jejich účinnost proti širšímu spektru flavivirů.

5.3 A helquat-like compound as a potent inhibitor of flaviviral and coronaviral polymerases

Nedávná pandemie COVID-19 způsobená virem SARS-CoV-2 ukázala pravý potenciál +RNA virů[61,107]. Od propuknutí pandemie se aktivně vyvíjejí inhibitory proti různým koronavirovým enzymům, jako je RdRp, proteáza 3CLpro, helikáza, endo- a exonukleáza či MTáza[92,108–111]. Na první dva zmíněné enzymy již dokonce byly nalezeny inhibitory, které byly následně schváleny jako léčiva, konkrétně remdesivir a molnupiravir cílící na RdRp a nirmatrelvir (prodávaný v kombinaci s látkou ritonavir pod názvem Paxlovid) inhibující 3CLpro proteázu[90–92,104].

Cílem však je vyvinout sloučeninu účinnou proti více virům či dokonce rodinám virů. Jedním takovým příkladem je již výše zmíněný remdesivir, který byl původně objeven proti respiračnímu syncytiálnímu viru a následně vyvinut k boji proti epidemii Eboly v roce 2014 a znovu použit proti SARS-CoV-2[90]. Nedávno bylo prokázáno, že je rovněž schopen inhibovat flavivirové RdRp[104].

V naší studii byla představena látka PR673, která, jak bylo experimentálně prokázáno, inhibuje RdRp, a to jak u SARS-CoV-2, tak u flavivirů.

Naše experimenty ukázaly, že námi představená látka označovaná PR673 funguje jako pseudo-obligátní terminátor syntézy RNA a dokáže tedy zastavit jeho syntézu. Na rozdíl od inhibitorů působících jako obligátní terminátory syntézy RNA, které se začlení do RNA a zabraňují tak začlenění dalšího nukleosidu, jako je třeba remdesivir[104], nedochází k začlenění této sloučeniny. Je možné, že PR673 soutěží o jedno z vazebných míst RNA. Tímto místem může být místo pro vstup či výstup RNA. Tyto oblasti jsou relativně konzervované u virových RdRp. Nelze rovněž vyloučit možnost, že PR673 je alosterický inhibitor. Tato hypotéza ovšem není příliš pravděpodobná, jelikož byla prokázána jeho aktivita na relativně odlišných RdRp, jejichž alosterická místa nejsou konzervována. V každém případě sloučenina PR673 ukazuje, že vývoj nenukleosidových antivirotik aktivních proti širokému spektru virů je možný.

5.4 Non-nucleotide RNA-dependent RNA polymerase inhibitor that blocks SARS-CoV-2 replication

Tato studie byla zaměřena na sloučeninu HeE1-2Tyr, která byla již dříve představena v práci Tarantina a kol.[103] jakožto nenukleosidového inhibitoru RdRp SARS-CoV-2 a její dva deriváty. Jak již bylo prokázáno v případě léčby HIV, kombinace nukleosidových a nenukleosidových inhibitorů reverzní transkriptázy může vést k efektivní léčbě i tak vážného onemocnění[112]. Podobně tomu bylo i v případě léčby hepatitidy B a C, kde inhibitory cílí primárně na polymerázu[113]. Není tedy překvapivé, že jedním z hlavních cílů vývoje inhibitorů proti SARS-CoV-2 je RdRp, jelikož hraje zásadní roli v replikaci virové RNA. Byly provedeny testy inhibiční aktivity těchto látek na již zmíněnou polymerázu *in vitro* a ty byly doplněny o testy na cytotoxicitu a antivirovou aktivitu v tkáňových systémech.

V naší práci jsme úspěšně ukázali, že nové nenukleosidové inhibitory HeE1-2Tyr a jeho deriváty 17 a 18 vykazují významnou antivirovou aktivitu proti SARS-CoV-2, což představuje slibnou alternativu k současným nukleosidovým analogům, jako je remdesivir. Způsob syntézy těchto inhibitorů, který zahrnoval modifikovaný přístup k zavedení substituentů namísto 8-OH v benzothiazolopyridinovém jádru, umožnil optimalizovat fyzikálně-chemické vlastnosti sloučenin. Byly tak vytvořeny účinné inhibitory RdRp, které fungují na jiném principu než remdesivir. Tyto látky pravděpodobně fungují jako kompetitivní inhibitory tím, že interagují s tunelem pro vstup RNA. Rozdílný mechanismus působení je velmi důležitý, protože nabízí potenciál pro kombinovanou terapii, což by mohlo přinést synergický efekt a snížit pravděpodobnost vzniku rezistence vůči léčivům.

Naše *in vitro* výsledky ukázaly, že HeE1-2Tyr (16) a sloučenina 17 účinně inhibovaly aktivitu RdRp a replikaci viru v testech na SARS-CoV-2 i na koronaviru koček (FIPV). Hodnoty IC50 získané pro HeE1-2Tyr a 17 byly srovnatelné s remdesivirem v buňkách Vero a Caco-2, i když strmější křivka inhibice růstu u remdesiviru naznačuje, že má remdesivir prudší závislost na dávce. Vysoký index selektivity a nízká cytotoxicita našich sloučenin ukazuje na jejich potenciál jako bezpečných a účinných antivirotik. Látka 18 byla méně účinná v testech *in vitro* a ukázala se neaktivní při stanovení aktivity proti viru SARS-CoV-2 ve tkáňových kulturách. Tato neaktivita by mohla být

způsobena špatným buněčným příjmem nebo metabolickou nestabilitou způsobenou degradací látek buněčnými katabolickými enzymy.

Přestože bude nutná další optimalizace ke klinickému využití sloučeniny HeE1-2Tyr a 17, jedná se o jeden z mála nenukleosidových inhibitorů replikace koronavirů, konkrétně jejich RdRp. Tyto sloučeniny představují významný krok na cestě k vývoji nových terapeutik zaměřených na virovou RdRp.

6 ZÁVĚR

Výzkum v rámci této disertační práce poskytl cenné informace ohledně strukturní a funkční podobnosti mezi MTázami nebo RdRp z různých flavivirů.

Srovnání enzymatických center potvrdilo, že tato rodina virů má aktivní místa konzervována jak u MTáz, tak u RdRp. Toto zjištění jen potvrzuje, že snahy o nalezení inhibitoru nebo inhibitorů, které budou aktivní proti celé rodině virů a případně i proti všem +RNA virům, jsou velmi slibné.

Naše výsledky ukazují, že je při vývoji širokospektrálních inhibitorů důležité zvolit správný cíl, jak bylo ukázáno v případě N kapsy v doméně RdRp. Ta zaujímá u různých flavivirů různý objem, což může způsobit rozdíly v účinnosti látek navržených právě na tuto kapsu.

Strukturní studie týkající se interakcí AT-9010 s flavivirovými MTázami se zaměřovala na využití této látky jakožto širokospektrálního antivirotika. Byl představen konzervovaný vazebný mód napříč různými flavivirovými MTázami, který podtrhuje potenciál AT-9010 jako slibného kandidáta pro budoucí vývoj antivirové terapie zaměřené na MTázové a RdRp domény u orthoflavivirů.

Další z testovaných látek byla HeE1-2Tyr a její dva deriváty. Testována byla tentokrát inhibiční aktivita *in vitro* a v buňkách. Tato látka rovněž inhibuje RdRp, a to jak u SARS-CoV-2, tak i u kočičího koronaviru FIPV. To opět potvrzuje důležitost snahy o vytvoření látky aktivní proti více rodinám virů.

Poslední námi testovanou látkou byla PR673, u které bylo prokázáno, že inhibuje RdRp jak u flavivirů, tak u koronavirů. Touto látkou jsme se opět přiblížili cíli pro nalezení látek proti různým virům. V tomto případě je velkým vzorem látka remdesivir, která již byla schválena jako léčivo. Tato látka byla také nejprve vyvinuta proti respiračnímu syncytiálnímu viru, později použita v boji proti Ebole a nyní byly prokázány její účinky na flavivirovou i koronavirovou RdRp.

Jak látka PR673, tak HeE1-2Tyr a její deriváty jsou nenukleosidové inhibitory a je tedy možná jejich kombinace s nukleosidovým inhibitorem, jako již bylo dříve ukázáno například při léčbě HIV. Tato kombinace může vést k vyšší efektivitě samotné léčby a vývoj takových látek použitelných v boji proti virům je tedy důležitý.

7 SEZNAM ZKRATEK

ATP	adenosintrifosfát, z angl. adenosine triphosphate
C protein	kapsidový protein, z angl. capsid protein
CC50	50% cytotoxická koncentrace, z angl. cytotoxic concentration 50
DENV	Dengue virus
dsRNA	dvojvláknová RNA, z angl. double-stranded RNA
E protein	obalový protein, z angl. enveloped protein
EC50	50% účinná koncentrace, z angl. effective concentration 50
ER	endoplazmatické retikulum
FDA	Úřad pro kontrolu potravin a léčiv, z angl. Food and Drug Administration
FIPV	virus infekční peritonitidy u koček, z angl. feline infectious peritonitis virus)
GMP	guanosinmonofosfát
GTP	guanosintrifosfát, z angl. guanosine triphosphate
HCoV	lidský koronavirus, z angl. human coronavirus
HIV	lidský virus imunitní nedostatečnosti, z angl. human immunodeficiency virus
IC50	50% inhibiční koncentrace, z angl. inhibition concentration 50
JEV	virus japonské encefalitidy, z angl. japanese encephalitis virus
M protein	membránový protein
MERS	blízkovýchodní respirační syndrom, z angl. Middle East respiratory syndrome
mRNA	mediátorová RNA
MTáza	methyltransferáza

N protein	nukleokapsidový protein
NendoU	nidovirová uridylyl-specifická endoribonukleáza, z angl. nidoviral uridylate-specific endoribonuclease
NS	nestrukturní protein (u flavivirů)
NSP1-16	nestrukturní protein 1-16, z angl. non-structural protein 1-16 (u koronavirů)
NTAV	Ntaya virus
NTP	nukleosidtrifosfát, z angl. nucleoside triphosphate
ORF	otevřený čtecí rámec, z angl. open reading frame
PEDV	virus prasečího epidemického průjmu, z angl. porcine epidemic diarrhea virus
prM	prekurzor membrány
RdRp	RNA-dependentní RNA polymeráza
RNA	ribonukleová kyselina, z angl. ribonucleic acid
+RNA	RNA s pozitivní polaritou
-RNA	RNA s negativní polaritou
RTPáza	RNA trifosfatáza, z angl. RNA triphosphatase
S protein	spike protein
SAH	S-adenosyl-L-homocystein
SAM	S-adenosyl-L-methionin
SARS-CoV	těžký akutní respirační syndrom způsobený koronavirem, z angl. severe acute respiratory syndrome coronavirus
SARS-CoV-2	těžký akutní respirační syndrom způsobený koronavirem 2, z angl. severe acute respiratory syndrome coronavirus 2
sgRNA	subgenomická RNA

ssRNA	jednovláknová RNA, z angl, single-stranded RNA
SLA	vlásenka se smyčkou A, z angl. stem loop A
TBEV	virus klíšťové encefalitidy, z angl. tick-borne encephalitis virus
TRS	transkripčně regulační sekvence
UTP	uridintrifosfát, z angl. uridine triphosphate
UTR	nepřekládaná oblast, z angl. untranslated region
WNV	západonilský virus, z angl. West Nile virus
YFV	virus žluté zimnice, z angl. yellow fever virus
ZIKV	Zika virus

8 SEZNAM POUŽITÉ LITERATURY

1. Simmonds, P., Becher, P., Bukh, J., Gould, E.A., Meyers, G., Monath, T., Muerhoff, S., Pletnev, A., Rico-Hesse, R., Smith, D.B., et al. (2017). ICTV Virus Taxonomy Profile: Flaviviridae. J. Gen. Virol. *98*, 2–3. https://doi.org/10.1099/jgv.0.000672.

2. MacNamara, F.N. (1954). Zika virus : A report on three cases of human infection during an epidemic of jaundice in Nigeria. Trans. R. Soc. Trop. Med. Hyg. *48*, 139–145. https://doi.org/10.1016/0035-9203(54)90006-1.

3. Uno, N., and Ross, T.M. (2018). Dengue virus and the host innate immune response. Emerg. Microbes Infect. *7*, 1–11. https://doi.org/10.1038/s41426-018-0168-0.

4. Waggoner, J.J., Rojas, A., and Pinsky, B.A. (2018). Yellow Fever Virus: Diagnostics for a Persistent Arboviral Threat. J. Clin. Microbiol. *56*, e00827-18. https://doi.org/10.1128/JCM.00827-18.

5. Bogovic, P. (2015). Tick-borne encephalitis: A review of epidemiology, clinical characteristics, and management. World J. Clin. Cases *3*, 430. https://doi.org/10.12998/wjcc.v3.i5.430.

6. Unni, S.K., Růžek, D., Chhatbar, C., Mishra, R., Johri, M.K., and Singh, S.K. (2011). Japanese encephalitis virus: from genome to infectome. Microbes Infect. *13*, 312–321. https://doi.org/10.1016/j.micinf.2011.01.002.

7. Smithburn, K.C., and Haddow, A.J. (1951). Ntaya Virus. A Hitherto Unknown Agent Isolated from Mosquitoes Collected in Uganda. Exp. Biol. Med. *77*, 130–133. https://doi.org/10.3181/00379727-77-18700.

8. Li, R., Niu, Z., Liu, Y., Bai, X., Wang, D., and Chen, C. (2022). Crystal structure and cap binding analysis of the methyltransferase of langat virus. Antiviral Res. *208*, 105459. https://doi.org/10.1016/j.antiviral.2022.105459.

9. Pierson, T.C., and Diamond, M.S. (2020). The continued threat of emerging flaviviruses. Nat. Microbiol. *5*, 796–812. https://doi.org/10.1038/s41564-020-0714-0.

10. Markoff, L. (2003). 5’- and 3’-noncoding regions in flavivirus RNA. Adv. Virus Res. *59*, 177–228. https://doi.org/10.1016/s0065-3527(03)59006-6.

11. Westaway, E.G., Brinton, M.A., Gaidamovich, Ya., Horzinek, M.C., Igarashi, A., Kääriäinen, L., Lvov, O.K., Porterfield, J.S., Russell, P.K., and Trent, D.W. (1985). Flaviviridae. Intervirology *24*, 183–192. https://doi.org/10.1159/000149642.

12. van der Schaar, H.M., Rust, M.J., Chen, C., van der Ende-Metselaar, H., Wilschut, J., Zhuang, X., and Smit, J.M. (2008). Dissecting the cell entry pathway of dengue

virus by single-particle tracking in living cells. PLoS Pathog. *4*, e1000244. https://doi.org/10.1371/journal.ppat.1000244.

13. Chu, J.J.H., and Ng, M.L. (2004). Infectious entry of West Nile virus occurs through a clathrin-mediated endocytic pathway. J. Virol. *78*, 10543–10555. https://doi.org/10.1128/JVI.78.19.10543-10555.2004.

14. Anwar, M.N., Akhtar, R., Abid, M., Khan, S.A., Rehman, Z.U., Tayyub, M., Malik, M.I., Shahzad, M.K., Mubeen, H., Qadir, M.S., et al. (2022). The interactions of flaviviruses with cellular receptors: Implications for virus entry. Virology *568*, 77–85. https://doi.org/10.1016/j.virol.2022.02.001.

15. Echavarria-Consuegra, L., Smit, J.M., and Reggiori, F. (2019). Role of autophagy during the replication and pathogenesis of common mosquito-borne flavi- and alphaviruses. Open Biol. *9*, 190009. https://doi.org/10.1098/rsob.190009.

16. Jones, C.T., Ma, L., Burgner, J.W., Groesch, T.D., Post, C.B., and Kuhn, R.J. (2003). Flavivirus capsid is a dimeric alpha-helical protein. J. Virol. *77*, 7143–7149. https://doi.org/10.1128/jvi.77.12.7143-7149.2003.

17. Zhang, X., Zhang, Y., Jia, R., Wang, M., Yin, Z., and Cheng, A. (2021). Structure and function of capsid protein in flavivirus infection and its applications in the development of vaccines and therapeutics. Vet. Res. *52*, 98. https://doi.org/10.1186/s13567-021-00966-2.

18. Byk, L.A., and Gamarnik, A.V. (2016). Properties and Functions of the Dengue Virus Capsid Protein. Annu. Rev. Virol. *3*, 263–281. https://doi.org/10.1146/annurev-virology-110615-042334.

19. Rey, F.A., Heinz, F.X., Mandl, C., Kunz, C., and Harrison, S.C. (1995). The envelope glycoprotein from tick-borne encephalitis virus at 2 Å resolution. Nature *375*, 291–298. https://doi.org/10.1038/375291a0.

20. Yu, I.-M., Zhang, W., Holdaway, H.A., Li, L., Kostyuchenko, V.A., Chipman, P.R., Kuhn, R.J., Rossmann, M.G., and Chen, J. (2008). Structure of the Immature Dengue Virus at Low pH Primes Proteolytic Maturation. Science *319*, 1834–1837. https://doi.org/10.1126/science.1153264.

21. Lorenz, I.C., Allison, S.L., Heinz, F.X., and Helenius, A. (2002). Folding and Dimerization of Tick-Borne Encephalitis Virus Envelope Proteins prM and E in the Endoplasmic Reticulum. J. Virol. *76*, 5480–5491. https://doi.org/10.1128/JVI.76.11.5480-5491.2002.

22. Elshuber, S., Allison, S.L., Heinz, F.X., and Mandl, C.W. (2003). Cleavage of protein prM is necessary for infection of BHK-21 cells by tick-borne encephalitis virus FN1. J. Gen. Virol. *84*, 183–191. https://doi.org/10.1099/vir.0.18723-0.

23. Akey, D.L., Brown, W.C., Dutta, S., Konwerski, J., Jose, J., Jurkiw, T.J., DelProposto, J., Ogata, C.M., Skiniotis, G., Kuhn, R.J., et al. (2014). Flavivirus NS1 Structures Reveal Surfaces for Associations with Membranes and the Immune System. Science *343*, 881–885. https://doi.org/10.1126/science.1247749.

24. Płaszczyca, A., Scaturro, P., Neufeldt, C.J., Cortese, M., Cerikan, B., Ferla, S., Brancale, A., Pichlmair, A., and Bartenschlager, R. (2019). A novel interaction between dengue virus nonstructural protein 1 and the NS4A-2K-4B precursor is required for viral RNA replication but not for formation of the membranous replication organelle. PLoS Pathog. *15*, e1007736. https://doi.org/10.1371/journal.ppat.1007736.

25. Xie, X., Gayen, S., Kang, C., Yuan, Z., and Shi, P.-Y. (2013). Membrane Topology and Function of Dengue Virus NS2A Protein. J. Virol. *87*, 4609–4622. https://doi.org/10.1128/JVI.02424-12.

26. Li, H., Clum, S., You, S., Ebner, K.E., and Padmanabhan, R. (1999). The Serine Protease and RNA-Stimulated Nucleoside Triphosphatase and RNA Helicase Functional Domains of Dengue Virus Type 2 NS3 Converge within a Region of 20 Amino Acids. J. Virol. *73*, 3108–3116. https://doi.org/10.1128/JVI.73.4.3108-3116.1999.

27. Zeidler, J.D., Fernandes-Siqueira, L.O., Barbosa, G.M., and Da Poian, A.T. (2017). Non-Canonical Roles of Dengue Virus Non-Structural Proteins. Viruses *9*, 42. https://doi.org/10.3390/v9030042.

28. Swarbrick, C.M.D., Basavannacharya, C., Chan, K.W.K., Chan, S.-A., Singh, D., Wei, N., Phoo, W.W., Luo, D., Lescar, J., and Vasudevan, S.G. (2017). NS3 helicase from dengue virus specifically recognizes viral RNA sequence to ensure optimal replication. Nucleic Acids Res. *45*, 12904–12920. https://doi.org/10.1093/nar/gkx1127.

29. Stern, O., Hung, Y.-F., Valdau, O., Yaffe, Y., Harris, E., Hoffmann, S., Willbold, D., and Sklan, E.H. (2013). An N-Terminal Amphipathic Helix in Dengue Virus Nonstructural Protein 4A Mediates Oligomerization and Is Essential for Replication. J. Virol. *87*, 4080–4085. https://doi.org/10.1128/JVI.01900-12.

30. Naik, N.G., and Wu, H.-N. (2015). Mutation of Putative N-Glycosylation Sites on Dengue Virus NS4B Decreases RNA Replication. J. Virol. *89*, 6746–6760. https://doi.org/10.1128/JVI.00423-15.

31. Umareddy, I., Chao, A., Sampath, A., Gu, F., and Vasudevan, S.G. (2006). Dengue virus NS4B interacts with NS3 and dissociates it from single-stranded RNA. J. Gen. Virol. *87*, 2605–2614. https://doi.org/10.1099/vir.0.81844-0.

32. Lu, G., and Gong, P. (2013). Crystal Structure of the Full-Length Japanese Encephalitis Virus NS5 Reveals a Conserved Methyltransferase-Polymerase Interface. PLoS Pathog. *9*, e1003549. https://doi.org/10.1371/journal.ppat.1003549.

33. Zhou, Y., Ray, D., Zhao, Y., Dong, H., Ren, S., Li, Z., Guo, Y., Bernard, K.A., Shi, P.-Y., and Li, H. (2007). Structure and Function of Flavivirus NS5 Methyltransferase. J. Virol. *81*, 3891–3903. https://doi.org/10.1128/JVI.02704-06.

34. Zhao, Y., Soh, T.S., Zheng, J., Chan, K.W.K., Phoo, W.W., Lee, C.C., Tay, M.Y.F., Swaminathan, K., Cornvik, T.C., Lim, S.P., et al. (2015). A Crystal Structure of the Dengue Virus NS5 Protein Reveals a Novel Inter-domain Interface Essential for Protein Flexibility and Virus Replication. PLOS Pathog. *11*, e1004682. https://doi.org/10.1371/journal.ppat.1004682.

35. Dong, H., Fink, K., Züst, R., Lim, S.P., Qin, C.-F., and Shi, P.-Y. (2014). Flavivirus RNA methylation. J. Gen. Virol. *95*, 763–778. https://doi.org/10.1099/vir.0.062208-0.

36. Gu, M., and Lima, C.D. (2005). Processing the message: structural insights into capping and decapping mRNA. Curr. Opin. Struct. Biol. *15*, 99–106. https://doi.org/10.1016/j.sbi.2005.01.009.

37. Furuichi, Y., and Shatkin, A.J. (2000). Viral and cellular mRNA capping: Past and prospects. In Advances in Virus Research (Elsevier), pp. 135–184. https://doi.org/10.1016/S0065-3527(00)55003-9.

38. Brecher, M.B., Li, Z., Zhang, J., Chen, H., Lin, Q., Liu, B., and Li, H. (2015). Refolding of a fully functional flavivirus methyltransferase revealed that S-adenosyl methionine but not S-adenosyl homocysteine is copurified with flavivirus methyltransferase. Protein Sci. *24*, 117–128. https://doi.org/10.1002/pro.2594.

39. Assenberg, R., Ren, J., Verma, A., Walter, T.S., Alderton, D., Hurrelbrink, R.J., Fuller, S.D., Bressanelli, S., Owens, R.J., Stuart, D.I., et al. (2007). Crystal structure of the Murray Valley encephalitis virus NS5 methyltransferase domain in complex with cap analogues. J. Gen. Virol. *88*, 2228–2236. https://doi.org/10.1099/vir.0.82757-0.

40. Geiss, B.J., Thompson, A.A., Andrews, A.J., Sons, R.L., Gari, H.H., Keenan, S.M., and Peersen, O.B. (2009). Analysis of Flavivirus NS5 Methyltransferase Cap Binding. J. Mol. Biol. *385*, 1643–1654. https://doi.org/10.1016/j.jmb.2008.11.058.

41. Duan, W., Song, H., Wang, H., Chai, Y., Su, C., Qi, J., Shi, Y., and Gao, G.F. (2017). The crystal structure of Zika virus NS 5 reveals conserved drug targets. EMBO J. *36*, 919–933. https://doi.org/10.15252/embj.201696241.

42. Jia, H., Zhong, Y., Peng, C., and Gong, P. (2022). Crystal Structures of Flavivirus NS5 Guanylyltransferase Reveal a GMP-Arginine Adduct. J. Virol. *96*, e00418-22. https://doi.org/10.1128/jvi.00418-22.

43. Ray, D., Shah, A., Tilgner, M., Guo, Y., Zhao, Y., Dong, H., Deas, T.S., Zhou, Y., Li, H., and Shi, P.-Y. (2006). West Nile Virus 5′-Cap Structure Is Formed by Sequential Guanine N-7 and Ribose 2′-O Methylations by Nonstructural Protein 5. J. Virol. *80*, 8362–8370. https://doi.org/10.1128/JVI.00814-06.

44. Choi, K.H., and Rossmann, M.G. (2009). RNA-dependent RNA polymerases from Flaviviridae. Curr. Opin. Struct. Biol. *19*, 746–751. https://doi.org/10.1016/j.sbi.2009.10.015.

45. Surana, P., Satchidanandam, V., and Nair, D.T. (2014). RNA-dependent RNA polymerase of Japanese encephalitis virus binds the initiator nucleotide GTP to form a mechanistically important pre-initiation state. Nucleic Acids Res. *42*, 2758–2773. https://doi.org/10.1093/nar/gkt1106.

46. Noble, C.G., Lim, S.P., Chen, Y.-L., Liew, C.W., Yap, L., Lescar, J., and Shi, P.-Y. (2013). Conformational Flexibility of the Dengue Virus RNA-Dependent RNA Polymerase Revealed by a Complex with an Inhibitor. J. Virol. *87*, 5291–5295. https://doi.org/10.1128/JVI.00045-13.

47. Dubankova, A., and Boura, E. (2019). Structure of the yellow fever NS5 protein reveals conserved drug targets shared among flaviviruses. Antiviral Res. *169*, 104536. https://doi.org/10.1016/j.antiviral.2019.104536.

48. Godoy, A.S., Lima, G.M.A., Oliveira, K.I.Z., Torres, N.U., Maluf, F.V., Guido, R.V.C., and Oliva, G. (2017). Crystal structure of Zika virus NS5 RNA-dependent RNA polymerase. Nat. Commun. *8*, 14764. https://doi.org/10.1038/ncomms14764.

49. Shu, B., and Gong, P. (2017). The uncoupling of catalysis and translocation in the viral RNA-dependent RNA polymerase. RNA Biol. *14*, 1314–1319. https://doi.org/10.1080/15476286.2017.1300221.

50. Yang, X., Smidansky, E.D., Maksimchuk, K.R., Lum, D., Welch, J.L., Arnold, J.J., Cameron, C.E., and Boehr, D.D. (2012). Motif D of Viral RNA-Dependent RNA Polymerases Determines Efficiency and Fidelity of Nucleotide Addition. Structure *20*, 1519–1527. https://doi.org/10.1016/j.str.2012.06.012.

51. Potapova, U., Feranchuk, S., Leonova, G., and Belikov, S. (2018). The rearrangement of motif F in the flavivirus RNA-directed RNA polymerase. Int. J. Biol. Macromol. *108*, 990–998. https://doi.org/10.1016/j.ijbiomac.2017.11.009.

52. Coronaviridae Study Group of the International Committee on Taxonomy of Viruses, Gorbalenya, A.E., Baker, S.C., Baric, R.S., De Groot, R.J., Drosten, C., Gulyaeva, A.A., Haagmans, B.L., Lauber, C., Leontovich, A.M., et al. (2020). The species Severe acute respiratory syndrome-related coronavirus: classifying 2019-nCoV and naming it SARS-CoV-2. Nat. Microbiol. *5*, 536–544. https://doi.org/10.1038/s41564-020-0695-z.

53. Corman, V.M., Muth, D., Niemeyer, D., and Drosten, C. (2018). Hosts and Sources of Endemic Human Coronaviruses. In Advances in Virus Research (Elsevier), pp. 163–188. https://doi.org/10.1016/bs.aivir.2018.01.001.

54. Perlman, S., and Netland, J. (2009). Coronaviruses post-SARS: update on replication and pathogenesis. Nat. Rev. Microbiol. *7*, 439–450. https://doi.org/10.1038/nrmicro2147.

55. Stertz, S., Reichelt, M., Spiegel, M., Kuri, T., Martínez-Sobrido, L., García-Sastre, A., Weber, F., and Kochs, G. (2007). The intracellular sites of early replication and budding of SARS-coronavirus. Virology *361*, 304–315. https://doi.org/10.1016/j.virol.2006.11.027.

56. Hamre, D., and Procknow, J.J. (1966). A New Virus Isolated from the Human Respiratory Tract. Exp. Biol. Med. *121*, 190–193. https://doi.org/10.3181/00379727-121-30734.

57. Lee, N., Hui, D., Wu, A., Chan, P., Cameron, P., Joynt, G.M., Ahuja, A., Yung, M.Y., Leung, C.B., To, K.F., et al. (2003). A Major Outbreak of Severe Acute Respiratory Syndrome in Hong Kong. N. Engl. J. Med. *348*, 1986–1994. https://doi.org/10.1056/NEJMoa030685.

58. Ge, X., Hu, B., and Shi, Z. (2015). Bat Coronaviruses. In Bats and Viruses, L. Wang and C. Cowled, eds. (Wiley), pp. 127–155. https://doi.org/10.1002/9781118818824.ch5.

59. Zhu, N., Zhang, D., Wang, W., Li, X., Yang, B., Song, J., Zhao, X., Huang, B., Shi, W., Lu, R., et al. (2020). A Novel Coronavirus from Patients with Pneumonia in China, 2019. N. Engl. J. Med. *382*, 727–733. https://doi.org/10.1056/NEJMoa2001017.

60. Kirtipal, N., Bharadwaj, S., and Kang, S.G. (2020). From SARS to SARS-CoV-2, insights on structure, pathogenicity and immunity aspects of pandemic human coronaviruses. Infect. Genet. Evol. *85*, 104502. https://doi.org/10.1016/j.meegid.2020.104502.

61. Cascella, M., Rajnik, M., Aleem, A., Dulebohn, S.C., and Di Napoli, R. (2024). Features, Evaluation, and Treatment of Coronavirus (COVID-19). In StatPearls (StatPearls Publishing).

62. Wu, F., Zhao, S., Yu, B., Chen, Y.-M., Wang, W., Song, Z.-G., Hu, Y., Tao, Z.-W., Tian, J.-H., Pei, Y.-Y., et al. (2020). A new coronavirus associated with human respiratory disease in China. Nature *579*, 265–269. https://doi.org/10.1038/s41586-020-2008-3.

63. Jackson, C.B., Farzan, M., Chen, B., and Choe, H. (2022). Mechanisms of SARS-CoV-2 entry into cells. Nat. Rev. Mol. Cell Biol. *23*, 3–20. https://doi.org/10.1038/s41580-021-00418-x.

64. V'kovski, P., Kratzel, A., Steiner, S., Stalder, H., and Thiel, V. (2021). Coronavirus biology and replication: implications for SARS-CoV-2. Nat. Rev. Microbiol. *19*, 155–170. https://doi.org/10.1038/s41579-020-00468-6.

65. Beniac, D.R., Andonov, A., Grudeski, E., and Booth, T.F. (2006). Architecture of the SARS coronavirus prefusion spike. Nat. Struct. Mol. Biol. *13*, 751–752. https://doi.org/10.1038/nsmb1123.

66. Neuman, B.W., Kiss, G., Kunding, A.H., Bhella, D., Baksh, M.F., Connelly, S., Droese, B., Klaus, J.P., Makino, S., Sawicki, S.G., et al. (2011). A structural analysis of M protein in coronavirus assembly and morphology. J. Struct. Biol. *174*, 11–22. https://doi.org/10.1016/j.jsb.2010.11.021.

67. Hurst, K.R., Koetzner, C.A., and Masters, P.S. (2009). Identification of In Vivo-Interacting Domains of the Murine Coronavirus Nucleocapsid Protein. J. Virol. *83*, 7221–7234. https://doi.org/10.1128/JVI.00440-09.

68. Klausegger, A., Strobl, B., Regl, G., Kaser, A., Luytjes, W., and Vlasak, R. (1999). Identification of a Coronavirus Hemagglutinin-Esterase with a Substrate Specificity Different from Those of Influenza C Virus and Bovine Coronavirus. J. Virol. *73*, 3737–3743. https://doi.org/10.1128/JVI.73.5.3737-3743.1999.

69. Afsar, M., Narayan, R., Akhtar, M.N., Das, D., Rahil, H., Nagaraj, S.K., Eswarappa, S.M., Tripathi, S., and Hussain, T. (2022). Drug targeting Nsp1-ribosomal complex shows antiviral activity against SARS-CoV-2. eLife *11*, e74877. https://doi.org/10.7554/eLife.74877.

70. Snijder, E.J., Decroly, E., and Ziebuhr, J. (2016). The Nonstructural Proteins Directing Coronavirus RNA Synthesis and Processing. In Advances in Virus Research (Elsevier), pp. 59–126. https://doi.org/10.1016/bs.aivir.2016.08.008.

71. Shin, D., Mukherjee, R., Grewe, D., Bojkova, D., Baek, K., Bhattacharya, A., Schulz, L., Widera, M., Mehdipour, A.R., Tascher, G., et al. (2020). Papain-like protease regulates SARS-CoV-2 viral spread and innate immunity. Nature *587*, 657–662. https://doi.org/10.1038/s41586-020-2601-5.

72. Angelini, M.M., Akhlaghpour, M., Neuman, B.W., and Buchmeier, M.J. (2013). Severe Acute Respiratory Syndrome Coronavirus Nonstructural Proteins 3, 4, and 6 Induce Double-Membrane Vesicles. mBio *4*, e00524-13. https://doi.org/10.1128/mBio.00524-13.

73. Roe, M.K., Junod, N.A., Young, A.R., Beachboard, D.C., and Stobart, C.C. (2021). Targeting novel structural and functional features of coronavirus protease nsp5 (3CLpro, Mpro) in the age of COVID-19. J. Gen. Virol. *102*. https://doi.org/10.1099/jgv.0.001558.

74. Te Velthuis, A.J.W., Van Den Worm, S.H.E., and Snijder, E.J. (2012). The SARS-coronavirus nsp7+nsp8 complex is a unique multimeric RNA polymerase capable of both de novo initiation and primer extension. Nucleic Acids Res. *40*, 1737–1747. https://doi.org/10.1093/nar/gkr893.

75. Chandel, V., Sharma, P.P., Raj, S., Choudhari, R., Rathi, B., and Kumar, D. (2022). Structure-based drug repurposing for targeting Nsp9 replicase and spike proteins of severe acute respiratory syndrome coronavirus 2. J. Biomol. Struct. Dyn. *40*, 249–262. https://doi.org/10.1080/07391102.2020.1811773.

76. Decroly, E., Debarnot, C., Ferron, F., Bouvet, M., Coutard, B., Imbert, I., Gluais, L., Papageorgiou, N., Sharff, A., Bricogne, G., et al. (2011). Crystal Structure and Functional Analysis of the SARS-Coronavirus RNA Cap 2′-O-Methyltransferase nsp10/nsp16 Complex. PLoS Pathog. *7*, e1002059. https://doi.org/10.1371/journal.ppat.1002059.

77. Gadhave, K., Kumar, P., Kumar, A., Bhardwaj, T., Garg, N., and Giri, R. (2021). Conformational dynamics of 13 amino acids long NSP11 of SARS-CoV-2 under membrane mimetics and different solvent conditions. Microb. Pathog. *158*, 105041. https://doi.org/10.1016/j.micpath.2021.105041.

78. Peng, Q., Peng, R., Yuan, B., Zhao, J., Wang, M., Wang, X., Wang, Q., Sun, Y., Fan, Z., Qi, J., et al. (2020). Structural and Biochemical Characterization of the nsp12-nsp7-nsp8 Core Polymerase Complex from SARS-CoV-2. Cell Rep. *31*, 107774. https://doi.org/10.1016/j.celrep.2020.107774.

79. Bouvet, M., Imbert, I., Subissi, L., Gluais, L., Canard, B., and Decroly, E. (2012). RNA 3'-end mismatch excision by the severe acute respiratory syndrome coronavirus nonstructural protein nsp10/nsp14 exoribonuclease complex. Proc. Natl. Acad. Sci. *109*, 9372–9377. https://doi.org/10.1073/pnas.1201130109.

80. Ivanov, K.A., and Ziebuhr, J. (2004). Human Coronavirus 229E Nonstructural Protein 13: Characterization of Duplex-Unwinding, Nucleoside Triphosphatase, and RNA 5′-Triphosphatase Activities. J. Virol. *78*, 7833–7838. https://doi.org/10.1128/JVI.78.14.7833-7838.2004.

81. Ahmed-Belkacem, R., Sutto-Ortiz, P., Guiraud, M., Canard, B., Vasseur, J.-J., Decroly, E., and Debart, F. (2020). Synthesis of adenine dinucleosides SAM analogs as specific inhibitors of SARS-CoV nsp14 RNA cap guanine-N7-methyltransferase. Eur. J. Med. Chem. *201*, 112557. https://doi.org/10.1016/j.ejmech.2020.112557.

82. Hong, S., Seo, S.H., Woo, S.-J., Kwon, Y., Song, M., and Ha, N.-C. (2021). Epigallocatechin Gallate Inhibits the Uridylate-Specific Endoribonuclease Nsp15 and Efficiently Neutralizes the SARS-CoV-2 Strain. J. Agric. Food Chem. *69*, 5948–5954. https://doi.org/10.1021/acs.jafc.1c02050.

83. Tazikeh-Lemeski, E., Moradi, S., Raoufi, R., Shahlaei, M., Janlou, M.A.M., and Zolghadri, S. (2021). Targeting SARS-COV-2 non-structural protein 16: a virtual drug repurposing study. J. Biomol. Struct. Dyn. *39*, 4633–4646. https://doi.org/10.1080/07391102.2020.1779133.

84. Sawicki, S.G., and Sawicki, D.L. (1995). Coronaviruses use Discontinuous Extension for Synthesis of Subgenome-Length Negative Strands. In Corona- and Related Viruses Advances in Experimental Medicine and Biology., P. J. Talbot and G. A. Levy, eds. (Springer US), pp. 499–506. https://doi.org/10.1007/978-1-4615-1899-0_79.

85. Sola, I., Almazán, F., Zúñiga, S., and Enjuanes, L. (2015). Continuous and Discontinuous RNA Synthesis in Coronaviruses. Annu. Rev. Virol. *2*, 265–288. https://doi.org/10.1146/annurev-virology-100114-055218.

86. De Clercq, E. (2011). A 40-Year Journey in Search of Selective Antiviral Chemotherapy*. Annu. Rev. Pharmacol. Toxicol. *51*, 1–24. https://doi.org/10.1146/annurev-pharmtox-010510-100228.

87. Jordheim, L.P., Durantel, D., Zoulim, F., and Dumontet, C. (2013). Advances in the development of nucleoside and nucleotide analogues for cancer and viral diseases. Nat. Rev. Drug Discov. *12*, 447–464. https://doi.org/10.1038/nrd4010.

88. Eyer, L., Nencka, R., De Clercq, E., Seley-Radtke, K., and Růžek, D. (2018). Nucleoside analogs as a rich source of antiviral agents active against arthropod-borne flaviviruses. Antivir. Chem. Chemother. *26*, 204020661876129. https://doi.org/10.1177/2040206618761299.

89. Gordon, C.J., Tchesnokov, E.P., Woolner, E., Perry, J.K., Feng, J.Y., Porter, D.P., and Götte, M. (2020). Remdesivir is a direct-acting antiviral that inhibits RNA-dependent RNA polymerase from severe acute respiratory syndrome coronavirus 2 with high potency. J. Biol. Chem. *295*, 6785–6797. https://doi.org/10.1074/jbc.RA120.013679.

90. Rubin, D., Chan-Tack, K., Farley, J., and Sherwat, A. (2020). FDA Approval of Remdesivir — A Step in the Right Direction. N. Engl. J. Med. *383*, 2598–2600. https://doi.org/10.1056/NEJMp2032369.

91. Fischer, W., Eron, J.J., Holman, W., Cohen, M.S., Fang, L., Szewczyk, L.J., Sheahan, T.P., Baric, R., Mollan, K.R., Wolfe, C.R., et al. (2021). Molnupiravir, an Oral Antiviral Treatment for COVID-19. Preprint, https://doi.org/10.1101/2021.06.17.21258639 https://doi.org/10.1101/2021.06.17.21258639.

92. Owen, D.R., Allerton, C.M.N., Anderson, A.S., Aschenbrenner, L., Avery, M., Berritt, S., Boras, B., Cardin, R.D., Carlo, A., Coffman, K.J., et al. (2021). An oral SARS-CoV-2 M^{pro} inhibitor clinical candidate for the treatment of COVID-19. Science *374*, 1586–1593. https://doi.org/10.1126/science.abl4784.

93. Hercik, K., Brynda, J., Nencka, R., and Boura, E. (2017). Structural basis of Zika virus methyltransferase inhibition by sinefungin. Arch. Virol. *162*, 2091–2096. https://doi.org/10.1007/s00705-017-3345-x.

94. Lowe, R., Barcellos, C., Brasil, P., Cruz, O.G., Honório, N.A., Kuper, H., and Carvalho, M.S. (2018). The Zika Virus Epidemic in Brazil: From Discovery to Future Implications. Int. J. Environ. Res. Public. Health *15*, 96. https://doi.org/10.3390/ijerph15010096.

95. Malet, H., Egloff, M.-P., Selisko, B., Butcher, R.E., Wright, P.J., Roberts, M., Gruez, A., Sulzenbacher, G., Vonrhein, C., Bricogne, G., et al. (2007). Crystal Structure of the RNA Polymerase Domain of the West Nile Virus Non-structural Protein 5. J. Biol. Chem. *282*, 10678–10689. https://doi.org/10.1074/jbc.M607273200.

96. Noble, C.G., Lim, S.P., Arora, R., Yokokawa, F., Nilar, S., Seh, C.C., Wright, S.K., Benson, T.E., Smith, P.W., and Shi, P.-Y. (2016). A Conserved Pocket in the Dengue Virus Polymerase Identified through Fragment-based Screening. J. Biol. Chem. *291*, 8541–8548. https://doi.org/10.1074/jbc.M115.710731.

97. Dong, H., Zhang, B., and Shi, P.-Y. (2008). Flavivirus methyltransferase: a novel antiviral target. Antiviral Res. *80*, 1–10. https://doi.org/10.1016/j.antiviral.2008.05.003.

98. Good, S.S., Shannon, A., Lin, K., Moussa, A., Julander, J.G., La Colla, P., Collu, G., Canard, B., and Sommadossi, J.-P. (2021). Evaluation of AT-752, a Double Prodrug of a Guanosine Nucleotide Analog with In Vitro and In Vivo Activity against Dengue and Other Flaviviruses. Antimicrob. Agents Chemother. *65*, e0098821. https://doi.org/10.1128/AAC.00988-21.

99. Feracci, M., Eydoux, C., Fattorini, V., Lo Bello, L., Gauffre, P., Selisko, B., Sutto-Ortiz, P., Shannon, A., Xia, H., Shi, P.-Y., et al. (2023). AT-752 targets multiple sites and activities on the Dengue virus replication enzyme NS5. Antiviral Res. *212*, 105574. https://doi.org/10.1016/j.antiviral.2023.105574.

100. de Wit, E., van Doremalen, N., Falzarano, D., and Munster, V.J. (2016). SARS and MERS: recent insights into emerging coronaviruses. Nat. Rev. Microbiol. *14*, 523–534. https://doi.org/10.1038/nrmicro.2016.81.

101. Paixão, E.S., Barreto, F., Teixeira, M. da G., Costa, M. da C.N., and Rodrigues, L.C. (2016). History, Epidemiology, and Clinical Manifestations of Zika: A Systematic Review. Am. J. Public Health *106*, 606–612. https://doi.org/10.2105/AJPH.2016.303112.

102. Vicenti, I., Zazzi, M., and Saladini, F. (2021). SARS-CoV-2 RNA-dependent RNA polymerase as a therapeutic target for COVID-19. Expert Opin. Ther. Pat. *31*, 325–337. https://doi.org/10.1080/13543776.2021.1880568.

103. Tarantino, D., Cannalire, R., Mastrangelo, E., Croci, R., Querat, G., Barreca, M.L., Bolognesi, M., Manfroni, G., Cecchetti, V., and Milani, M. (2016). Targeting flavivirus RNA dependent RNA polymerase through a pyridobenzothiazole inhibitor. Antiviral Res. *134*, 226–235. https://doi.org/10.1016/j.antiviral.2016.09.007.

104. Konkolova, E., Dejmek, M., Hřebabecký, H., Šála, M., Böserle, J., Nencka, R., and Boura, E. (2020). Remdesivir triphosphate can efficiently inhibit the RNA-dependent RNA polymerase from various flaviviruses. Antiviral Res. *182*, 104899. https://doi.org/10.1016/j.antiviral.2020.104899.

105. Konkolova, E., Krejčová, K., Eyer, L., Hodek, J., Zgarbová, M., Fořtová, A., Jirasek, M., Teply, F., Reyes-Gutierrez, P.E., Růžek, D., et al. (2022). A Helquat-like Compound as a Potent Inhibitor of Flaviviral and Coronaviral Polymerases. Mol. Basel Switz. *27*, 1894. https://doi.org/10.3390/molecules27061894.

106. Milisavljevic, N., Konkolová, E., Kozák, J., Hodek, J., Veselovská, L., Sýkorová, V., Čížek, K., Pohl, R., Eyer, L., Svoboda, P., et al. (2021). Antiviral Activity of 7-Substituted 7-Deazapurine Ribonucleosides, Monophosphate Prodrugs, and Triphoshates against Emerging RNA Viruses. ACS Infect. Dis. *7*, 471–478. https://doi.org/10.1021/acsinfecdis.0c00829.

107. Asselah, T., Durantel, D., Pasmant, E., Lau, G., and Schinazi, R.F. (2021). COVID-19: Discovery, diagnostics and drug development. J. Hepatol. *74*, 168–184. https://doi.org/10.1016/j.jhep.2020.09.031.

108. Dejmek, M., Konkoľová, E., Eyer, L., Straková, P., Svoboda, P., Šála, M., Krejčová, K., Růžek, D., Boura, E., and Nencka, R. (2021). Non-Nucleotide RNA-Dependent RNA Polymerase Inhibitor That Blocks SARS-CoV-2 Replication. Viruses *13*, 1585. https://doi.org/10.3390/v13081585.

109. Newman, J.A., Douangamath, A., Yadzani, S., Yosaatmadja, Y., Aimon, A., Brandão-Neto, J., Dunnett, L., Gorrie-stone, T., Skyner, R., Fearon, D., et al. (2021). Structure, mechanism and crystallographic fragment screening of the SARS-CoV-2 NSP13 helicase. Nat. Commun. *12*, 4848. https://doi.org/10.1038/s41467-021-25166-6.

110. Otava, T., Šála, M., Li, F., Fanfrlík, J., Devkota, K., Perveen, S., Chau, I., Pakarian, P., Hobza, P., Vedadi, M., et al. (2021). The Structure-Based Design of SARS-CoV-2 nsp14 Methyltransferase Ligands Yields Nanomolar Inhibitors. ACS Infect. Dis. *7*, 2214–2220. https://doi.org/10.1021/acsinfecdis.1c00131.

111. Perveen, S., Khalili Yazdi, A., Devkota, K., Li, F., Ghiabi, P., Hajian, T., Loppnau, P., Bolotokova, A., and Vedadi, M. (2021). A High-Throughput RNA Displacement Assay for Screening SARS-CoV-2 nsp10-nsp16 Complex toward Developing Therapeutics for COVID-19. SLAS Discov. *26*, 620–627. https://doi.org/10.1177/2472555220985040.

112. Pedersen, O.S., and Pedersen, E.B. (1999). Non-Nucleoside Reverse Transcriptase Inhibitors: The NNRTI Boom. Antivir. Chem. Chemother. *10*, 285–314. https://doi.org/10.1177/095632029901000601.

113. Wang, L.-C., Chen, E.-Q., Cao, J., Liu, L., Wang, J.-R., Lei, B.-J., and Tang, H. (2010). Combination of Lamivudine and adefovir therapy in HBeAg-positive chronic hepatitis B patients with poor response to adefovir monotherapy. J. Viral Hepat. *17*, 178–184. https://doi.org/10.1111/j.1365-2893.2009.01164.x.

9 PŘÍLOHY

Article

Structure

Structural and functional insights in flavivirus NS5 proteins gained by the structure of Ntaya virus polymerase and methyltransferase

Graphical abstract

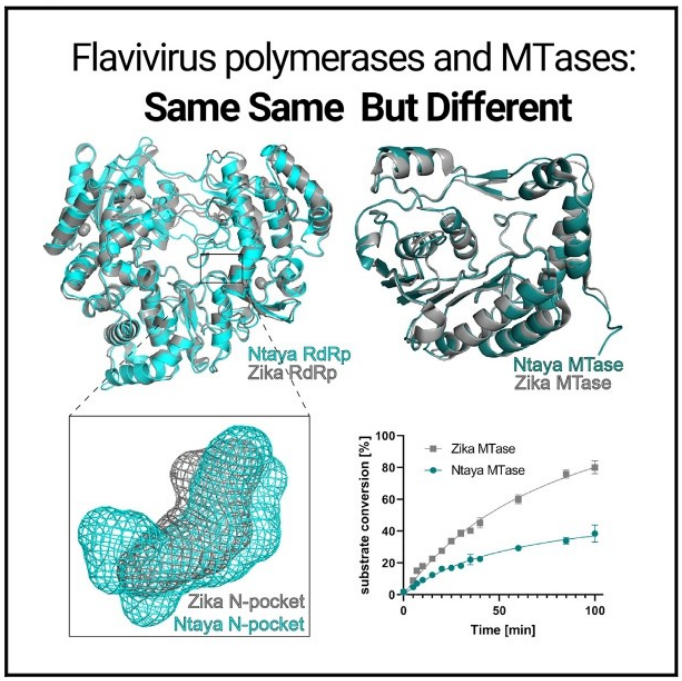

Authors

Kateřina Krejčová, Petra Krafcikova, Martin Klima, Dominika Chalupska, Karel Chalupsky, Eva Zilecka, Evzen Boura

Correspondence

boura@uochb.cas.cz

In brief

Krejcova et al. solved the crystal structure of the polymerase and methyltransferase of the Ntaya virus, an emerging flavivirus, revealing significant differences from other flaviviruses, such as the polymerase N pocket's shape and size and varied enzymatic activities of methyltransferases within flaviviruses.

Highlights

- Structural conservation of the enzymatic centers of flaviviral RdRps and MTases
- Different enzymatic activities of MTase domains from medically important flaviviruses
- Different sizes and shapes of the N-pockets of flaviviral RdRps
- Different conformations of the priming loops of the RdRps

Krejčová et al., 2024, Structure *32*, 1099–1109
August 8, 2024
https://doi.org/10.1016/j.str.2024.04.020

CellPress

Structure

CellPress
OPEN ACCESS

Article

Structural and functional insights in flavivirus NS5 proteins gained by the structure of Ntaya virus polymerase and methyltransferase

Kateřina Krejčová,[1,2] Petra Krafcikova,[1] Martin Klima,[1] Dominika Chalupska,[1] Karel Chalupsky,[1] Eva Zilecka,[1] and Evzen Boura[1,3,*]

[1]Institute of Organic Chemistry and Biochemistry, Academy of Sciences of the Czech Republic, v.v.i, Flemingovo nám. 2, 166 10 Prague 6, Czech Republic

[2]Faculty of Sciences, Charles University, Albertov 6, 128 00 Prague 2, Czech Republic

[3]Lead contact

*Correspondence: boura@uochb.cas.cz

https://doi.org/10.1016/j.str.2024.04.020

SUMMARY

Flaviviruses are single-stranded positive-sense RNA (+RNA) viruses that are responsible for several (re) emerging diseases such as yellow, dengue, or West Nile fevers. The Zika epidemic highlighted their dangerousness when a relatively benign virus known since the 1950s turned into a deadly pathogen. The central protein for their replication is NS5 (non-structural protein 5), which is composed of the N-terminal methyltransferase (MTase) domain and the C-terminal RNA-dependent RNA-polymerase (RdRp) domain. It is responsible for both RNA replication and installation of the 5′ RNA cap. We structurally and biochemically analyzed the Ntaya virus MTase and RdRp domains and we compared their properties to other flaviviral NS5s. The enzymatic centers are well conserved across *Flaviviridae*, suggesting that the development of drugs targeting all flaviviruses is feasible. However, the enzymatic activities of the isolated proteins were significantly different for the MTase domains.

INTRODUCTION

Single-stranded positive-sense RNA (+RNA) viruses are responsible for most of the recent virus outbreaks, local epidemics, and most importantly, the COVID-19 pandemic. *Flaviviridae* are one of the +RNA virus families that contain relatively benign or animal pathogens as well as dangerous human pathogens. This family consists of four genera: flavivirus, hepacivirus, pegivirus, and pestivirus.[1] Flaviviruses contain most human pathogens within this family. Yellow fever, caused by the yellow fever virus (YFV) was considered the worst disease of the 19th century and was only contained after a vaccine was developed in the 1930s[2] Recently, we have witnessed outbreaks of other flaviviruses, most importantly the mosquito-borne West Nile virus (WNV),[3] dengue virus (DENV),[4] and Zika virus (ZIKV)[5] in the Americas and the tick-borne encephalitis virus (TBEV) in Europe and Asia.[6,7]

Ntaya virus (NTAV) was first isolated from mosquitos in Uganda in 1951.[8] However, the exact mosquito species that serves as a vector is unknown although the genus *Culex* is the most probable.[9] Together with several other flaviviruses, it comprises the Ntaya virus group, which used to have four other viral species besides NTAV: Bagaza virus (BAGV), Israel turkey meningoencephalitis virus (ITV), Ilheus virus (ILHV), and Tembusu virus (TMUV).[10] However, recently it was shown that BAGV and ITV are actually the same virus.[11] Antibodies against Ntaya virus have been discovered in a variety of migratory birds[12] and domestic mammals, such as sheep, cattle, goats, and pigs.[13] In birds, the virus is neurotropic and causes hemorrhages in the brain and other organs.[14] Antibodies against Ntaya virus have also been discovered in humans from West, Central, and East African regions and the virus is suspected to cause an illness that manifests itself with fever and headache.[15]

Ntaya virus and other flaviviruses encode several non-structural proteins (NS1, NS2A, NS2B, NS3, NS4A, NS4B, and NS5) that ensure their replication in infected cells.[16] Some of them are enzymes; for example, NS2B-NS3 is a protease, NS3 functions also as a helicase, and the NS5 protein bears the most crutial enzymatic activity for an RNA virus—the RNA-dependent RNA-polymerase (RdRp). In addition, the NS5 protein has an N-terminal methyltransferase (MTase) domain that is responsible for RNA cap formation, a process necessary for efficient viral RNA (vRNA) translation and immune evasion.[17,18] There are more than 50 species within the genus flavivirus, of which more than 40 are human pathogens.[19,20] However, only a handful of crystal structures of the RdRp domain are available from the most medically important flaviviruses including Zika, dengue, West Nile, Japanese encephalitis, and yellow fever viruses.[21–25] The structure of the first flavivirus RdRp (dengue) complexed with RNA was recently solved using cryoelectron microscopy

(cryo-EM),[26] whereas a crystal structure of the related hepacivirus HCV RdRp in complex with RNA has been available for almost a decade.[27] The MTase domains are more explored, and crystal structures of MTases from less-known flavivirus such as the Langat or Usutu viruses are available.[28,29] We aimed to better understand the NS5 protein function. We chose the Ntaya virus NS5 protein for analysis and solved the crystal structures of the RdRp and MTase domains. We also performed a structural and functional comparison of flaviviral RdRps and MTases, which revealed their common features and surprising differences in the enzymatic activities of the MTase domains.

RESULTS

Crystal structure of Ntaya RdRp

We aimed to solve the crystal structure of the Ntaya polymerase to gain more insights into the replication of flaviviruses. Eventually we obtained crystals that belonged to the monoclinic $P2_1$ space group and diffracted to 2.8 Å resolution. The structure was solved by molecular replacement and revealed a fold resembling a cupped human right hand with fingers, palm, and thumb, which is typical for viral polymerases (Figure 1). It is a predominantly α-helical fold composed of twenty-seven helices (helices α10–α36 and helices α1–α9 of the NS5 protein are located in the N-terminal MTase domain) with five small β-sheets. Interestingly, all eleven β-strands (β10–β20) forming these β-sheets are oriented in an antiparallel manner (Figure 1D). The flaviviral RdRp domain also contains two zinc fingers that are important for the overall fold stability;[25] one is located in the vicinity of helices α10, α14, α16, and α22 and is formed by two cysteine residues (Cys449 and Cys452), one histidine (His444), and one glutamate (Glu440) residues ($Cys_2HisGlu$, Figure 1C). This is somewhat different from the canonical Cys_2His_2 zinc finger that is widespread in DNA binding motifs.[30] However, Glu440 is absolutely conserved among flaviviral RdRps (Figure S1). The second zinc finger is localized above the β18–β19 sheet and between helices α33 and α35 and it is formed by cysteine residues Cys733 and Cys852 and histidine residues His717 and His719 (Cys_2His_2-type, Figure 1C). The conserved motifs A–G that bear most of the catalytically important residues are arranged along the template entry channel (F and G), the active site (A, B, D, and E), and the dsRNA exit channel (C), as expected based on their conserved functions: (1) template binding (B and C), (2) incoming nucleotide binding and its stabilization in a proper conformation (E, F, and G), (3) priming (D), and (4) the formation of the phosphodiester bond (A).

The overall fold of the Ntaya RdRp domain is in good agreement with previously described flaviviral RdRps (Figures 2A and S2). The most similar seems to be the RdRp from the Zika virus (RMSD of superposed structures = 0.866, ΔD_{max} = 1.27 Å) while the most different one (RMSD of superposed structures = 1.708, ΔD_{max} = 3.43 Å) was the one from the West Nile virus (Figure 2A). Most of the structural differences are in the conformations of loops, among them the priming loop is the most important for the enzymatic function—flaviviral RdRps belong to the primer-independent polymerases. The closed conformation of flaviviral RdRp allows only for the entry of ssRNA and the initiation of RNA synthesis is by the *de novo* mechanism where the priming loop partially fulfills the function of the primer. We examined the conformation of the Ntaya priming loop in detail and compared it to ZIKV and WNV priming loops (Figures 2B and 2C). While the beginning and end of these priming loops (Trp792 and Glu812) are always in the same conformation, the rest significantly differs. The ZIKV priming loop is virtually in the same conformation as that of Ntaya, with the only difference being a different rotamer of Trp800, a residue important for the stabilization of the initiation complex.[31] In contrast, in the case of WNV, Trp800 is displaced. Actually, the overall conformation of WNV priming loop is different; another significantly displaced residue is the His803 residue (Figure 2C), which could play a role in stabilizing the initiation complex via a stacking interaction with the base of a priming NTP.[31] Interestingly, the position of Trp808 is absolutely conserved among all analyzed flaviviral polymerases (Figures 2 and S2) suggesting that this residue is important for the function of the priming loop.

Recently a novel, druggable pocket was discovered within the flavivirus RdRp in the vicinity of its active site located at the interface of the thumb and palm subdomains and was termed the N pocket.[32–34] Importantly, it was shown, using the dengue virus, that compounds targeting the N pocket are effective inhibitors of dengue virus replication, and based on conservation of several residues in WNV and JEV, it was suggested that this pocket could be utilized to target multiple flaviviruses.[32,33]

We compared the N pockets of Ntaya RdRp against those of Zika and dengue (Figures 2D–2H). We employed the tool CavitOmiX (Innophore GmbH) to visualize and measure these N pockets. Remarkably, we observed significant variations in both the overall volume and the shape of these pockets. The N pocket of Ntaya was the largest, reaching ~350 $Å^3$, whereas the Zika N pocked was notably smaller, with a volume of ~190 $Å^3$, and the dengue N pocked was in between, with a volume of ~300 $Å^3$. These large discrepancies in sizes also explain their different shapes. Given that the N pocket of Ntaya is almost twice as large as that of Zika, maintaining a similar shape between them would be difficult.

Ntaya MTase crystal structure

While RdRps are well-established drug targets, MTases have only recently attracted significant scientific attention as promising targets for several viral families, including coronaviruses, flaviviruses, and poxviruses.[35–42] Therefore, we aimed to solve the crystal structure of the MTase domain of NS5. We supplemented the protein with the pan-MTase inhibitor sinefungin and obtained well-diffracting crystals with a resolution of 2.3 Å (Table S1). The structure was solved by molecular replacement (detailed in the STAR Methods section) and revealed the overall fold of the Ntaya MTase which was in good agreement with previously solved structures of flaviviral MTases.[43,44] It is a mixed α-β fold (Figure 3B) that resembles a sandwich, where a central β-sheet is surrounded by α-helices (Figure 3). The central β-sheet is composed of seven β-strands (β4, β3, β2, β5, β6, β8, and β7 as viewed from the S-adenosyl-methionine [SAM] binding pocket) and, together with β1 and β9, form β-sheets that resemble the letter *J* (Figure 3C). These *J* β-sheets are well conserved among analyzed flaviviral MTases (Figure 3C). A three-helix bundle (α1, α2, and α8) contacts and stabilizes the loop connecting β7 and β8 strands, and a four-helix bundle (α6, α5, α4, and α3) together with a small β1 and β9 sheet is

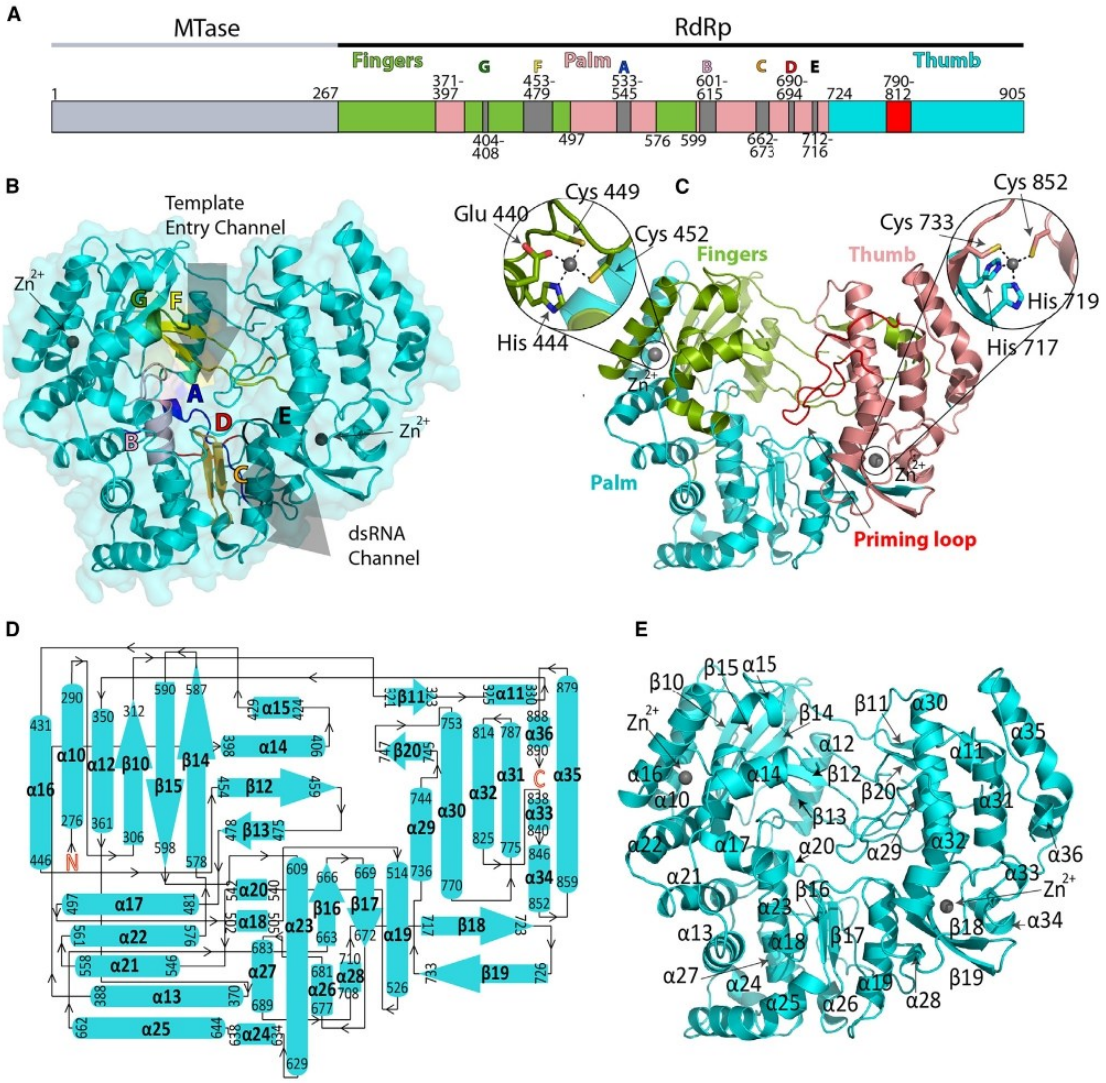

Figure 1. Crystal structure of the Ntaya RdRp domain

(A) Schematic representation of the NS5 protein which is composed of the MTase and RdRp domains. Palm, thumb, and finger subdomains and motifs A–G are shown.

(B) Overall structure of Ntaya RdRp, template entry, dsRNA channels and motifs A–G are highlighted.

(C) The three subdomains are depicted in different colors: fingers (green), palm (cyan), thumb (pink), and the priming loop (red). Two zinc-binding fingers are zoomed.

(D) Topological representation of the secondary structure of the Ntaya RdRp.

(E) Secondary structure elements are labeled.

located above the central sheet, while helices α7 and α9 are located below.

Sinefungin binding mode

The electron density for sinefungin was clearly visible upon molecular replacement (Figure 3A). Sinefungin was located in the SAM binding pocket, which is defined by four β-strands (β4, β3, β2, and β5) and three helices (α3, α4, and α5). The sinefungin molecule is bound to the SAM binding pocket mainly through hydrogen bonds. The 2′ hydroxyl of the ribose ring forms a hydrogen bond with the side chain of Glu111. The adenosine ring forms hydrogen bonds to the backbones of Lys105 and

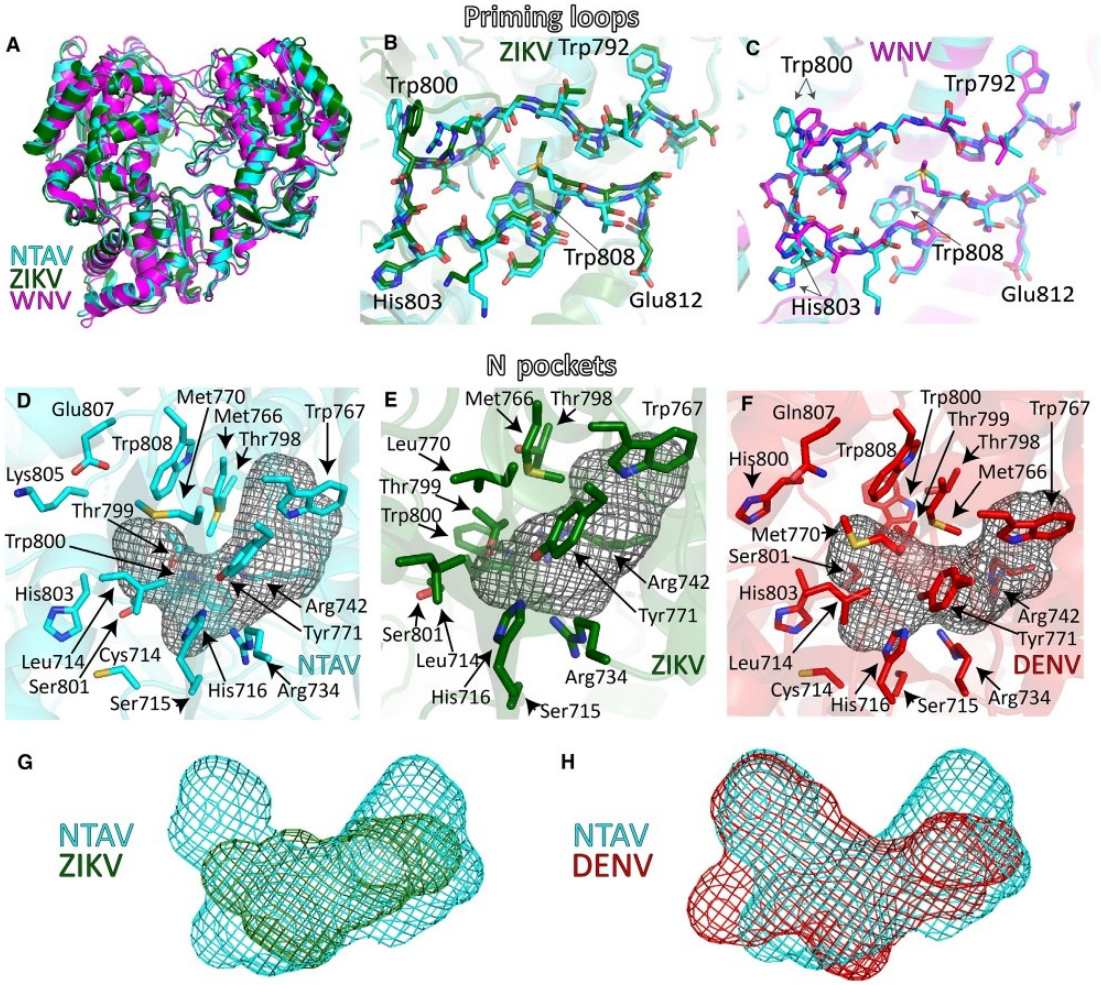

Figure 2. Structural alignment of flaviviral RdRp domains

(A) The overall structural alignment of Ntaya (cyan), Zika (dark green, PDB: 5M2Z), and West Nile (magenta, PDB: 2HFZ) RdRps.

(B and C) Structural superposition of NTAV (cyan) and ZIKV (dark green) or WNV (magenta) priming loops. The key residue Trp800 (Trp797 in case of ZIKV), which is involved in the stabilization of the priming nucleotide, is indicated.

(D–F) A detailed view of Ntaya (cyan), Zika (green), or dengue (red) N-pockets. Key residues are shown.

(G and H) Comparison of size and shape of N-pockets of (G) Ntaya (cyan, 349 Å^3) and Zika (green, 186 Å^3), and (H) dengue (red, 303 Å^3).

Val132 and its 6-amino group interacts with the side chain of Asp131. The amino acid moiety of sinefungin is coordinated by hydrogen bonds to Trp87, Asp146, Ser56, and Gly86 (Figure 3D). Superposition of Ntaya and Zika virus MTases revealed that the catalytic tetrad KDKE (residues Lys61, Asp146, Lys182, and Glu218) is in the same conformation (Figure 3D), which is not surprising given the absolute conservation of these residues for all the analyzed flaviviral MTases (Figure S1).

GTP binding mode

The NS5 protein, specifically its MTase domain, is also an RNA guanylyltransferase,[45] and thus its MTase domain has a GTP binding site.[46] We were interested in the GTP binding mode and aimed to solve a crystal structure with GTP bound. To begin, crystals of Ntaya MTase were prepared without the presence of sinefungin, resulting in the presence of S-adenosyl-homocysteine (SAH) from bacteria bound in the SAM binding pocket of the recombinant protein. Subsequently, the crystals were soaked overnight with GTP and magnesium as described in the STAR Methods section. These soaked crystals diffracted at a resolution of 2 Å, revealing clear electron density for both ligands (Figure S3A), with each ligand localized at its respective site (Figure 4A). The GTP molecule formed hydrogen bonds with key residues within the GTP/cap-binding pocket. The 2′

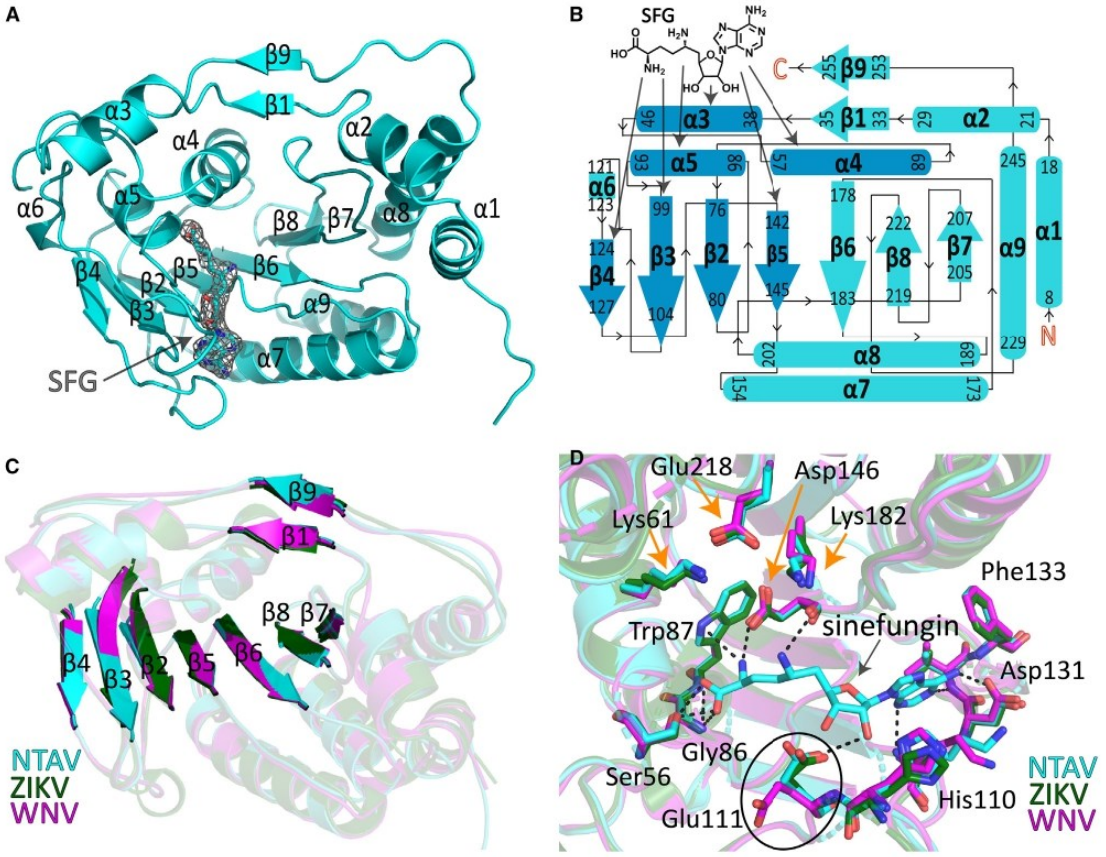

Figure 3. Crystal structure of the Ntaya MTase domain

(A) Overall fold of the Ntaya MTase domain with sinefungin bound. An Fo-Fc omit map contoured at 2σ is shown around the sinefungin.

(B) Topological representation of the Ntaya MTase secondary structure.

(C) Structural superposition of Ntaya (cyan), Zika (dark green, PDB: 5MRK), and West-Nile (magenta, PDB: 4R8S) MTase domains, the β-sheets are highlighted.

(D) Structural comparison of the SAM binding pockets. Hydrogen bonds between sinefungin and key residues are shown, with their distances available in Table S2. The residues of the catalytic tetrad are highlighted by orange arrows.

hydroxyl group of the ribose ring of GTP interacts with the side chains of Gln17 and Lys13. Actually, Lys13 forms hydrogen bonds with both the 2′ and 3′ hydroxyl groups. Also, the main chains of Ser151 and Pro152 are involved in hydrogen bonding with the 3′ hydroxyl group. The 2-amino group of the guanine ring forms hydrogen bond with the backbones of Leu16, Gln17, and Leu19. The phosphate groups are stabilized by hydrogen bonds to Arg28, Arg213, and Ser215 (Figure 4B). The magnesium atom was clearly visible and was coordinated by six oxygen atoms—three from the phosphate groups of GTP (one oxygen from each phosphate group) and three water molecules (Figure S3B). In fact, this octahedral coordination is used to distinguish magnesium from water.[47] However, a structural comparison with the crystal structure of Zika MTase bound to GTP revealed a different conformation of the triphosphates (Figure 4C). This is most likely caused by the lack of magnesium in the crystal structure of the Zika MTase/GTP complex in the study of Zhang et al.[48] Magnesium is present in the cytoplasm where the flaviviruses replicate; therefore, we believe our structure represents the physiological state. We also observed the SAH molecule, and its binding mode was the same as the binding mode of sinefungin with the obvious exception that SAH does not have an amine group that could hydrogen bond with Asp146 (Figure 4D).

RdRps enzymatic activities

We were also interested in the functional comparison of RdRps from various flaviviruses. We chose the NTAV, JEV, WNV, YF, and ZIKV RdRp domains of NS5 proteins for this comparison. We used a classical primer extension assay, where one primer was fluorescently labeled, and we monitored the progress of the reaction using denaturing PAGE (Figure 5). Consistent with the high structural homology of their active sites, the activity of these enzymes was similar. The most active enzyme was from ZIKV, but all the RdRps exhibited fair activity (Figure 5).

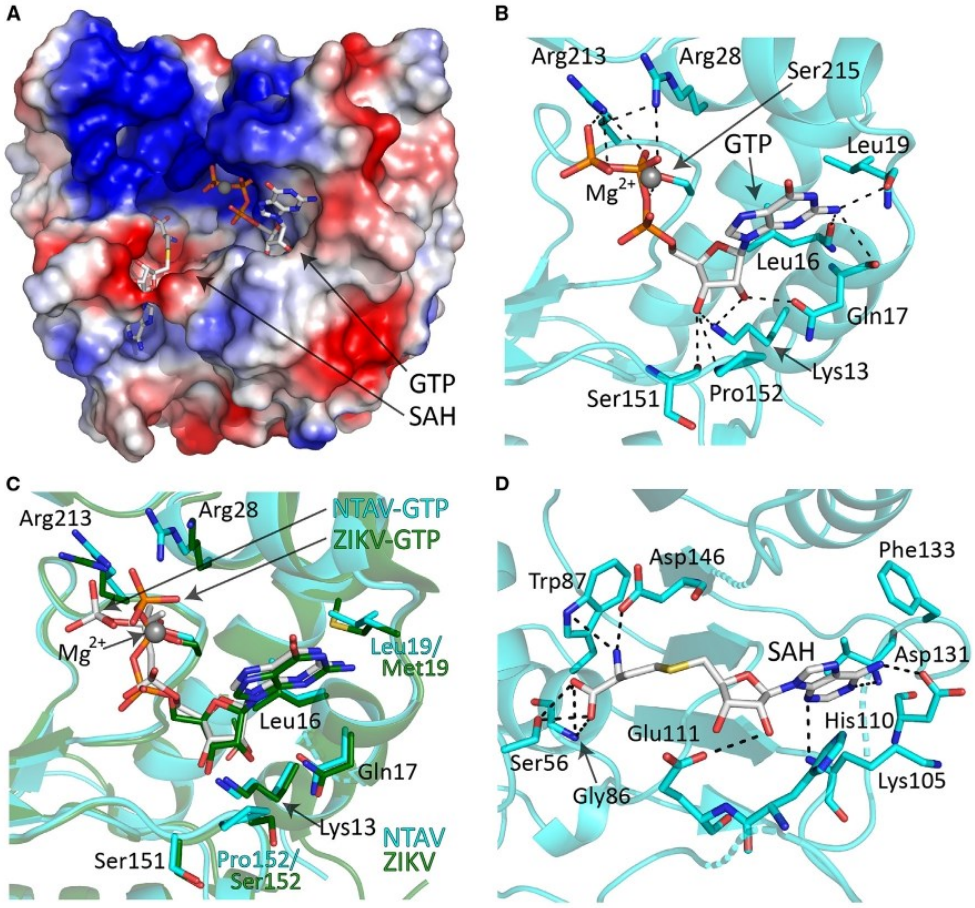

Figure 4. Crystal structure of the Ntaya MTase domain in complex with GTP and SAH

(A) SAH and GTP bound to the Ntaya MTase domain. The surface is colored according to the electrostatic potential and SAH and SAM are shown in stick representation.

(B) A detailed view of GTP bound to key residues of the GTP/cap-binding pocket. Selected hydrogen bonds between GTP and the key residues are depicted and labeled.

(C) Structural alignment of GTP/cap-binding pocket of Ntaya (cyan) and Zika (dark green, PDB: 5GOZ) with GTP bound.

(D) A detailed view of SAH bound to key residues of the SAM binding pocket.

Furthermore, consistently with our previous work,[49–51] the Ntaya RdRp could be inhibited by nucleoside and non-nucleoside inhibitors (Figure S4).

To further validate our structural findings, we selected several residues (Lys404, Arg484, Asp536, and Trp540) located near the active site for mutational analysis. Lys404 and Arg484 are predicted to play crucial roles in RNA binding, while Asp536 is implicated in metal coordination. In contrast, Trp540 was selected as negative control due to the general importance of tryptophan residues in protein stability and function, despite our structure not indicating any particular importance for Trp540 (Figure 6A). As expected, mutations of Lys404, Arg484, and Asp536 to alanine completely abolished the enzymatic activity of Ntaya RdRp, while mutation of Trp540 to alanine only moderately reduced its enzymatic activity (Figure 6).

MTase enzymatic activities

We also aimed to compare enzymatic activities of the recombinant Ntaya MTase domain to those of better characterized flaviviruses (DENV3, WNV, ZIKV, TBEV, JEV, and YFV). We prepared all these domains as recombinant proteins and measured their 2′-*O*-RNA MTase activity using ~100 bp of their respective m7GpppA capped genomic RNA and SAM as substrates. For each methylated RNA molecule, one SAH molecule is produced and this SAH was quantified using mass spectroscopy. Surprisingly, we observed large differences among the various MTases. The most active was the Zika virus MTase, which converted 76% of substrate SAM to the product SAH in 85 min. NTAV, DENV, WNV, TBEV, and JEV MTases showed 47% ± 3%, 45% ± 3%, 22% ± 2%, 9% ± 1%, and 9% ± 1% of ZIKV MTase activity, respectively. Surprisingly, the activity of the YFV MTase was

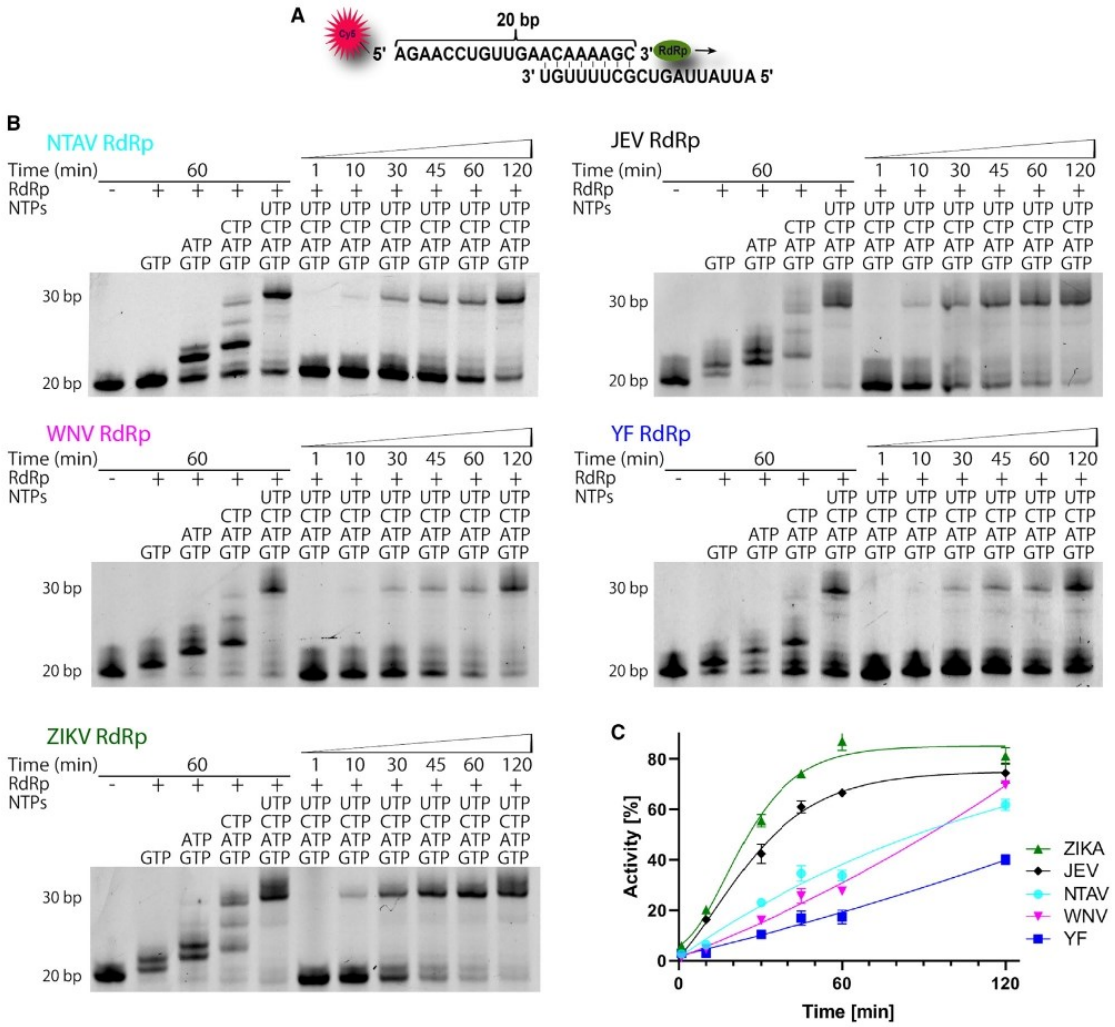

Figure 5. Analysis of polymerase activity of various flaviviral RdRps using a primer extension assay

(A) RNA oligonucleotides used in this study. The fluorescent label (Cy5) at the 5′ end of one of the oligonucleotides is highlighted in red. The arrow indicates the direction of the primer extension.

(B) Incorporation of individual mixes of nucleotides in the RNA polymerase assay. The reaction contained 30 nM NS5 protein, 10 nM oligonucleotide duplex and was initiated by the addition of 10μM NTPs. All reactions were stopped at the given timepoint and resolved on 20% denaturing PAGE gel.

(C) Graphical representation of RdRps activity (%) plotted against time (min). Error bars represent the standard deviation from three independent measurements.

almost at the detection limit and almost inactive—only 3% ± 1% of ZIKV MTase activity (Figure 7A).

Based on our structure, we selected several residues (Asp131, Val132, and Lys182) for mutational analysis. Both Asp131 and Val132 form the SAM binding pocket and are conserved; Asp131 is absolutely conserved, while Val132 is, in some instances, replaced with the very similar isoleucine residue (Figure S1). However, our structure predicts that only mutation of Asp131 to alanine would be detrimental because this residue forms a hydrogen bond with the adenine base of SAH (Figure 7B). Indeed, the Asp131Ala mutation proved to be detrimental for the enzyme, while the Val132Ala mutation only lowered the activity by about ~50% (Figure 7C), probably because the SAM binding pocket became suboptimal but remained functional. As a control, we also selected Lys182, an absolutely conserved amino acid residue that is a part of the catalytic tetrad.[52] As expected, this mutation was detrimental to the Ntaya MTase (Figure 7C).

DISCUSSION

Ntaya virus is primarily a zoonotic virus that is sometimes transmitted to humans and causes fever and headache.[15] It was

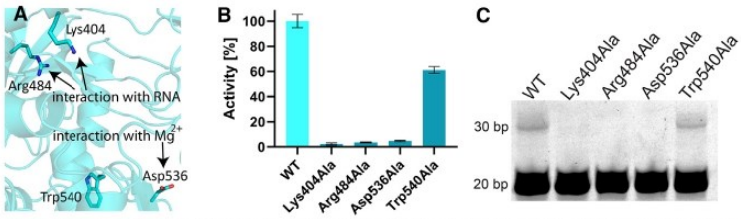

Figure 6. Mutational analysis of enzymatic activity of Ntaya RdRp

(A) A detailed view of the amino acids selected for mutational analysis.

(B) Graphical representation of RdRps activity (%) in 60 min reaction of the mutants prepared. Error bars represent the standard deviation from three independent measurements.

(C) Incorporation of nucleotides in the RNA polymerase assay. The reaction contained 30 nM protein, 10 nM oligonucleotide duplex, and was initiated by the addition of 10 μM NTPs. All reactions were stopped at the given time point and resolved on a 20% denaturing PAGE gel.

discovered in the early fifties and is not considered too dangerous. In this respect, it resembles the Zika virus before the Zika epidemic that started in Brazil in 2015.[53] Together with other recent outbreaks of +RNA zoonotic viruses (SARS, Middle East respiratory syndrome [MERS], Tick-borne encephalitis virus [TBEV], and severe acute respiratory syndrome coronavirus 2 [SARS-CoV-2]) and old foes such as YFV and WNV, there is a strong case advocating for considerable better understanding of +RNA viruses. In this study, we characterized the key protein responsible for RNA replication, NS5, of the Ntaya virus.

Our structural analysis revealed some differences in the conformations of several important regions such as the priming loop in the RdRp (Figure 2) or different conformations of Glu111 in the SAM binding pocket (Figure 3D). Glu111 forms a hydrogen bond with the 2′ hydroxyl group of the ribose ring in most of the structures of flaviviral MTases,[54] but its ability to adopt a non-bonding conformation could help explain the mechanism of SAH leaving the active site because structurally, SAH and SAM are bound in the same way.[17,55–58] Although there are differences among them, our structural comparison with previously available structures shows that the active sites in these +RNA viruses are conserved, indicating that there is significant evolutionary pressure to maintain these functional regions. This observation is encouraging because it suggests that a therapeutic compound active against one flaviviral enzyme should also be effective against all members of the flavivirus family. However, the N pocket, previously suggested as a potential binding site for pan-flaviviral inhibitors[32,33] and shown to be druggable, is actually not conserved among medically important flaviviruses (Figure 2). Consequently, inhibitors targeting this pocket would be effective against a specific subgroup of flaviviruses but not all of them.

Nevertheless, designing pan-flaviviral inhibitors appears feasible. Many (non-)nucleoside inhibitors were described for the dengue RdRp[59–62] that have potential to be developed into broad-spectrum antivirals. Moreover, we have recently measured the activity of remdesivir triphosphate *in vitro* against various flaviviral polymerases, and it was very similar, ranging from 0.3 to 2.1 μM.[49] Similar results were obtained for another more unusual inhibitor, PR673.[50] These results correspond to our enzymatic analysis of recombinant flaviviral RdRps (Figure 5). The most active enzyme (ZIKV) was about 4× more active than the least active one (YFV). A different situation was observed among the MTase domains. Again, the MTase from ZIKV was the most active, but this time, more than an order of magnitude (30× actually) than the least active enzyme, which was again from YFV (Figure 7). These results are difficult to explain from the structural point of view. In any case, the RdRp has to synthesize the whole genome which is about 10 000–11 000 catalytic steps. At the same time, the MTase domain must perform one guanylyl transfer reaction, one N7 and one 2′-O methylation reactions. There might not be any evolutionary pressure for speed in the case of MTase domains explaining the differences we observe; a slow MTase domain could be just as good as a fast one.

Concluding remarks

RNA viruses, particularly +RNA viruses, pose a significant threat to humanity. To develop effective treatments against future epidemics, a thorough molecular understanding of these viruses is essential. Our study highlights the structural conservation of the enzymatic centers of both flaviviral RdRps and MTases, which offers promising opportunities for designing antivirals effective against all flaviviruses. Notably, although the enzymatic properties of recombinant MTases were very diverse, all of the recombinant RdRps exhibited similar behavior.

STAR★METHODS

Detailed methods are provided in the online version of this paper and include the following:

- KEY RESOURCES TABLE
- RESOURCE AVAILABILITY
  - Lead contact
  - Materials availability
  - Data and code availability
- EXPERIMENTAL MODEL AND STUDY PARTICIPANT DETAILS
  - Bacterial strains
- METHOD DETAILS
  - Protein expression and purification
  - Crystallization and crystallographic analysis
  - Primer extension polymerase activity assay
  - RNA preparation
  - MTase activity assay
- QUANTIFICATION AND STATISTICAL ANALYSIS
  - Crystallographic data collection and processing

SUPPLEMENTAL INFORMATION

Supplemental information can be found online at https://doi.org/10.1016/j.str.2024.04.020.

ACKNOWLEDGMENTS

We thank the Helmholtz-Zentrum Berlin für Materialien und Energie for the allocation of synchrotron radiation beamtime. This research was funded by the Czech Science Foundation (21-25280S) (to E.B.) and by the Grant Agency of

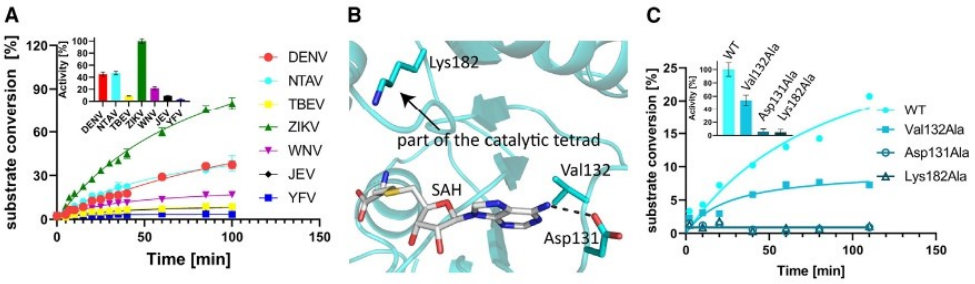

Figure 7. Analysis of the enzymatic activity of selected flaviviral MTases

(A) The rate of MTase activity was measured as the amount of the substrate (SAM) converted to the product of the reaction (SAH). Data points are presented as mean values ± standard deviations from triplicates. For comparison of measured MTase activities the values of substrate conversion in 85 min reaction were expressed as percent of the value of ZIKV MTase substrate conversion.

(B) A detailed view of residues (Asp131, Lys182, and Val132) which were mutated to alanine for mutational analysis.

(C) MTase activity of NTAV MTase mutants (Asp131, Val132, and Lys182) compared to the WT NTAV MTase. For comparison, the measured activities of NTAV MTase mutants in 80 min reaction time were expressed as percent of the activity of WT NTAV MTase.

Charles University (grant no. 408422) (to K.K.). The National Institute Virology and Bacteriology (Program EXCELES, project no. LX22NPO5103)—Funded by the European Union—Next Generation EU and The Academy of Sciences of the Czech Republic, RVO: 61388963, are also acknowledged.

AUTHOR CONTRIBUTIONS

K.K, P.K., E.Z., and D.C. performed experiments. M.K., K.K., and E.B. analyzed data. K.K. and E.B. wrote the manuscript. E.B. conceived the project. E.B. and K.K. obtained funding.

DECLARATION OF INTERESTS

The authors declare no competing interests.

Received: May 10, 2023
Revised: April 4, 2024
Accepted: April 26, 2024
Published: May 22, 2024

REFERENCES

1. Simmonds, P., Becher, P., Bukh, J., Gould, E.A., Meyers, G., Monath, T., Muerhoff, S., Pletnev, A., Rico-Hesse, R., Smith, D.B., et al. (2017). ICTV Virus Taxonomy Profile: Flaviviridae. J. Gen. Virol. *98*, 2–3. https://doi.org/10.1099/jgv.0.000672.
2. Oldstone, M.B.A. (2020). Viruses, Plagues, and History : Past, Present, and Future, Third edition (Oxford University Press).
3. Hadfield, J., Brito, A.F., Swetnam, D.M., Vogels, C.B.F., Tokarz, R.E., Andersen, K.G., Smith, R.C., Bedford, T., and Grubaugh, N.D. (2019). Twenty years of West Nile virus spread and evolution in the Americas visualized by Nextstrain. PLoS Pathog. *15*, e1008042. https://doi.org/10.1371/journal.ppat.1008042.
4. Bhatt, P., Sabeena, S.P., Varma, M., and Arunkumar, G. (2021). Current Understanding of the Pathogenesis of Dengue Virus Infection. Curr. Microbiol. *78*, 17–32. https://doi.org/10.1007/s00284-020-02284-w.
5. Lowe, R., Barcellos, C., Brasil, P., Cruz, O.G., Honório, N.A., Kuper, H., and Carvalho, M.S. (2018). The Zika Virus Epidemic in Brazil: From Discovery to Future Implications. Int. J. Environ. Res. Public Health *15*, 96. https://doi.org/10.3390/ijerph15010096.
6. Lickova, M., Fumacova Havlikova, S., Slavikova, M., and Klempa, B. (2021). Alimentary Infections by Tick-Borne Encephalitis Virus. Viruses *14*, 56. https://doi.org/10.3390/v14010056.
7. Im, J.H., Baek, J.H., Durey, A., Kwon, H.Y., Chung, M.H., and Lee, J.S. (2020). Geographic distribution of Tick-borne encephalitis virus complex. J. Vector Borne Dis. *57*, 14–22. https://doi.org/10.4103/0972-9062.308794.
8. Smithburn, K.C., and Haddow, A.J. (1951). Ntaya virus; a hitherto unknown agent isolated from mosquitoes collected in Uganda. Proc. Soc. Exp. Biol. Med. *77*, 130–133. https://doi.org/10.3181/00379727-77-18700.
9. Braack, L., Gouveia de Almeida, A.P., Cornel, A.J., Swanepoel, R., and de Jager, C. (2018). Mosquito-borne arboviruses of African origin: review of key viruses and vectors. Parasit. Vectors *11*, 29. https://doi.org/10.1186/s13071-017-2559-9.
10. Weissenbock, H., Hubalek, Z., Bakonyi, T., and Nowotny, N. (2010). Zoonotic mosquito-borne flaviviruses: Worldwide presence of agents with proven pathogenicity and potential candidates of future emerging diseases. Vet. Microbiol. *140*, 271–280. https://doi.org/10.1016/j.vetmic.2009.08.025.
11. Kuno, G., and Chang, G.J.J. (2007). Full-length sequencing and genomic characterization of Bagaza, Kedougou, and Zika viruses. Arch. Virol. *152*, 687–696. https://doi.org/10.1007/s00705-006-0903-z.
12. Antipa, C., Girjabu, E., Iftimovici, R., and Drăgănescu, N. (1984). Serological investigations concerning the presence of antibodies to arboviruses in wild birds. Virologie *35*, 5–9.
13. Dilcher, M., Sall, A.A., Hufert, F.T., and Weidmann, M. (2013). Full-length genome sequence of Ntaya virus. Virus Gene. *46*, 162–164. https://doi.org/10.1007/s11262-012-0825-7.
14. Davidson, I. (2015). A New Look at Avian Flaviviruses. Isr. J. Vet. Med. *70*, 3–8.
15. Woodruff, A.W., Bowen, E.T., and Platt, G.S. (1978). Viral infections in travellers from tropical Africa. Br. Med. J. *1*, 956–958. https://doi.org/10.1136/bmj.1.6118.956.
16. da Fonseca, N.J., Jr., Lima Afonso, M.Q., Pedersolli, N.G., de Oliveira, L.C., Andrade, D.S., and Bleicher, L. (2017). Sequence, structure and function relationships in flaviviruses as assessed by evolutive aspects of its conserved non-structural protein domains. Biochem. Biophys. Res. Commun. *492*, 565–571. https://doi.org/10.1016/j.bbrc.2017.01.041.
17. Dong, H., Fink, K., Züst, R., Lim, S.P., Qin, C.F., and Shi, P.Y. (2014). Flavivirus RNA methylation. J. Gen. Virol. *95*, 763–778. https://doi.org/10.1099/vir.0.062208-0.
18. Hyde, J.L., and Diamond, M.S. (2015). Innate immune restriction and antagonism of viral RNA lacking 2-O methylation. Virology *479–480*, 66–74. https://doi.org/10.1016/j.virol.2015.01.019.

19. Moureau, G., Cook, S., Lemey, P., Nougairede, A., Forrester, N.L., Khasnatinov, M., Charrel, R.N., Firth, A.E., Gould, E.A., and de Lamballerie, X. (2015). New Insights into Flavivirus Evolution, Taxonomy and Biogeographic History, Extended by Analysis of Canonical and Alternative Coding Sequences. PLoS One *10*, e0117849. https://doi.org/10.1371/journal.pone.0117849.

20. Kuno, G., Chang, G.J., Tsuchiya, K.R., Karabatsos, N., and Cropp, C.B. (1998). Phylogeny of the genus Flavivirus. J. Virol. *72*, 73–83. https://doi.org/10.1128/Jvi.72.1.73-83.1998.

21. Upadhyay, A.K., Cyr, M., Longenecker, K., Tripathi, R., Sun, C., and Kempf, D.J. (2017). Crystal structure of full-length Zika virus NS5 protein reveals a conformation similar to Japanese encephalitis virus NS5. Acta Crystallogr. F Struct. Biol. Commun. *73*, 116–122. https://doi.org/10.1107/S2053230X17001601.

22. Zhao, Y., Soh, T.S., Zheng, J., Chan, K.W.K., Phoo, W.W., Lee, C.C., Tay, M.Y.F., Swaminathan, K., Cornvik, T.C., Lim, S.P., et al. (2015). A crystal structure of the Dengue virus NS5 protein reveals a novel inter-domain interface essential for protein flexibility and virus replication. PLoS Pathog. *11*, e1004682. https://doi.org/10.1371/journal.ppat.1004682.

23. Malet, H., Egloff, M.P., Selisko, B., Butcher, R.E., Wright, P.J., Roberts, M., Gruez, A., Sulzenbacher, G., Vonrhein, C., Bricogne, G., et al. (2007). Crystal structure of the RNA polymerase domain of the West Nile virus non-structural protein 5. J. Biol. Chem. *282*, 10678–10689. https://doi.org/10.1074/jbc.M607273200.

24. Lu, G., and Gong, P. (2013). Crystal Structure of the full-length Japanese encephalitis virus NS5 reveals a conserved methyltransferase-polymerase interface. PLoS Pathog. *9*, e1003549. https://doi.org/10.1371/journal.ppat.1003549.

25. Dubankova, A., and Boura, E. (2019). Structure of the yellow fever NS5 protein reveals conserved drug targets shared among flaviviruses. Antivir. Res. *169*, 104536. https://doi.org/10.1016/j.antiviral.2019.104536.

26. Osawa, T., Aoki, M., Ehara, H., and Sekine, S.I. (2023). Structures of dengue virus RNA replicase complexes. Mol. Cell *83*, 2781–2791.e4. https://doi.org/10.1016/j.molcel.2023.06.023.

27. Appleby, T.C., Perry, J.K., Murakami, E., Barauskas, O., Feng, J., Cho, A., Fox, D., 3rd, Wetmore, D.R., McGrath, M.E., Ray, A.S., et al. (2015). Viral replication. Structural basis for RNA replication by the hepatitis C virus polymerase. Science *347*, 771–775. https://doi.org/10.1126/science.1259210.

28. Li, R., Niu, Z., Liu, Y., Bai, X., Wang, D., and Chen, C. (2022). Crystal structure and cap binding analysis of the methyltransferase of langat virus. Antivir. Res. *208*, 105459. https://doi.org/10.1016/j.antiviral.2022.105459.

29. Ferrero, D.S., Albentosa-González, L., Mas, A., and Verdaguer, N. (2022). Structure and function of the NS5 methyltransferase domain from Usutu virus. Antivir. Res. *208*, 105460. https://doi.org/10.1016/j.antiviral.2022.105460.

30. Razin, S.V., Borunova, V.V., Maksimenko, O.G., and Kantidze, O.L. (2012). Cys2His2 zinc finger protein family: classification, functions, and major members. Biochemistry *77*, 217–226. https://doi.org/10.1134/S0006297912030017.

31. Malet, H., Massé, N., Selisko, B., Romette, J.L., Alvarez, K., Guillemot, J.C., Tolou, H., Yap, T.L., Vasudevan, S., Lescar, J., and Canard, B. (2008). The flavivirus polymerase as a target for drug discovery. Antivir. Res. *80*, 23–35. https://doi.org/10.1016/j.antiviral.2008.06.007.

32. Noble, C.G., Lim, S.P., Arora, R., Yokokawa, F., Nilar, S., Seh, C.C., Wright, S.K., Benson, T.E., Smith, P.W., and Shi, P.Y. (2016). A Conserved Pocket in the Dengue Virus Polymerase Identified through Fragment-based Screening. J. Biol. Chem. *291*, 8541–8548. https://doi.org/10.1074/jbc.M115.710731.

33. Lim, S.P., Noble, C.G., Nilar, S., Shi, P.Y., and Yokokawa, F. (2018). Discovery of Potent Non-nucleoside Inhibitors of Dengue Viral RNA-Dependent RNA Polymerase from Fragment Screening and Structure-Guided Design. Adv. Exp. Med. Biol. *1062*, 187–198. https://doi.org/10.1007/978-981-10-8727-1_14.

34. Lim, S.P., Noble, C.G., Seh, C.C., Soh, T.S., El Sahili, A., Chan, G.K.Y., Lescar, J., Arora, R., Benson, T., Nilar, S., et al. (2016). Potent Allosteric Dengue Virus NS5 Polymerase Inhibitors: Mechanism of Action and Resistance Profiling. PLoS Pathog. *12*, e1005737. https://doi.org/10.1371/journal.ppat.1005737.

35. Devkota, K., Schapira, M., Perveen, S., Khalili Yazdi, A., Li, F., Chau, I., Ghiabi, P., Hajian, T., Loppnau, P., Bolotokova, A., et al. (2021). Probing the SAM Binding Site of SARS-CoV-2 Nsp14 In Vitro Using SAM Competitive Inhibitors Guides Developing Selective Bisubstrate Inhibitors. SLAS Discov. *26*, 1200–1211. https://doi.org/10.1177/24725552211026261.

36. Li, F., Ghiabi, P., Hajian, T., Klima, M., Li, A.S.M., Khalili Yazdi, A., Chau, I., Loppnau, P., Kutera, M., Seitova, A., et al. (2023). SS148 and WZ16 inhibit the activities of nsp10-nsp16 complexes from all seven human pathogenic coronaviruses. Biochim. Biophys. Acta Gen. Subj. *1867*, 130319. https://doi.org/10.1016/j.bbagen.2023.130319.

37. Otava, T., Šála, M., Li, F., Fanfrlík, J., Devkota, K., Perveen, S., Chau, I., Pakarian, P., Hobza, P., Vedadi, M., et al. (2021). The Structure-Based Design of SARS-CoV-2 nsp14 Methyltransferase Ligands Yields Nanomolar Inhibitors. ACS Infect. Dis. *7*, 2214–2220. https://doi.org/10.1021/acsinfecdis.1c00131.

38. Silhan, J., Klima, M., Otava, T., Skvara, P., Chalupska, D., Chalupsky, K., Kozic, J., Nencka, R., and Boura, E. (2023). Discovery and structural characterization of monkeypox virus methyltransferase VP39 inhibitors reveal similarities to SARS-CoV-2 nsp14 methyltransferase. Nat. Commun. *14*, 2259. https://doi.org/10.1038/s41467-023-38019-1.

39. Coutard, B., Barral, K., Lichiere, J., Selisko, B., Martin, B., Aouadi, W., Lombardia, M.O., Debart, F., Vasseur, J.J., Guillemot, J.C., et al. (2017). Zika Virus Methyltransferase: Structure and Functions for Drug Design Perspectives. J. Virol. *91*, e02202-16. https://doi.org/10.1128/JVI.02202-16.

40. Zgarbova, M., Otava, T., Silhan, J., Nencka, R., Weber, J., and Boura, E. (2023). Inhibitors of mpox VP39 2'-O methyltransferase efficiently inhibit the monkeypox virus. Antivir. Res. *218*, 105714. https://doi.org/10.1016/j.antiviral.2023.105714.

41. Skvara, P., Chalupska, D., Klima, M., Kozic, J., Silhan, J., and Boura, E. (2023). Structural basis for RNA-cap recognition and methylation by the mpox methyltransferase VP39. Antivir. Res. *216*, 105663. https://doi.org/10.1016/j.antiviral.2023.105663.

42. Dostalik, P., Krafcikova, P., Silhan, J., Kozic, J., Chalupska, D., Chalupsky, K., and Boura, E. (2021). Structural Analysis of the OC43 Coronavirus 2 '-O-RNA Methyltransferase. J. Virol. *95*, e0046321. https://doi.org/10.1128/JVI.00463-21.

43. Dong, H., Zhang, B., and Shi, P.Y. (2008). Flavivirus methyltransferase: a novel antiviral target. Antivir. Res. *80*, 1–10. https://doi.org/10.1016/j.antiviral.2008.05.003.

44. Zhou, Y., Ray, D., Zhao, Y., Dong, H., Ren, S., Li, Z., Guo, Y., Bernard, K.A., Shi, P.Y., and Li, H. (2007). Structure and function of flavivirus NS5 methyltransferase. J. Virol. *81*, 3891–3903. https://doi.org/10.1128/JVI.02704-06.

45. Issur, M., Geiss, B.J., Bougie, I., Picard-Jean, F., Despins, S., Mayette, J., Hobdey, S.E., and Bisaillon, M. (2009). The flavivirus NS5 protein is a true RNA guanylyltransferase that catalyzes a two-step reaction to form the RNA cap structure. RNA *15*, 2340–2350. https://doi.org/10.1261/rna.1609709.

46. Egloff, M.P., Benarroch, D., Selisko, B., Romette, J.L., and Canard, B. (2002). An RNA cap (nucleoside-2 '-O-)-methyltransferase in the flavivirus RNA polymerase NS5: crystal structure and functional characterization. EMBO J. *21*, 2757–2768. https://doi.org/10.1093/emboj/21.11.2757.

47. Smola, M., Birkus, G., and Boura, E. (2019). No magnesium is needed for binding of the stimulator of interferon genes to cyclic dinucleotides. Acta Crystallogr. F Struct. Biol. Commun. *75*, 593–598. https://doi.org/10.1107/S2053230X19010999.

48. Zhang, C., Feng, T., Cheng, J., Li, Y., Yin, X., Zeng, W., Jin, X., Li, Y., Guo, F., and Jin, T. (2017). Structure of the NS5 methyltransferase from Zika

virus and implications in inhibitor design. Biochem. Biophys. Res. Commun. *492*, 624–630. https://doi.org/10.1016/j.bbrc.2016.11.098.

49. Konkolova, E., Dejmek, M., Hřebabecký, H., Šála, M., Bőserle, J., Nencka, R., and Boura, E. (2020). Remdesivir triphosphate can efficiently inhibit the RNA-dependent RNA polymerase from various flaviviruses. Antivir. Res. *182*, 104899. https://doi.org/10.1016/j.antiviral.2020.104899.
50. Konkolova, E., Krejcova, K., Eyer, L., Hodek, J., Zgarbova, M., Fortova, A., Jirasek, M., Teply, F., Reyes-Gutierrez, P.E., Ruzek, D., et al. (2022). A Helquat-like Compound as a Potent Inhibitor of Flaviviral and Coronaviral Polymerases. Molecules *27*, 1894. https://doi.org/10.3390/molecules27061894.
51. Milisavljevic, N., Konkolová, E., Kozák, J., Hodek, J., Veselovská, L., Sýkorová, V., Čížek, K., Pohl, R., Eyer, L., Svoboda, P., et al. (2021). Antiviral Activity of 7-Substituted 7-Deazapurine Ribonucleosides, Monophosphate Prodrugs, and Triphoshates against Emerging RNA Viruses. ACS Infect. Dis. *7*, 471–478. https://doi.org/10.1021/acsinfecdis.0c00829.
52. Milani, M., Mastrangelo, E., Bollati, M., Selisko, B., Decroly, E., Bouvet, M., Canard, B., and Bolognesi, M. (2009). Flaviviral methyltransferase/RNA interaction: Structural basis for enzyme inhibition. Antivir. Res. *83*, 28–34. https://doi.org/10.1016/j.antiviral.2009.03.001.
53. Baud, D., Gubler, D.J., Schaub, B., Lanteri, M.C., and Musso, D. (2017). An update on Zika virus infection. Lancet *390*, 2099–2109. https://doi.org/10.1016/S0140-6736(17)31450-2.
54. Hercik, K., Brynda, J., Nencka, R., and Boura, E. (2017). Structural basis of Zika virus methyltransferase inhibition by sinefungin. Arch. Virol. *162*, 2091–2096. https://doi.org/10.1007/s00705-017-3345-x.
55. Bradrick, S.S. (2017). Causes and Consequences of Flavivirus RNA Methylation. Front. Microbiol. *8*, 2374. https://doi.org/10.3389/fmicb.2017.02374.
56. Byszewska, M., Śmietański, M., Purta, E., and Bujnicki, J.M. (2014). RNA methyltransferases involved in 5 ' cap biosynthesis. RNA Biol. *11*, 1597–1607. https://doi.org/10.1080/15476286.2015.1004955.
57. Wu, J., Liu, W., and Gong, P. (2015). A Structural Overview of RNA-Dependent RNA Polymerases from the Flaviviridae Family. Int. J. Mol. Sci. *16*, 12943–12957. https://doi.org/10.3390/ijms160612943.
58. Nencka, R., Silhan, J., Klima, M., Otava, T., Kocek, H., Krafcikova, P., and Boura, E. (2022). Coronaviral RNA-methyltransferases: function, structure and inhibition. Nucleic Acids Res. *50*, 635–650. https://doi.org/10.1093/nar/gkab1279.
59. Nascimento, I.J.D., Santos, P.F.D., de Aquino, T.M., de Araujo, J.X., and da Silva, E.F. (2021). Insights on Dengue and Zika NS5 RNA-dependent RNA polymerase (RdRp) inhibitors. Eur. J. Med. Chem. *224*, 113698. https://doi.org/10.1016/j.ejmech.2021.113698.
60. Shimizu, H., Saito, A., Mikuni, J., Nakayama, E.E., Koyama, H., Honma, T., Shirouzu, M., Sekine, S.I., and Shioda, T. (2019). Discovery of a small molecule inhibitor targeting dengue virus NS5 RNA-dependent RNA polymerase. PLoS Negl. Trop. Dis. *13*, e0007894. https://doi.org/10.1371/journal.pntd.0007894.
61. Abdelaziz, O.S., and Waffa, Z. (2020). Neuropathogenic human coronaviruses: A review. Rev. Med. Virol. *30*, e2118. https://doi.org/10.1002/rmv.2118.
62. Feracci, M., Eydoux, C., Fattorini, V., Lo Bello, L., Gauffre, P., Selisko, B., Sutto-Ortiz, P., Shannon, A., Xia, H., Shi, P.Y., et al. (2023). AT-752 targets multiple sites and activities on the Dengue virus replication enzyme NS5. Antivir. Res. *212*, 105574. https://doi.org/10.1016/j.antiviral.2023.105574.
63. Krafcikova, P., Silhan, J., Nencka, R., and Boura, E. (2020). Structural analysis of the SARS-CoV-2 methyltransferase complex involved in RNA cap creation bound to sinefungin. Nat. Commun. *11*, 3717. https://doi.org/10.1038/s41467-020-17495-9.
64. Hercik, K., Kozak, J., Sala, M., Dejmek, M., Hrebabecky, H., Zbornikova, E., Smola, M., Ruzek, D., Nencka, R., and Boura, E. (2017). Adenosine triphosphate analogs can efficiently inhibit the Zika virus RNA-dependent RNA polymerase. Antivir. Res. *137*, 131–133. https://doi.org/10.1016/j.antiviral.2016.11.020.
65. Kabsch, W. (2010). Xds. Acta Crystallogr. D Biol. Crystallogr. *66*, 125–132. https://doi.org/10.1107/S0907444909047337.
66. Liebschner, D., Afonine, P.V., Baker, M.L., Bunkóczi, G., Chen, V.B., Croll, T.I., Hintze, B., Hung, L.W., Jain, S., McCoy, A.J., et al. (2019). Macromolecular structure determination using X-rays, neutrons and electrons: recent developments in Phenix. Acta Crystallogr. D *75*, 861–877. https://doi.org/10.1107/S2059798319011471.
67. Emsley, P., Lohkamp, B., Scott, W.G., and Cowtan, K. (2010). Features and development of Coot. Acta Crystallogr. D Biol. Crystallogr. *66*, 486–501. https://doi.org/10.1107/S0907444910007493.
68. Dubankova, A., Humpolickova, J., Klima, M., and Boura, E. (2017). Negative charge and membrane-tethered viral 3B cooperate to recruit viral RNA dependent RNA polymerase 3D (pol). Sci. Rep. *7*, 17309. https://doi.org/10.1038/s41598-017-17621-6.
69. Konkolova, E., Klima, M., Nencka, R., and Boura, E. (2020). Structural analysis of the putative SARS-CoV-2 primase complex. J. Struct. Biol. *211*, 107548. https://doi.org/10.1016/j.jsb.2020.107548.
70. Mueller, U., Darowski, N., Fuchs, M.R., Förster, R., Hellmig, M., Paithankar, K.S., Pühringer, S., Steffien, M., Zocher, G., and Weiss, M.S. (2012). Facilities for macromolecular crystallography at the Helmholtz-Zentrum Berlin. J. Synchrotron Radiat. *19*, 442–449. https://doi.org/10.1107/S0909049512006395.
71. McCoy, A.J., Grosse-Kunstleve, R.W., Adams, P.D., Winn, M.D., Storoni, L.C., and Read, R.J. (2007). Phaser crystallographic software. J. Appl. Crystallogr. *40*, 658–674. https://doi.org/10.1107/S0021889807021206.
72. Afonine, P.V., Grosse-Kunstleve, R.W., Echols, N., Headd, J.J., Moriarty, N.W., Mustyakimov, M., Terwilliger, T.C., Urzhumtsev, A., Zwart, P.H., and Adams, P.D. (2012). Towards automated crystallographic structure refinement with phenix.refine. Acta Crystallogr. D Biol. Crystallogr. *68*, 352–367. https://doi.org/10.1107/S0907444912001308.

STAR★METHODS

KEY RESOURCES TABLE

REAGENT or RESOURCE	SOURCE	IDENTIFIER
Bacterial and virus strains		
Escherichia coli BL21 DE3 RIL strain	Agilent	230245
Chemicals, peptides, and recombinant proteins		
m7GpppA	Jena Bioscience	NU-535L
GTP	Thermo Fisher Scientific	R0461
Sinefungin	(Krafcikova et al., 2020)[63]	N/A
2′-C-methylated nucleotide	(Hercik et al., 2017)[64]	N/A
PR673	(Konkolova et al., 2022)[50]	N/A
HisPur Ni-NTA Superflow Agarose	Thermo Fisher Scientific	25216
Critical commercial assays		
Phusion Site/Dorected Mutagenesis Kit	Thermo Fisher Scientific	F541
TranscriptAid T7 High Yield Transcription Kit	Thermo Fisher Scientific	K0441
Deposited data		
Mtase + sinefungin	This paper	PDB: 8QDJ
Mtase + sinefungin	This paper	PDB: 8BXK
Mtase + SAH + GTP	This paper	PDB: 8CQH
RdRp	This paper	PDB: 7ZIU
Oligonucleotides		
DENV3 CAGTAATACGACTCACTATAGttgtt agtctacgtggaccgacaagaacagtttcgactcg gaagcttgcttaacgtagtgctgacagtttttattag agagcagatctctga	This paper	N/A
NTAV CAGTAATACGACTCACTATAGaagttcatctg tgtgaacttcgtgattgacagctcaacacgagtgcgggcaacc gtaaacacagtttgaacgtttttggagagagactact	This paper	N/A
TBEV CAGTAATACGACTCACTATAG attttcttgcacgtgcgtgcgtttgcttcggacagcattagc agcggttggtttgaaagaaatattcttttgtttttaccagtcgtga acgtgttgagaaaaagacagcttaggagaacaagagctgggg	This paper	N/A
ZIKV CAGTAATACGACTCACTATAG ttgttgatctgtgtgagtcagactgcgacagttcga gtctgaagcgagagctaacaacagtatcaacag gtttaatttggatttggaaacgagagtttctggtc	This paper	N/A
WNV CAGTAATACGACTCACTATAGtagttcg cctgtgtgagctgacaaacttagtagtgtttgtgaggattaa caacaattaacacagtgcgagctgtttcttggcacgaagatctcg	This paper	N/A
JEV CAGTAATACGACTCACTATAGaagtttatctgtgtg aacttcttggcttagtatcgttgagaagaatcgagagattagtgca gtttaaacagtttttagaacggaagataacc	This paper	N/A
YFV CAGTAATACGACTCACTATAG taaatcctgtgtgctaattgaggtgcattggtctgca aatcgagttgctaggcaataaacacatttggattaat tttaatcgttcgttgagcgattagcagagaactgaccagaac	This paper	N/A
Recombinant DNA		
plasmid pET28bRdRp WT	This paper	N/A
plasmid pET28bRdRp Lys404Ala	This paper	N/A
plasmid pET28bRdRp Arg484Ala	This paper	N/A
plasmid pET28bRdRp Asp536Ala	This paper	N/A

(*Continued on next page*)

Continued

REAGENT or RESOURCE	SOURCE	IDENTIFIER
plasmid pET28bRdRp Trp540Ala	This paper	N/A
plasmid pSUMO-Mtase WT	This paper	N/A
plasmid pSUMO-Mtase Asp131Ala	This paper	N/A
plasmid pSUMO-Mtase Val132Ala	This paper	N/A
plasmid pSUMO-Mtase Lys182Ala	This paper	N/A
Software and algorithms		
XDS	(Kabsch et al., 2010)[65]	https://xds.mr.mpg.de/
Phenix v1.20.1-4487	(Liebschner et al., 2019)[66]	https://phenix-online.org/
Coot v0.9.8.7	(Emsley et al., 2010)[67]	https://www2.mrc-lmb.cam.ac.uk/personal/pemsley/coot/
Grade2 v1.3.1	Global Phasing Ltd.	https://grade.globalphasing.org/cgi-bin/grade2_server.cgi
PyMol v2.0	Schrödinger, LLC	https://pymol.org/
Prism 7.05	GraphPad Software	https://www.graphpad.com/

RESOURCE AVAILABILITY

Lead contact

Further information and requests for resources and reagents should be directed to and will be fulfilled by the lead contact, Evzen Boura (boura@uochb.cas.cz).

Materials availability

All unique/stable reagents generated in this study will be made available on request, but we may require a payment and/or a completed materials transfer agreement if there is potential for commercial application.

Data and code availability

The structural data (atomic coordinates and structural factors) have been deposited in the Protein Data Bank (https://www.rcsb.org) and are publicly available as of the date of publication. Accession numbers are listed in the key resources table.

This paper does not report original code.

Any additional information required to reanalyze the data reported in this paper is available from the lead contact upon request.

EXPERIMENTAL MODEL AND STUDY PARTICIPANT DETAILS

Bacterial strains

All proteins used for biochemical studies were recombinantly expressed in Escherichia coli BL21 DE3 RIL strain (Agilent, 230245).

METHOD DETAILS

Protein expression and purification

An artificial gene encoding the Ntaya NS5 protein (GeneBank: KF917539.1) was obtained from the European Virus Archive goes Global (EVAg). The sequence encoding the RdRp domain was cloned into pET28b vector using Gibson assembly. The resulting proteins contained an N-terminal 6× His-tag followed by TEV cleavage site. The sequence encoding the MTase domain was cloned into a home-made pSUMO vector[54] using restriction cloning (BamHI and XhoI sites). The resulting protein contained an N-terminal 8x-His-SUMO tag. All mutants were prepared using Phusion Site-Directed Mutagenesis Kit (Thermo Fisher Scientific) and the sequence was verified by DNA sequencing.

All proteins were expressed and purified using our standard protocols for viral enzymes in *E. coli*.[68,69] In brief, the genes were expressed in *E.coli* strain BL21-CodonPlus (DE3) RIL in LB medium supplemented with 50 μM $ZnSO_4$ and 1 mM $MgCl_2$. The bacteria were harvested by centrifugation, resuspended and sonicated in lysis buffer (50 mM Tris-HCl pH 8.0, 20 mM imidazole, 500 mM NaCl, 10% (v/v) glycerol, 3 mM β-mercaptoethanol). After lysis, the supernatant was immobilized on Ni-NTA agarose beads (Machery-Nagel), washed with lysis buffer supplemented with 1M NaCl and the protein was eluted using lysis buffer supplemented with 300 mM imidazole.

For all the RdRps, the 6× His-tag was digested using TEV protease at 4°C overnight and the RdRps were further purified by affinity chromatography using HiTrap Heparin HP, HiTrap Q HP or Hi Trap SP HP columns (Cytiva). This was followed by size exclusion chromatography using Superdex 200 16/600 (GE Life Sciences) in 20 mM CHES pH 9.5, 800 mM NaCl, 10% (v/v) glycerol, 0.02% NaN_3.

For the MTases, after elution from the Ni-NTA agarose beads, the proteins were supplemented with yeast sumo-protease Ulp1 and dialyzed against the lysis buffer overnight. The 8x-His-SUMO tag was removed by Ni-NTA agarose beads and the proteins were further purified by size exclusion chromatography using Superdex 75 16/600 (GE Life Sciences) in 25 mM HEPES pH 7.5, 500 mM NaCl, 5% glycerol and 1 mM TCEP. Finally, the pure proteins were concentrated to 4 mg/ml (RdRps) or 10 mg/ml (MTases) and stored at -80°C until needed.

Crystallization and crystallographic analysis

Crystals of Ntaya RdRp and MTase in complex with SAH grew in 7 days at 18°C in sitting drops consisting of 1:1 mixture (200 nl each) of the protein and the well solution (0.1 M Trizma/Bicine pH 8.5, 0.02M monosacharides, 10% (w/v) PEG4000, 20% (v/v) glycerol). GTP soaking was carried overnight in the presence of 1 mM Mg^{2+}, the GTP concentration was 10 mM. The Ntaya MTase crystals in complex with sinefungin grew in two weeks in sitting drops prepared using the same procedure, but the well solution was 4.0 M sodium formate. These crystals did not require cryo-protection and were flash frozen in liquid nitrogen. During revisions of our study, we also prepared new crystals of Ntaya MTase in complex with SAH. These grew in three days at 18°C in sitting drops consisting of 1:1 mixture (200 nl each) of the protein and the well solution (0.2 M $MgCl_2$, 0.1 M Bis-Tris pH 5.5, 25 % (w/v) PEG 3350). Before harvesting the crystals were cryo-protected in well solution supplemented with 20% (v/v) glycerol and flash frozen in liquid nitrogen. These crystals diffracted to 1.8 Å and belonged to the $P12_11$ spacegroup.

The MTase datasets were collected using our home-source (rotating anode, Rigaku micromax-007 HF) while the RdRp dataset was collected at BESSY II electron storage ring operated by the Helmoltz-Zentrum Berlin (HZB).[70] The data was integrated and scaled using XDS.[65] The structures of the NTAV MTase and NTAV RdRp were solved by molecular replacement using the structures of Zika MTase (pdb entry 5MRK)[54] and Yellow fever virus polymerase NS5A (pdb entry 6QSN),[25] respectively, as search models. The initial models were obtained with Phaser[71] from the Phenix package.[66] The models were further improved using automatic model refinement with Phenix.refine[72] followed by manual model building with Coot.[67] Statistics for data collection and processing, structure solution and refinement are summarized in Table S1. Structural figures were generated with the PyMOL Molecular Graphics System v2.0 (Schrödinger, LLC). The atomic coordinates and structural factors were deposited in the Protein Data Bank (https://www.rcsb.org).

Primer extension polymerase activity assay

The polymerase activity of the NS5 RdRp domain and its mutants was determined in a primer extension reaction using a fluorescently labeled primer (Cy5 5'-AGAACCUGUUGAACAAAAGC-3') and a template (5'-AUUAUUAGCUGCUUUUGU-3'). The reaction was performed in a reaction mix containing 30 nM NS5 protein, 10 nM template/primer complex, 10 μM NTPs in the reaction buffer (5mM Tris-HCl pH 7.4, 10mM DTT, 0.5% Triton X-100, 1% glycerol, 3mM $MnCl_2$) in a total volume of 20 μl. The data were quantified using ImageJ (NIH) and fitted to sigmoidal dose-response curves using GraphPad Prism (Dotmatics).

RNA preparation

The DNA templates (Table S3) for each flaviviral RNA were used for *in vitro* transcription in the presence of m7GpppA cap using the TranscriptAid T7 High Yield Transcription Kit (ThermoFisher Scientific). The obtained m7Gp3A capped RNAs were purified using RNA Clean and Concentrator (Zymo Research) and frozen in - 20°C until needed.

MTase activity assay

The methyltransferase activity was measured using the MTase domains of NS5 proteins from NTAV and its mutants, DENV3, WNV, ZIKV, TBEV, JEV and YFV. m7Gp3A capped RNA of the appropriate sequence for each virus (Table S3) was used as a substrate for the MTase assay. The reaction mixture contained 4 μM SAM and 4 μM m7Gp3A capped RNA in the reaction buffer (5 mM Tris pH 8.0, 1 mM TCEP, 0.1 mg/ml BSA, 0.005% Triton X-100, 1 mM $MgCl_2$) and was started by the addition of the MTase to final concentration 0.5 μM in total volume 6 μl. The reaction mixture was incubated at 25°C for 0 – 100 min and analyzed using an Echo system coupled with a Sciex 6500 triple-quadrupole mass spectrometer operating with an electrospray ionization source. The rate of MTase activity was measured as the amount of the product of the reaction, SAH. The spectrometer was run in the multiple-reaction-monitoring (MRM) mode with the interface heated to 350°C. The declustering potential was 20 V, the entrance potential was 10 V, and the collision energy 28 eV. 10 nl of each sample was injected into the mobile phase (flow rate of 0.40 ml/min; 100% methanol). The characteristic product ion of SAH (m/z 385.1 > 134.1) was used for quantification.

QUANTIFICATION AND STATISTICAL ANALYSIS

Crystallographic data collection and processing

Statistics for crystallographic data collection and processing, structure solution and refinement were calculated with the phenix.table_one tool from the Phenix package v1.20.1-4487.[66] These statistics are summarized in Table S1.

Structural basis for broad spectrum binding of AT-9010 to flaviviral methyltransferases

Katerina Krejcova[1], Evzen Boura[1,*]

[1]Institute of Organic Chemistry and Biochemistry, Academy of Sciences of the Czech Republic, v.v.i, Flemingovo nám. 2, 166 10 Prague 6, Czech Republic.

[*]correspondence to boura@uochb.cas.cz

Abstract

AT-9010 (2'-methyl-2'-fluoro guanosine triphosphate) is a GTP analog that is, or more precisely its prodrug AT-752, considered in human medicine as a drug against certain flaviviruses. It was believed to act as an obligatory chain terminator, thereby inhibiting viral replication. However, recently it was discovered that it also binds the GTP binding site of the methyltransferase (MTase) domain of the orthoflavivirus polymerase, thus interfering with proper RNA capping. Here, we investigated the binding of AT-9010 to Ntaya and Zika methyltransferases (MTases). Our structural analysis revealed conserved interactions between AT-9010's base and sugar with key residues in both MTases, though differences in hydrogen bonding were observed. Our analysis also suggested that the triphosphate part of AT-9010 is flexible. Despite these variations, the overall binding mode of AT-9010 remained well conserved across the analyzed flaviviral MTases providing structural basis of AT-9010's efficacy against multiple orthoflavivirus MTases.

Introduction

The family *Flaviviridae* contains four genera [1]. Among them, the NS5 protein of the genus Orthoflavivirus (previously genus Flavivirus) is composed of two domains: the N-terminal methyltransferase (MTase domain) and the C-terminal RdRp domain. The RdRp is a well-described and established antiviral target [2-5]. Several compounds targeting orthoflaviviral RdRps have been described [6-8], including many nucleotide triphosphate analogs such as remdesivir triphosphate and AT-9010 [9-11]. Its active site is homologous to HCV, which explains why most compounds are active against RdRps from the entire *Flaviviridae* family (HCV also belongs to the family *Flaviviridae* but to the genus Hepacivirus).

The orthoflaviviral MTase domain has several enzymatic functions, it binds GTP and acts as a guanylyltransferase and also has two MTase activities: N7 and 2′-O [12] suggesting an important role in viral replication and implicating the MTase domain as an target for antivirals [13, 14].

The development of inhibitors against viral MTases started more than a decade ago [15, 16]. However, MTases, like other viral enzymes, became the focus of scientific scrutiny particularly during the COVID-19 pandemic, when the MTases from SARS-CoV-2 were characterized and specific inhibitors for these enzymes were developed [17-22]. Interestingly, during the same period, MTases from other unrelated viruses, including the Mpox virus, were also characterized, and their inhibitors were developed [23-25]. MTases from the most medically important flaviviruses had already been characterized before the COVID-19 pandemic [3, 4, 26]. Later, during and after the pandemic, crystal structures of flaviviral MTases from lesser-known flaviviruses such as the Usutu, Langat, and Ntaya viruses also became available [27-29].

Most of the MTase inhibitors target the SAM or RNA binding site, with the exception of AT-9010,

which is a fluorinated analog of GTP (2'-methyl-2'-fluoro guanosine triphosphate). The presence of the fluorine atom, instead of a 2′ hydroxyl group, in the ribose ring inevitably leads to the termination of RNA replication when a non-proofreading RNA-dependent RNA polymerase (RdRp) uses it instead of the GTP molecule. Notably, most viral RdRps lack proofreading activity with the exception of Nidovirales where the replication complex includes an exonuclease which enables proofreading [30].

However, as a triphosphate, AT-9010 cannot cross the plasma membrane. To overcome this limitation, prodrugs have been designed: AT-752 and AT-281. Both these prodrugs have low cytotoxicity and are converted to the active triphosphate form within cells through a series of enzymatic reactions [31]. AT-282 and AT-752 were effective against flaviviruses in cell culture [32]. AT-752 also exhibited promising results when tested in the hamster model of yellow fever [33] and was shown to be non-toxic in humans [34]. Due to its chemical structure, it was believed that the sole target is the RdRp. However, it was recently shown that AT-9010 also binds the GTP binding site of the methyltransferase (MTase) domain of the flaviviral RdRp polymerase NS5 [32]. In this study, we decided to analyze the binding mode of AT-9010 with other flaviviral MTases. We chose the Zika and Ntaya MTase domains, solved their crystal structures in complex with AT-9010, and compared the binding modes to that of AT-9010 with the Dengue MTase.

Materials and Methods

Protein expression and purification - Zika and Ntaya MTase domains were cloned into home-made pSUMO vector [35], so that the recombinant protein contained an N-terminal 8x-His-SUMO solubilisation/purification tag. Proteins were expressed and purified as described before [29, 36]. Briefly, the genes for Ntaya and Zika MTase were expressed in *E.coli* BL21-CodonPlus (DE3)

RIL in LB medium. The harvested bacteria were resuspended in lysis buffer containing 50 mM Tris pH 8.0, 500 mM NaCl, 20 mM imidazole, 10% (v/v) glycerol, and 3mM β-mercaptoethanol. The supernatant was then immobilized on Ni-NTA agarose beads (Machery-Nagel) and eluted using lysis buffer supplemented with 300 mM imidazole. Subsequently, the 8x-His-SUMO tag was cleaved by the Ulp1 protease at 4°C overnight while dialyzing against the lysis buffer. The 8x-His-SUMO tag and any traces of uncleaved protein were separated using Ni-NTA agarose beads. Subsequently, the proteins were purified by size exclusion chromatography (SEC) using Superdex 75 16/600 (GE Life Sciences) running in SEC buffer (25 mM HEPES pH 7.5, 500 mM NaCl, 5% (v/v) glycerol, and 1mM TCEP). Finally, the proteins were concentrated to 10 mg/ml and used for crystallization trials or stored in -80°C until needed.

Crystallization and crystallographic analysis. - Crystals of Ntaya and Zika MTase domains grew in 4 days at 18°C in sitting drops. The proteins were mixed 1:1 with the well solution. The composition of well solution for Ntaya was 0.2M Sodium acetate trihydrate, 0.1M Sodium HEPES pH 7.5, 25% (w/v) PEG 3350 and for Zika 0.2 M $MgCl_2$, 0.1 M HEPES pH 7.5, 25% (w/v) PEG 3350.

Crystals of MTases were then soaked with 10 mM compound AT-9010 overnight in presence of 1 mM Mg^{2+}. The soaked crystals were then cryo-protected in well solution supplemented with 20% (v/v) glycerol and flash frozen in liquid nitrogen. The crystals of both Zika and Ntaya MTase domains belonged to the $P2_1$ spacegroup and diffracted to 2 Å and 1.8 Å respectively.

The datasets were collected at our home-source (rotating anode, Rigaku micromax-007 HF). The data was integrated and scaled using XDS [37]. The structures were solved using molecular replacement using the structure of Ntaya MTase (pdb entry: 8QDJ)[29] and Zika MTase (PDB

entry 5MRK)[36]. The initial models were obtained with Phaser from the Phenix package [38]. The models were further improved using automatic model refinement with Phenix.refine followed by manual model building with Coot [39]. Statistics for data collection and processing, structure solution and refinement are summarized in Table 1. Structural figures were generated with the PyMOL Molecular Graphics System v2.0 (Schrödinger, LLC). The atomic coordinates and structural factors were deposited in the Protein Data Bank (https://www.rcsb.org).

Results and Discussion

We prepared crystals of Ntaya and Zika MTases as previously described [29, 36], and soaked them overnight with 10 mM AT-9010. The structures were solved by molecular replacement and the electron density for both expected ligands, AT-9010 and SAH, was clearly visible. The AT-9010 molecule was in both cases located in the GTP binding site, as expected. However, the electron density was better defined for the AT-9010 molecule that was bound to the Ntaya MTase (Figure 1). In fact, in case of the Zika-bound AT-9010 we did not observe any density corresponding to the AT-9010's γ-phosphate and therefore we did not model it. This observation suggests that the γ-phosphate is highly flexible in this case. However, in a previous structural analysis of Zika MTase in complex with GTP, all three phosphates were visible [40].

Both crystal structures had high resolution (2 Å and 1.8 Å) that allowed us to model the ligand precisely and to describe the binding of AT-9010 to both MTase domains in atomic details (Figure 2). The AT9 molecule forms hydrogen bonds with key residues at the GTP binding sites of both Ntaya and Zika, however we noted some differences. In Ntaya MTase, the amino group of the guanine ring forms hydrogen bonds with the main chains of Leu16 and Leu19 (Figure 2A), while in Zika MTase, there is an additional interaction with the main chain of residue Asn17 (Figure

2B). The 3′-hydroxyl group of the modified ribose ring interacts with main chains of Ser151 and Pro152 and side chain of Lys13 in the Ntaya MTase. However, Lys13 adopts a slightly different conformation in the Zika MTase, positioning its amino group 4.5 Å away from the 3′-hydroxyl group of the sugar, thereby not allowing for the formation of a hydrogen bond. In addition, Zika has a serine residue at position 152 (Figure 2D) which does not form a hydrogen bond with the sugar ring whereas the Pro152 in Ntaya does. As stated above, in the Ntaya MTase structure bound with AT9, all three phosphate groups are present, whereas in the Zika MTase structure the γ-phosphate group was not modeled as we did not observe any electron density for it. We suspected that the electrostatic interactions might be responsible. However, our analysis revealed that in both cases the phosphates are located in a highly positively charged canyon (Figure 3).

Next, we compared binding of AT-9010 in Ntaya and Zika MTases and compared it to the binding of GTP (Figure 4A, B). We observed that the positions of the base, sugar, and α-phosphate are more or less conserved. While the β- and γ-phosphates are flexible. Comparison of AT-9010 binding mode in Ntaya, Zika and Dengue MTases also revealed conserved position of the sugar and base (Figure 4C, D). Taken together, we observed that the binding mode of AT-9010 is conserved in flaviviral MTases especially for the base and sugar. However, differences do exist, as documented by the comparison of the Zika and Ntaya structures where the sugar part of AT-9010 form significantly more hydrogen bonds with Ntaya MTase as compared to Zika. In each case, structural comparisons revealed flexibility in the triphosphate portion of the AT-9010 molecule. One contributing factor is residue 28, which may be either lysine or arginine. Zika has a lysine at this position, forming a hydrogen bond with the α-phosphate, whereas Ntaya's Arg28 does not. However, the AT-9010 binding mode is sufficiently conserved, thereby providing a structural basis for the function of AT-9010 against multiple orthoflavivirus MTases.

Declaration of Generative AI and AI-assisted technologies in the writing process

During the preparation of this work ChatGPT 3.5 was used in order to check spelling and to correct the grammar. After using this tool, the authors reviewed and edited the content and take full responsibility for the content of the publication.

Declaration of Competing Interest

The authors declare no competing interests.

Data availability

The structures and related structure factors were deposited in the PDB database under the accession codes 9GJZ (Ntaya MTase in complex with AT-9010) and 8PEM (Zika MTase in complex with AT-9010).

Acknowledgment

This research was funded by the project the National Institute Virology and Bacteriology (Programme EXCELES, Project No. LX22NPO5103) - Funded by the European Union - Next Generation EU. RVO: 61388963 is also acknowledged.

Author Contribution

K.K. performed experiments, analyzed data and prepared the figures. E.B. conceived the project, analyzed data and wrote the manuscript.

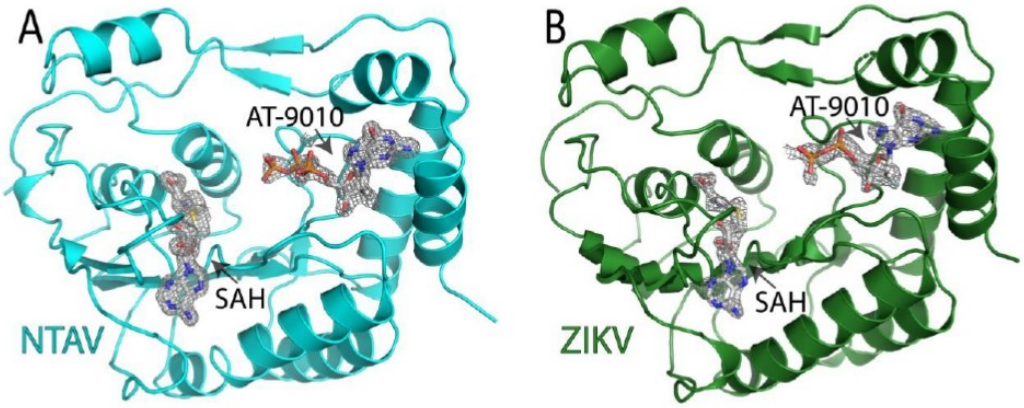

Figure 1. **Crystal structure of Ntaya and Zika MTase domains in complex with AT-9010 and SAH.** A) Overall structure of the Ntaya MTase domain with bound AT-9010 and SAH is shown. The Fo-Fc omit electron density maps contoured at 3σ are displayed for the AT-9010 and SAH molecules. B) Overall structure of the Zika MTase domain with bound AT-9010 and SAH is shown. The Fo-Fc omit electron density map is contoured at 3σ for the SAH molecule and at 2σ for the AT-9010.

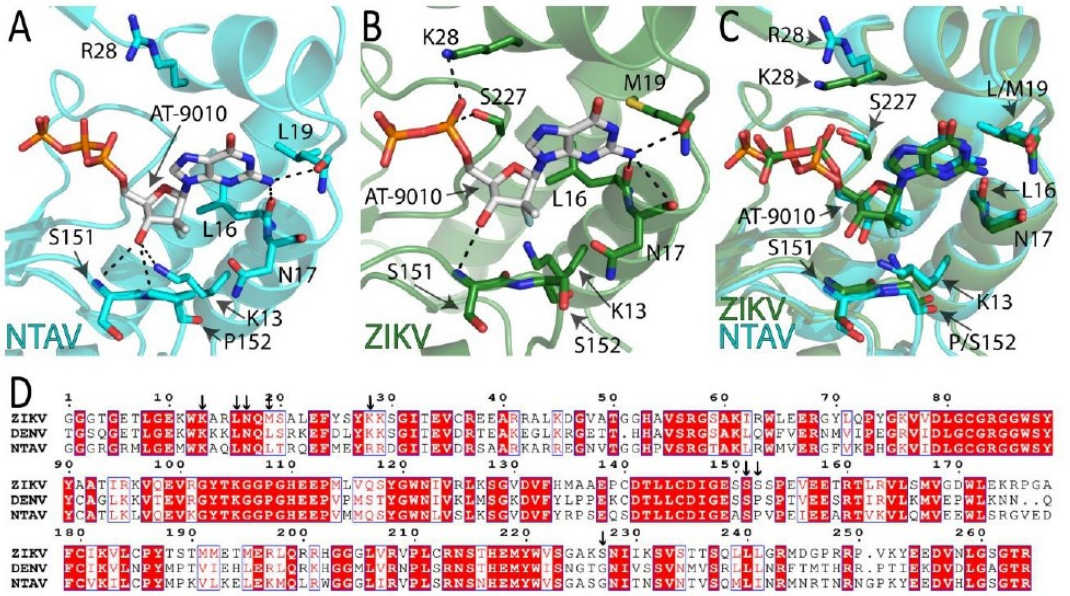

Figure 2: **Binding of AT-9010 to the Ntaya and Zika MTase domains.** A) A detailed view of residues of the GTP binding site of the Ntaya MTase domain that interact with AT-9010. Hydrogen bonds are depicted, and key residues are labeled. B) A detailed view of AT-9010 bound to residues of the GTP binding site of the Zika MTase domain that interact with AT-9010. Hydrogen bonds are depicted, and key residues are labeled. C) Structural alignment of the AT-9010 binding sites of Ntaya (cyan) and Zika (green). The phosphors of AT-9010 in Ntaya structure are colored orange, and those in Zika are colored green. Key residues are labeled. D) Primary sequence alignment of selected flaviviral MTase domains. Conserved residues are highlighted in red. The alignment was generated using the ESPript 3.0 online program (https://espript.ibcp.fr/ESPript/ESPript/).

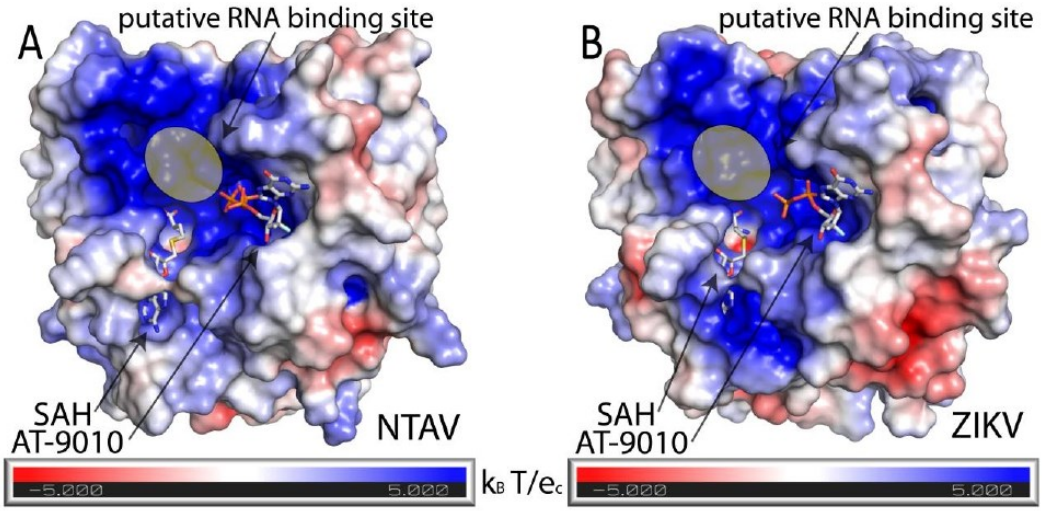

Figure 3: Electrostatic potential visualization of Ntaya and Zika MTase domains in complex with AT-9010 and SAH. A/B) The surface of Ntaya (panel A) and Zika (panel B) MTase domains is colored according to the electrostatic potential from red (negative charge) to blue (positive charge). AT-9010 and SAH are shown in stick representation and labeled. The putative RNA binding site is highlighted.

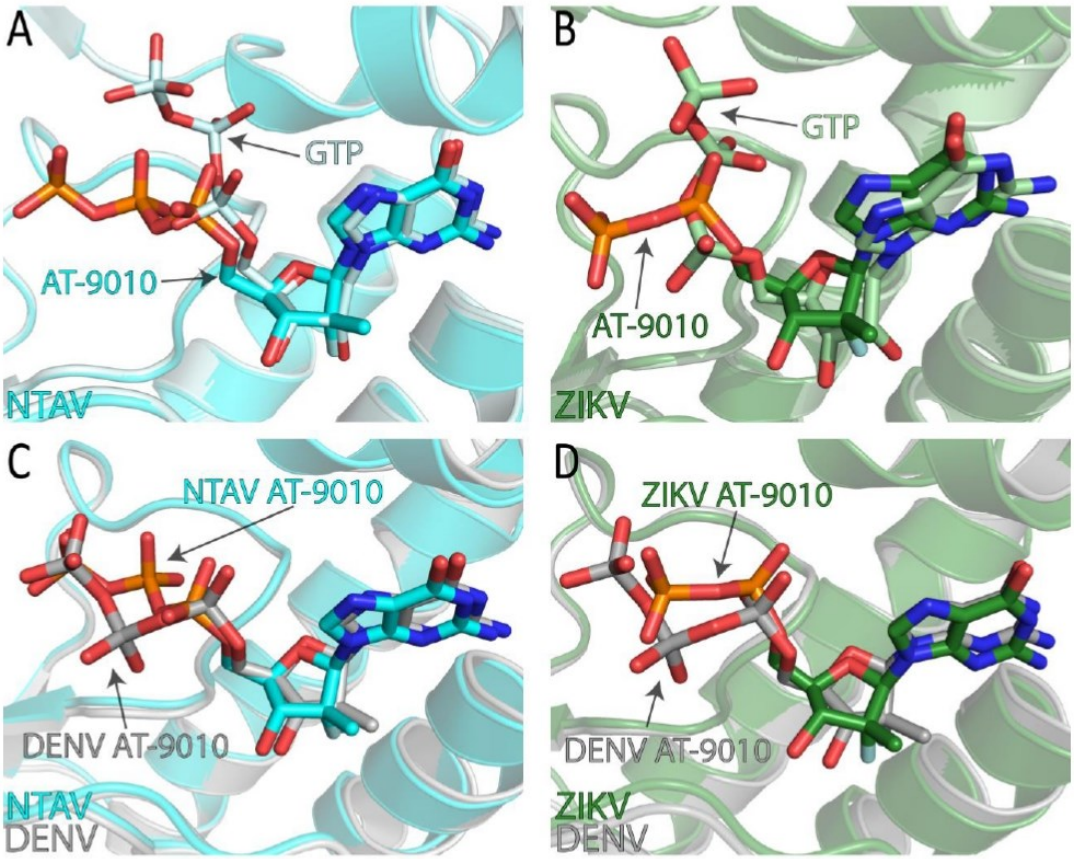

Figure 4: **Structural comparison of selected flaviviral MTase domains bound to AT-9010 or GTP.** A) Structural alignment of the Ntaya MTase domain bound to AT-9010 (cyan) and GTP (palecyan, PDB ID: 8CQH). The phosphors of AT-9010 are colored orange, and those of GTP are colored palecyan. B) Structural alignment of the Zika MTase domain bound to AT-9010 (green) and GTP (palegreen, PDB ID: 5GOZ). The phosphors of AT-9010 are colored orange, and those of GTP are colored palegreen C) Structural comparison of Ntaya (cyan) and Dengue (gray, PDB ID: 8BCR) MTase domains bound to AT-9010. The phosphors of AT-9010 interacting with Ntaya MTase are colored orange, and those interacting with Dengue MTase are colored grey. D) Structural comparison of Zika (green) and Dengue (gray, PDB ID: 8BCR) MTase domains bound to AT-9010. The phosphors of AT-9010 in Zika MTase structure are colored orange, and those in the Dengue are colored grey.

Crystal	Zika MTase+AT9010	Ntaya MTase+AT9010
PDB accession code	8PEM	
Data collection and processing		
Space group	$P2_1$	$P2_1$
Cell dimensions - a, b, c (Å)	39.56, 41.02, 69.03	38.33, 71.58, 50.33
Cell dimensions - α, β, γ (°)	90.00, 96.25, 90.00	90, 92.64, 90
Resolution range (Å)	28.38 – 2 (2.074–2.002)	35.79 - 1.74 (1.81 - 1.74)
No. of unique reflections	14679 (1430)	49191 (5018)
Completeness (%)	97.20(94.75)	95.24 (87.59)
Multiplicity	3.2 (3.2)	1.8 (1.8)
Mean I/σ(I)	4.90 (1.24)	6.87 (1.32)
$CC_{1/2}$	0.975 (0.385)	0.991 (0.443)
CC*	0.994 (0.746)	0.998 (0.784)
Structure solution and refinement		
R-work (%)	22.82 (30.60)	17.28 (26.16)
R-free (%)	26.21 (32.47)	20.03 (27.35)
R.m.s.d. - bonds (Å) / angles (°)	0.003 / 0.69	0.006 / 0.86
Average B factors ($Å^2$)	21.65	18.64
protein	21.39	17.02
ligand	36.96	24.79
solvent	21.58	27.44
Clashscore	2.5	3.98
Ramachandran favored/outliers (%)	98.05 / 0	98.85 / 0

Table 1. **Data-collection and processing statistics.** Values in parentheses are for the highest resolution shell.

1. Postler, T.S., M. Beer, B.J. Blitvich, J. Bukh, X. de Lamballerie, J.F. Drexler, A. Imrie, A. Kapoor, G.G. Karganova, P. Lemey, V. Lohmann, P. Simmonds, D.B. Smith, J.T. Stapleton, and J.H. Kuhn, *Renaming of the genus*

and extension of binomial species names within the family. Archives of Virology, 2023. **168**(9).
2. Yap, T.L., T. Xu, Y.L. Chen, H. Malet, M.P. Egloff, B. Canard, S.G. Vasudevan, and J. Lescar, *Crystal structure of the dengue virus RNA-dependent RNA polymerase catalytic domain at 1.85-angstrom resolution.* J Virol, 2007. **81**(9): p. 4753-65.
3. Dubankova, A. and E. Boura, *Structure of the yellow fever NS5 protein reveals conserved drug targets shared among flaviviruses.* Antiviral Res, 2019. **169**: p. 104536.
4. Upadhyay, A.K., M. Cyr, K. Longenecker, R. Tripathi, C. Sun, and D.J. Kempf, *Crystal structure of full-length Zika virus NS5 protein reveals a conformation similar to Japanese encephalitis virus NS5.* Acta Crystallogr F Struct Biol Commun, 2017. **73**(Pt 3): p. 116-122.
5. Sebera, J., A. Dubankova, V. Sychrovsky, D. Ruzek, E. Boura, and R. Nencka, *The structural model of Zika virus RNA-dependent RNA polymerase in complex with RNA for rational design of novel nucleotide inhibitors.* Sci Rep, 2018. **8**(1): p. 11132.
6. Noble, C.G., S.P. Lim, Y.L. Chen, C.W. Liew, L. Yap, J. Lescar, and P.Y. Shi, *Conformational flexibility of the Dengue virus RNA-dependent RNA polymerase revealed by a complex with an inhibitor.* J Virol, 2013. **87**(9): p. 5291-5.
7. Arora, R., C.W. Liew, T.S. Soh, D.A. Otoo, C.C. Seh, K. Yue, S. Nilar, G. Wang, F. Yokokawa, C.G. Noble, Y.L. Chen, P.Y. Shi, J. Lescar, T.M. Smith, T.E. Benson, and S.P. Lim, *Two RNA Tunnel Inhibitors Bind in Highly Conserved Sites in Dengue Virus NS5 Polymerase: Structural and Functional Studies.* Journal of Virology, 2020. **94**(24).
8. Konkolova, E., K. Krejcova, L. Eyer, J. Hodek, M. Zgarbova, A. Fortova, M. Jirasek, F. Teply, P.E. Reyes-Gutierrez, D. Ruzek, J. Weber, and E. Boura, *A Helquat-like Compound as a Potent Inhibitor of Flaviviral and Coronaviral Polymerases.* Molecules, 2022. **27**(6).
9. Good, S.S., J. Westover, K.H. Jung, X.J. Zhou, A. Moussa, P. La Colla, G. Collu, B. Canard, and J.P. Sommadossi, *AT-527, a Double Prodrug of a Guanosine Nucleotide Analog, Is a Potent Inhibitor of SARS-CoV-2 In Vitro and a Promising Oral Antiviral for Treatment of COVID-19.* Antimicrob Agents Chemother, 2021. **65**(4).
10. Konkolova, E., M. Dejmek, H. Hrebabecky, M. Sala, J. Boserle, R. Nencka, and E. Boura, *Remdesivir triphosphate can efficiently inhibit the RNA-dependent RNA polymerase from various flaviviruses.* Antiviral Res, 2020. **182**: p. 104899.
11. Milisavljevic, N., E. Konkolova, J. Kozak, J. Hodek, L. Veselovska, V. Sykorova, K. Cizek, R. Pohl, L. Eyer, P. Svoboda, D. Ruzek, J. Weber, R. Nencka, E. Boura, and M. Hocek, *Antiviral Activity of 7-Substituted 7-Deazapurine Ribonucleosides, Monophosphate Prodrugs, and Triphoshates against Emerging RNA Viruses.* ACS Infect Dis, 2021. **7**(2): p. 471-478.
12. Dong, H., K. Fink, R. Zust, S.P. Lim, C.F. Qin, and P.Y. Shi, *Flavivirus RNA methylation.* J Gen Virol, 2014. **95**(Pt 4): p. 763-778.
13. Song, W., H. Zhang, Y. Zhang, Y. Chen, Y. Lin, Y. Han, and J. Jiang, *Identification and Characterization of Zika Virus NS5 Methyltransferase Inhibitors.* Front Cell Infect Microbiol, 2021. **11**: p. 665379.
14. Delgado-Maldonado, T., A. Moreno-Herrera, G. Pujadas, L.K. Vazquez-Jimenez, A. Gonzalez-Gonzalez, and G. Rivera, *Recent advances in the development of methyltransferase (MTase) inhibitors against (re)emerging arboviruses diseases dengue and Zika.* Eur J Med Chem, 2023. **252**: p. 115290.
15. Dong, H., B. Zhang, and P.Y. Shi, *Flavivirus methyltransferase: a novel antiviral target.* Antiviral Res, 2008. **80**(1): p. 1-10.
16. Milani, M., E. Mastrangelo, M. Bollati, B. Selisko, E. Decroly, M. Bouvet, B. Canard, and M. Bolognesi, *Flaviviral methyltransferase/RNA interaction: Structural basis for enzyme inhibition.* Antiviral Research, 2009. **83**(1): p. 28-34.
17. Kottur, J., O. Rechkoblit, R. Quintana-Feliciano, D. Sciaky, and A.K. Aggarwal, *High-resolution structures of the SARS-CoV-2 N7-methyltransferase inform therapeutic development.* Nat Struct Mol Biol, 2022. **29**(9): p. 850-853.
18. Ahmed-Belkacem, R., M. Hausdorff, A. Delpal, P. Sutto-Ortiz, A.M.G. Colmant, F. Touret, N.S. Ogando,

E.J. Snijder, B. Canard, B. Coutard, J.J. Vasseur, E. Decroly, and F. Debart, *Potent Inhibition of SARS-CoV-2 nsp14 N7-Methyltransferase by Sulfonamide-Based Bisubstrate Analogues.* J Med Chem, 2022. **65**(8): p. 6231-6249.
19. Otava, T., M. Sala, F. Li, J. Fanfrlik, K. Devkota, S. Perveen, I. Chau, P. Pakarian, P. Hobza, M. Vedadi, E. Boura, and R. Nencka, *The Structure-Based Design of SARS-CoV-2 nsp14 Methyltransferase Ligands Yields Nanomolar Inhibitors.* ACS Infect Dis, 2021. **7**(8): p. 2214-2220.
20. Zilecka, E., M. Klima, M. Stefek, M. Dejmek, R. Nencka, and E. Boura, *Structure of SARS-CoV-2 MTase nsp14 with the inhibitor STM957 reveals inhibition mechanism that is shared with a poxviral MTase VP39.* Journal of Structural Biology: X, 2024: p. 100109.
21. Kocek, H., D. Chalupská, M. Dejmek, A. Dvořáková, M. Zgarbová, M. Šála, K. Chalupský, P. Krafčíková, T. Otava, and M. Drexler, *Discovery of highly potent SARS-CoV-2 nsp14 methyltransferase inhibitors based on adenosine 5'-carboxamides.* RSC Medicinal Chemistry, 2024.
22. Klima, M., A. Khalili Yazdi, F. Li, I. Chau, T. Hajian, A. Bolotokova, H.U. Kaniskan, Y. Han, K. Wang, D. Li, M. Luo, J. Jin, E. Boura, and M. Vedadi, *Crystal structure of SARS-CoV-2 nsp10-nsp16 in complex with small molecule inhibitors, SS148 and WZ16.* Protein Sci, 2022. **31**(9): p. e4395.
23. Silhan, J., M. Klima, D. Chalupska, J. Kozic, and E. Boura, *The structure of monkeypox virus 2'-O-ribose methyltransferase VP39 in complex with sinefungin provides the foundation for inhibitor design.* bioRxiv, 2022: p. 2022.09. 27.509668.
24. Skvara, P., D. Chalupska, M. Klima, J. Kozic, J. Silhan, and E. Boura, *Structural basis for RNA-cap recognition and methylation by the mpox methyltransferase VP39.* Antiviral Res, 2023. **216**: p. 105663.
25. Zgarbova, M., T. Otava, J. Silhan, R. Nencka, J. Weber, and E. Boura, *Inhibitors of mpox VP39 2'-O methyltransferase efficiently inhibit the monkeypox virus.* Antiviral Res, 2023. **218**: p. 105714.
26. Yap, L.J., D. Luo, K.Y. Chung, S.P. Lim, C. Bodenreider, C. Noble, P.Y. Shi, and J. Lescar, *Crystal structure of the dengue virus methyltransferase bound to a 5'-capped octameric RNA.* PLoS One, 2010. **5**(9).
27. Ferrero, D.S., L. Albentosa-Gonzalez, A. Mas, and N. Verdaguer, *Structure and function of the NS5 methyltransferase domain from Usutu virus.* Antiviral Res, 2022. **208**: p. 105460.
28. Li, R., Z. Niu, Y. Liu, X. Bai, D. Wang, and C. Chen, *Crystal structure and cap binding analysis of the methyltransferase of langat virus.* Antiviral Res, 2022. **208**: p. 105459.
29. Krejcova, K., P. Krafcikova, M. Klima, D. Chalupska, K. Chalupsky, E. Zilecka, and E. Boura, *Structural and functional insights in flavivirus NS5 proteins gained by the structure of Ntaya virus polymerase and methyltransferase.* Structure, 2024.
30. Posthuma, C.C., A.J.W. Te Velthuis, and E.J. Snijder, *Nidovirus RNA polymerases: Complex enzymes handling exceptional RNA genomes.* Virus Res, 2017. **234**: p. 58-73.
31. Good, S.S., A. Shannon, K. Lin, A. Moussa, J.G. Julander, P. La Colla, G. Collu, B. Canard, and J.P. Sommadossi, *Evaluation of AT-752, a Double Prodrug of a Guanosine Nucleotide Analog with In Vitro and In Vivo Activity against Dengue and Other Flaviviruses.* Antimicrob Agents Chemother, 2021. **65**(11): p. e0098821.
32. Feracci, M., C. Eydoux, V. Fattorini, L. Lo Bello, P. Gauffre, B. Selisko, P. Sutto-Ortiz, A. Shannon, H.J. Xia, P.Y. Shi, M. Noel, F. Debart, J.J. Vasseur, S. Good, K. Lin, A. Moussa, J.P. Sommadossi, A. Chazot, K. Alvarez, J.C. Guilemot, E. Decroly, F. Ferron, and B. Canard, *AT-752 targets multiple sites and activities on the Dengue virus replication enzyme NS5.* Antiviral Research, 2023. **212**.
33. Lin, K., S.S. Good, J.G. Julander, A.E. Weight, A. Moussa, and J.P. Sommadossi, *AT-752, a double prodrug of a guanosine nucleotide analog, inhibits yellow fever virus in a hamster model.* PLoS Negl Trop Dis, 2022. **16**(1): p. e0009937.
34. Zhou, X.J., J. Lickliter, M. Montrond, L. Ishak, K. Pietropaolo, D. James, B. Belanger, A. Horga, and J. Hammond, *First-in-human trial evaluating safety and pharmacokinetics of AT-752, a novel nucleotide prodrug with pan-serotype activity against dengue virus.* Antimicrob Agents Chemother, 2024. **68**(5): p. e0161523.
35. Dubankova, A., V. Horova, M. Klima, and E. Boura, *Structures of kobuviral and siciniviral polymerases reveal conserved mechanism of picornaviral polymerase activation.* J Struct Biol, 2019. **208**(2): p. 92-98.
36. Hercik, K., J. Brynda, R. Nencka, and E. Boura, *Structural basis of Zika virus methyltransferase inhibition by sinefungin.* Arch Virol, 2017. **162**(7): p. 2091-2096.
37. Kabsch, W., *Xds.* Acta Crystallogr D Biol Crystallogr, 2010. **66**(Pt 2): p. 125-32.
38. Liebschner, D., P.V. Afonine, M.L. Baker, G. Bunkoczi, V.B. Chen, T.I. Croll, B. Hintze, L.W. Hung, S. Jain, A.J. McCoy, N.W. Moriarty, R.D. Oeffner, B.K. Poon, M.G. Prisant, R.J. Read, J.S. Richardson, D.C. Richardson, M.D. Sammito, O.V. Sobolev, D.H. Stockwell, T.C. Terwilliger, A.G. Urzhumtsev, L.L. Videau,

C.J. Williams, and P.D. Adams, *Macromolecular structure determination using X-rays, neutrons and electrons: recent developments in Phenix.* Acta Crystallographica Section D-Structural Biology, 2019. **75**: p. 861-877.

39. Emsley, P., B. Lohkamp, W.G. Scott, and K. Cowtan, *Features and development of Coot.* Acta Crystallogr D Biol Crystallogr, 2010. **66**(Pt 4): p. 486-501.
40. Zhang, C., T. Feng, J. Cheng, Y. Li, X. Yin, W. Zeng, X. Jin, Y. Li, F. Guo, and T. Jin, *Structure of the NS5 methyltransferase from Zika virus and implications in inhibitor design.* Biochem Biophys Res Commun, 2016.

molecules

MDPI

Article

A Helquat-like Compound as a Potent Inhibitor of Flaviviral and Coronaviral Polymerases

Eva Konkolova [1,†], Kateřina Krejčová [1,†], Luděk Eyer [2,†], Jan Hodek [1], Michala Zgarbová [1], Andrea Fořtová [2], Michael Jirasek [1], Filip Teply [1], Paul E. Reyes-Gutierrez [1], Daniel Růžek [2,3,4], Jan Weber [1] and Evzen Boura [1,*]

[1] Institute of Organic Chemistry and Biochemistry, Academy of Sciences of the Czech Republic, v.v.i., Flemingovo nám. 2, 16610 Prague, Czech Republic; eva.konkolova@uochb.cas.cz (E.K.); krejcova@uochb.cas.cz (K.K.); jan.hodek@uochb.cas.cz (J.H.); michala.zgarbova@uochb.cas.cz (M.Z.); michal.jirasek@uochb.cas.cz (M.J.); filip.teply@uochb.cas.cz (F.T.); reyes.gutierrez@uochb.cas.cz (P.E.R.-G.); jan.weber@uochb.cas.cz (J.W.)
[2] Laboratory of Emerging Viral Diseases, Veterinary Research Institute, Hudcova 296/70, 62100 Brno, Czech Republic; eyer@vri.cz (L.E.); andrea.fortova@vri.cz (A.F.); ruzekd@paru.cas.cz (D.R.)
[3] Institute of Parasitology, Biology Centre of the Czech Academy of Sciences, Branišovská 1160/31, 37005 Ceske Budejovice, Czech Republic
[4] Department of Experimental Biology, Faculty of Science, Masaryk University, 62500 Brno, Czech Republic
* Correspondence: boura@uochb.cas.cz
† These authors contributed equally to this work.

Abstract: Positive-sense single-stranded RNA (+RNA) viruses have proven to be important pathogens that are able to threaten and deeply damage modern societies, as illustrated by the ongoing COVID-19 pandemic. Therefore, compounds active against most or many +RNA viruses are urgently needed. Here, we present PR673, a helquat-like compound that is able to inhibit the replication of SARS-CoV-2 and tick-borne encephalitis virus in cell culture. Using in vitro polymerase assays, we demonstrate that PR673 inhibits RNA synthesis by viral RNA-dependent RNA polymerases (RdRps). Our results illustrate that the development of broad-spectrum non-nucleoside inhibitors of RdRps is feasible.

Keywords: helquat-like compound; RNA-dependent RNA-polymerase; SARS-CoV-2; Flaviviruses; antiviral agents

Citation: Konkolova, E.; Krejčová, K.; Eyer, L.; Hodek, J.; Zgarbová, M.; Fořtová, A.; Jirasek, M.; Teply, F.; Reyes-Gutierrez, P.E.; Růžek, D.; et al. A Helquat-like Compound as a Potent Inhibitor of Flaviviral and Coronaviral Polymerases. *Molecules* **2022**, *27*, 1894. https://doi.org/10.3390/molecules27061894

Academic Editors: Francesc Xavier Ruiz and Joy Y. Feng

Received: 21 February 2022
Accepted: 9 March 2022
Published: 15 March 2022

1. Introduction

Flaviviruses (family *Flaviviridae*) and coronaviruses (family *Coronaviridae*) both belong among single-stranded positive-sense RNA (+RNA) viruses. Members of these viral families include important human pathogens, such as the yellow fever virus (YFV), Zika virus (ZIKV), tick-borne encephalitis virus (TBEV), West Nile virus (WNV), Middle East respiratory syndrome coronavirus (MERS-CoV), severe acute respiratory syndrome coronavirus (SARS-CoV), OC43 coronavirus (OC43-CoV) and the severe acute respiratory syndrome coronavirus 2 (SARS-CoV-2) [1–4]. Unfortunately, both families have proved that they hold pandemic potential, as demonstrated recently by the ZIKV, MERS-CoV and SARS-CoV outbreaks [5–8]. Nonetheless, the ZIKV, MERS-CoV and SARS-CoV viruses were contained. It was the SARS-CoV-2 that revealed the full potential of +RNA viruses to cause harm to humans. According to the WHO (https://covid19.who.int/, accessed on 20 February 2022), the COVID-19 pandemic has already claimed 6 million lives worldwide at the beginning of March 2022.

Small molecule-based antiviral treatments are urgently needed. The first FDA-approved small molecule to be used against COVID-19 was remdesivir [9], and recently orally available drugs molnupiravir and Paxlovid were approved in several countries as well. Molnupiravir targets the RNA-dependent RNA polymerase (RdRp), a key enzyme in the replication of RNA viruses [10]. The primary target of Paxlovid is the SARS-CoV-2 main protease, which is involved in the processing of the coronaviral polyprotein [11]. Importantly, new

SARS-CoV-2 variants, such as omicron, that partially escape vaccine-induced immunity are sensitive to these compounds [12]. In addition, other coronaviral enzymes, including exonuclease, endonuclease, helicase and methyltransferase, have recently been biochemically and structurally described [13–17], and their inhibitors have been reported [18–21]; however, none of these compounds have been developed enough to enter clinical trials. Furthermore, often, the simultaneous administration of several compounds is necessary to efficiently combat a virus and to prevent the development of escape mutants, as illustrated by the highly efficient highly active antiretroviral therapy (HAART) against the HIV virus [22].

Here, we present compound PR673 bearing a rather unusual helquat-like chemical structure (Figure 1A) that was discovered while screening against the SARS-CoV-2 virus, but is actually more active against flaviviruses. We use in vitro polymerase assays to show that this compound interferes with RNA syntheses performed by the viral RdRps.

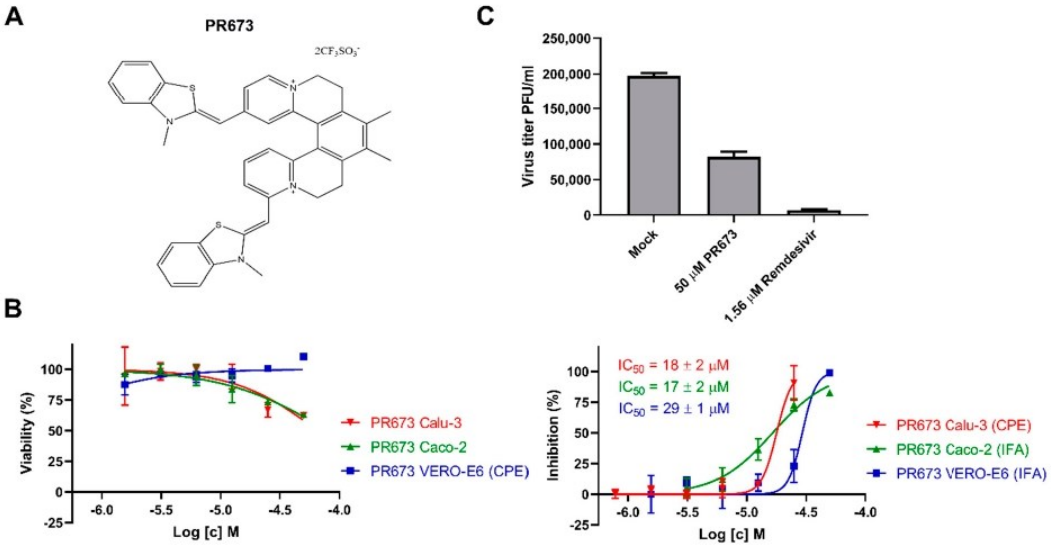

Figure 1. Inhibitory activity of PR673 against SARS-CoV-2. (**A**) The chemical structure of PR673. (**B**) Left panels: dependence of viability of VERO-E6, Calu-3 and Caco-2 cells on PR673 concentration; right panels: dependence of inhibition of SARS-CoV-2 in VERO-E6, Calu-3 and Caco-2 cells on PR673 concentration. (**C**) Comparison of PR673 and remdesivir in SARS-CoV-2 yield reduction assay. The VERO-E6 cells were incubated with PR673, remdesivir and a mock followed by SARS-CoV-2 infection at MOI 0.04 for 3 days, and the virus yield was determined by plaque assay in VERO-E6 cells.

2. Results

2.1. Identification of PR673

We screened the IOCB library [23] using a phenotypic assay against SARS-CoV-2. Briefly, the IOCB-library compounds were screened at a 64 µM concentration in triplicates in VERO-E6 cells against SARS-CoV-2, and the inhibition of the virus-induced cytopathic effect (CPE) was monitored. We identified an interesting helquat-like compound (PR673) (Figure 1A) that inhibited the replication of the virus in VERO-E6 cells. This activity was further verified in VERO-E6 and Caco-2 cells using SARS-CoV-2 nucleoprotein expression detected by the immunofluorescence assay (IFA) (Figure 1B, Supplementary Figure S1), which we could also confirm using the protection of cells from the virus-induced cytopathic effect (CPE) in Calu-3 cells (Figure 1B). PR673 inhibited SARS-CoV-2 with an EC_{50} value of 29 µM in VERO-E6 cells (Figure 1B) and yielded a 58% reduction in viral plaques at 50 µM (Figure 1C), while exhibiting no cell toxicity in Vero E6 cells (Figure 1B). The compound effectively inhibited virus-induced CPE in Calu-3 cells and virus replication in Caco-2 cells, with EC_{50} values of 18 µM and 17 µM, respectively. We observed mild cytotoxicity at the highest used concentration for Caco-2 and Calu-3 cell lines, but the CC_{50} of PR673 for both

cell lines was above 50 μM (Figure 1B). Nonetheless, it must be noted that PR673 was much less active than the COVID-19 drug remdesivir (Figure 1C).

2.2. PR673 Inhibits the Coronaviral RdRp

We next aimed to discover the molecular target of this compound. Based on the chemical structure, we speculated that the RdRp is the target of PR673. The SARS-CoV-2 RdRp is a heterotrimeric protein complex composed of nsp7, nsp8 and nsp12. We prepared this RdRp recombinantly, as reported before [21], and measured the inhibitory activity of PR673. Indeed, it targeted the SARS-CoV-2 RdRp: the synthesis of RNA was totally blocked at a PR673 concentration above 12.5 μM (Figure 2, SARS-CoV-2 panel).

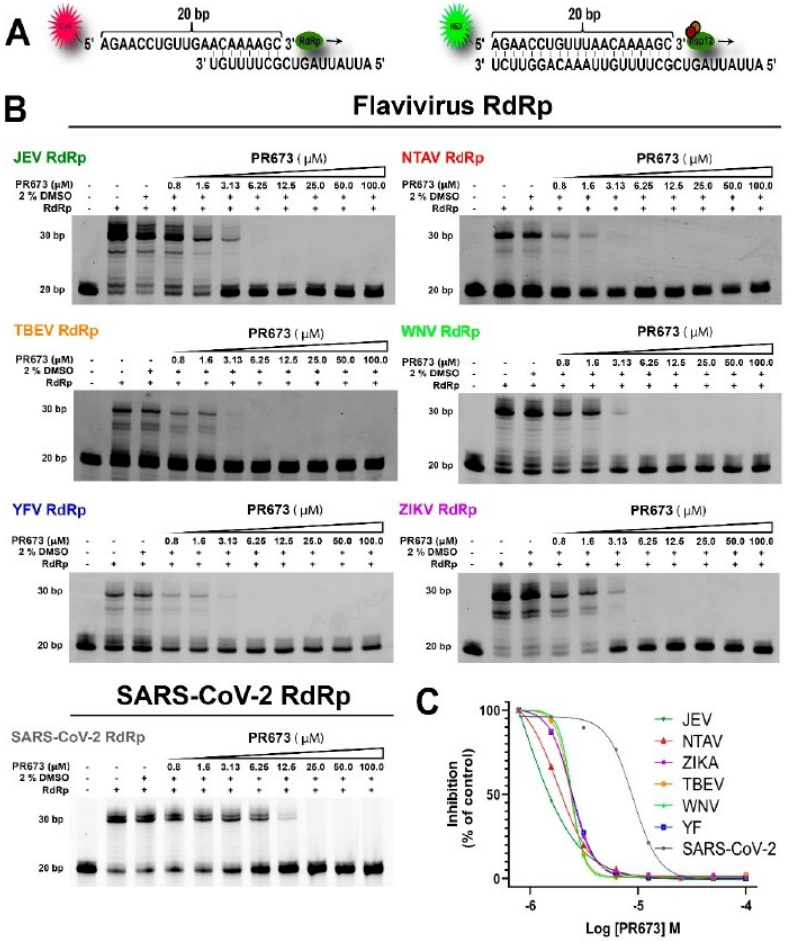

Figure 2. Analysis of PR673 inhibitory activity against various RdRps using a primer extension assay. (**A**) The RNA primer and RNA templates used in this assay. The RNA primer contains a fluorescent label at the 5′ end (Cy5 or Hex for flaviviral RdRp, or SARS-CoV-2 RdRp, respectively). The arrow indicates the direction of primer extension. (**B**) Serial dilutions of PR673 (in μM), as indicated on the top of the gel, and a constant concentration of the polymerase (20 nM) and template/primer (10 nM) were used in the assay. The reactions were initiated by adding 10 μM NTPs. The reactions continued at 33 °C for 1 h; then, the reactions were stopped by the addition of stop buffer, and the products were separated on denaturing polyacrylamide gels. (**C**) The percentages of inhibition (against control) in panel B were plotted against the logarithm of concentrations of PR673; the results were fitted to sigmoidal dose–response curves.

2.3. PR673 Inhibitory Activity against Flaviviral RdRps

Further, we sought to decipher whether PR673 inhibited other viral RdRps. We chose several members of the *Flaviviridae* family, namely the Japanese encephalitis virus (JEV), Ntaya virus (NTAV), tick-borne encephalitis virus (TBEV), yellow fever virus (YFV) and Zika virus (ZIKV), and we prepared their polymerases recombinantly. In each case, we observed a strong inhibition of RNA synthesis in low micromolar concentrations of PR673 (Figures 2 and 3).

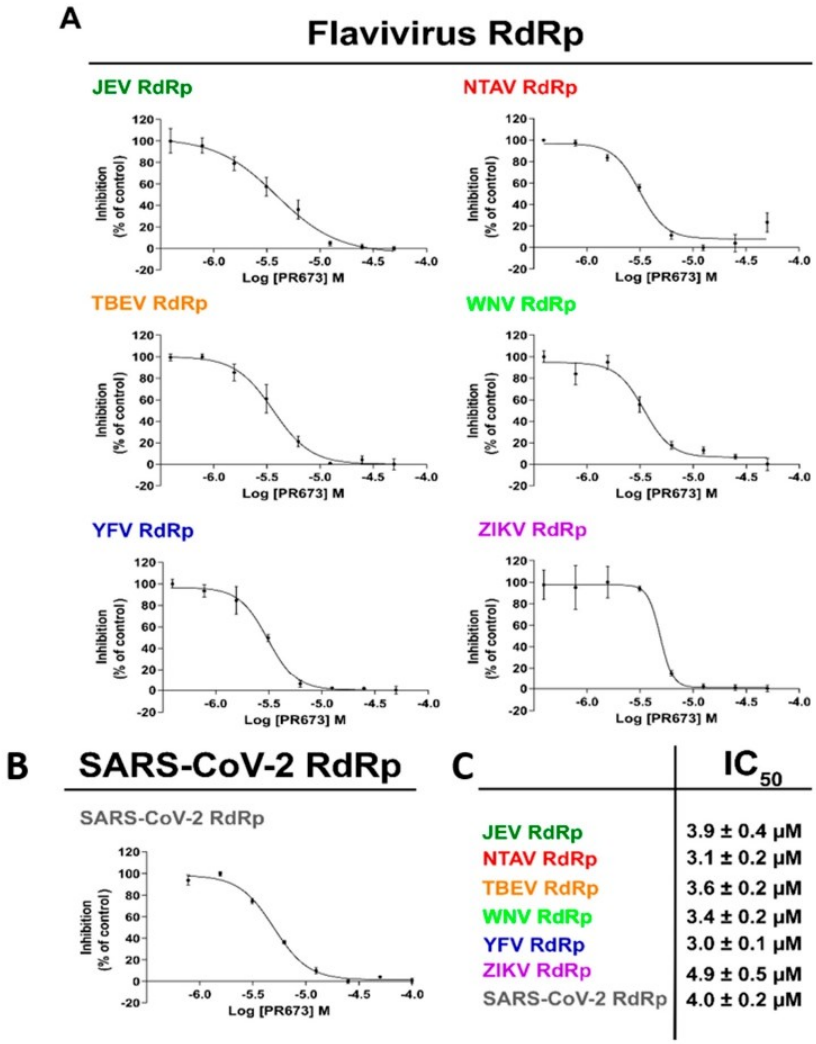

Figure 3. Measurement of the IC_{50} values of PR673. The IC_{50} values were established for each tested polymerase with PR673 using radioactively labeled elongation products. (**A**) The RNA hairpin used in this assay. The arrow indicates the direction of primer extension. (**B**) The percentages of inhibition (against control) were plotted against the logarithm of concentrations of PR673, and the results were fitted to sigmoidal dose–response curves. Error bars represent the standard error of three independent measurements. (**C**) The table of IC_{50} values. The IC_{50} values were extrapolated from $LogIC_{50}$ according to the GraphPad algorithm.

We then established IC_{50} values for each of the aforementioned RdRp enzymes using a radioactive assay because it is more sensitive and accurate than alternative methods. The reaction mixture contained the viral RdRp, the hairpin-containing RNA as the template

and radioactively labeled ATP ([α-^{32}P]-ATP). Our results showed that PR673 inhibits all of the tested polymerases, with IC_{50} values ranging from 3.0 ± 0.1 μM to 4.9 ± 0.5 μM (Figure 4). The yellow fever virus RdRp was inhibited the most and the Zika RdRp the least; however, the observed differences were rather low.

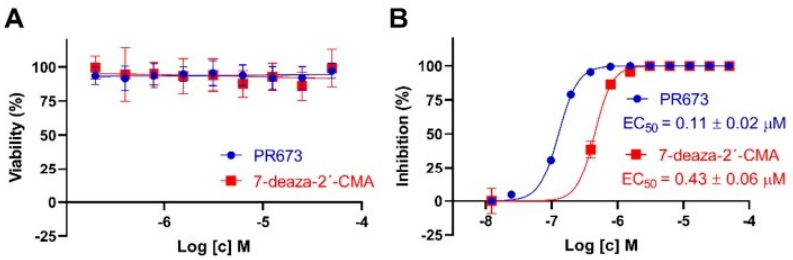

Figure 4. Cytotoxicity and anti-TBEV activity of PR673 in PS cells. (**A**) Cytotoxicity of PR673 for PS cells expressed as percentage of cell viability at the indicated drug concentrations. The cells were seeded in 96-well plates for 24 h, then treated with the compounds and incubated for 48 h. Cell viabilities were measured by Cell Counting Kit-8. (**B**) Anti-TBEV activity of PR673 in PS cells. The cell monolayers were treated with the compounds (0 to 50 μM) and infected simultaneously with TBEV (Hypr) at MOI of 0.1. The infected cells were then incubated for 48 h, after which, cell media were collected and viral titers determined using a plaque assay. The obtained titers were used to construct dose-dependent inhibition curves (as indicated) and to calculate EC_{50} values. 7-deaza-2′-CMA (in the same concentration range) was used as a positive control.

2.4. PR673 Inhibits Replication of the TBEV in Cell Culture

Since we observed a strong inhibition of all tested flaviviral RdRps in vitro, we decided to test whether PR673 could inhibit a flavivirus in cell culture. We used the TBEV (strain Hypr) for which we have well established assays [24,25]. We first tested the cytotoxicity of PR673 in porcine kidney stable cells (PS cells) that are widely used for TBEV multiplication, anti-TBEV assays and TBEV-based plaque assays [26]. We also used 7-deaza-2′-C-methyladenosine (7-deaza-2′-CMA) as a positive control because this compound is a well-established inhibitor of the TBEV RdRp [25]. The cytotoxicity was evaluated in a concentration range of 0 to 50 μM; both compounds appeared as non-cytotoxic for PS cells up to 50 μM when incubated with the cells for 48 h. Similarly to 7-deaza-2′-CMA, the CC_{50} values of PR673 were estimated to be >50 μM (Figure 4A).

Next, we tested the anti-TBEV activity of PR673 in PS cells and compared its anti-TBEV activity with that of 7-deaza-2′-CMA. PR673 exerted a dose-dependent anti-TBEV effect, with an EC_{50} value of 0.11 μM. The complete inhibition of TBEV replication was observed at a compound concentration of 0.4 μM. The anti-TBEV activity of PR673 was almost four-fold higher in comparison to 7-deaza-2′-CMA (Figure 4B).

3. Discussion

More small molecules active against SARS-CoV-2 are needed. Two compounds targeting the RdRp (remdesivir and molnupiravir) and the 3C-like protease inhibitor nirmatrelvir (sold under the name Paxlovid) are already available as human medicines. In addition, inhibitors of other coronaviral enzymes, such as the helicase [27,28], endo- and exonuclease [29,30] or the methyltransferases [18,19,31], have been actively developed. However, the goal is to develop compounds that would be active against multiple viruses or even multiple viral families. These so-called broad-spectrum antivirals could be a powerful weapon to combat future pandemics. One such example is remdesivir. It was originally discovered by Gilead when screening for compounds active against the respiratory syncytial virus, and was later both developed to combat the Ebola outbreak in 2014 and repurposed against SARS-CoV-2 [32–34]. Recently, we showed that it can also effectively inhibit flaviviral RdRps [35]. Remdesivir is a nucleotide analog that is metabolized into remdesivir triphosphate; upon incorporation into RNA, it acts as a delayed chain terminator. In fact,

nucleoside analogs can be divided into three classes: (*i*) mutagenic nucleosides, such as ribavirin, that are able to cause mutational catastrophe [36]; (*ii*) obligate chain terminators that usually lack the ribosyl C3′-hydroxyl group [37]; and (*iii*) delayed chain terminators, such as remdesivir [38]. Our experiments with PR673 demonstrate that it acts as a pseudo-obligate chain terminator. It can clearly stop the synthesis of RNA in vitro by recombinant RdRps (Figure 2), which explains its effect on the replication of SARS-CoV-2 and TBEV (Figures 1 and 4). However, obligate chain terminators are incorporated into RNA, and their chemical nature prevents the incorporation of another nucleoside [39], which is clearly not the case for PR673. It could possibly compete for one of the RNA binding sites that are present and relatively conserved at viral RdRps, such as the entry site or the exit tunnel [40–42]. We cannot rule out the possibility that PR673 is an allosteric inhibitor; however, this is not probable because it is active on relatively distant RdRps, where an allosteric site is unlikely to be conserved. In any case, PR673 illustrates that the development of non-nucleoside antivirals active against a broad spectrum of viruses is feasible.

4. Material and Methods

4.1. Anti-SARS-CoV-2 Activity Determination Using Immunofluorescence Assay

Anti-SARS-CoV-2 activity was tested in VERO-E6 (ATCC CRL-1586) and Caco-2 cells (ATCC HTB-37) using immunofluorescence assay. VERO-E6 cells were seeded one day before experiment in DMEM medium with 10% FBS, 100 U of penicillin/mL and 100 µg of streptomycin/mL (all Merck KGaA, Darmstadt, Germany) in 96-well plate. Day after, two-fold serial dilution of compound was added to the cells in triplicate in complete DMEM medium with 2% FBS. After one hour, cells were infected with SARS-CoV-2 (hCoV-19/Czech Republic/NRL_6632_2/2020, multiplicity of infection MOI = 0.02) and incubated for 3 days in 5% CO_2 at 37 °C. After incubation, medium was removed, cells were fixed using 4% paraformaldehyde (PFA), washed 3× with PBS, permeabilized with 0.2% Triton-X100 for 5 min at room temperature and incubated for 2 h with anti-SARS-CoV-2 antibody (mouse monoclonal anti-nucleoprotein IgG, Institute of Molecular Genetics, Czech Republic). Subsequently, cells were washed 3× with PBS and incubated for 1.5 h with 1:250 dilution of Cy3-labeled donkey anti-mouse IgG (Jackson ImmunoResearch, Cambridgeshire) at RT, and fluorescent foci were visualized using a fluorescence microscope (Olympus IX 81, Hamburg, Germany). Cellular DNA was labeled with DAPI (4′,6-diamidino-2-phenylindole) (Merck KGaA, Darmstadt, Germany) nucleic acid stain. Cells were incubated with DAPI (0.1 µg/mL) for 10 min and subsequently washed with 1× PBS. Immunofluorescence assay in Caco-2 cells was performed similarly as above, with following changes. The MOI of SARS-CoV-2 was 0.002, permeabilization was performed with methanol at −20 °C for ten minutes and, as a secondary antibody, the 1:200 dilution of FITC-labelled goat anti-mouse IgG (Jackson ImmunoResearch) was used. The fluorescent images of both cell lines were analyzed by ImageJ (NIH) and the compound concentration required to reduce fluorescence by 50% (EC_{50}) was calculated using nonlinear regression analysis with GraphPad Prism software.

4.2. Anti-SARS-CoV-2 Activity Determination Using Cytopathic Effect-Based Assay

For CPE-based assay, two-fold serial dilutions of compounds were added in triplicate in a 96-well plate with Calu-3 cells (ATCC HTB-55) seeded day before in DMEM medium with 10% FBS, 100 U of penicillin/mL and 100 µg of streptomycin/mL. After 1 h incubation, SARS-CoV-2 was added at MOI 0.04. Following a three-day incubation at 37 °C in 5% CO_2 the cell viability was evaluated by XTT cell viability assay. Four hours after addition of XTT solution, the absorbance was measured using EnVision plate reader (PerkinElmer) and the compound concentrations required to reduce viral cytopathic effect by 50% (EC_{50}) were calculated using nonlinear regression analysis using GraphPad Prism software.

4.3. Cytotoxicity Determination in SARS-CoV-2 Assays

Cytotoxicity was evaluated by incubating the same two-fold serial dilutions of compound as in antiviral assays with VERO-E6, Caco-2 and Calu-3 cells. After three days' incubation at 37 °C in 5% CO_2, the cell viability was determined by addition of 50:1 mixture of XTT labeling reagent (1 mg/mL) and PMS electron-coupling reagent (0.383 mg/mL) (both Merck KGaA, Darmstadt, Germany), and the compound concentrations resulting in 50% reduction in viability (CC_{50}) were calculated as above in the antiviral activity determination using CPE-based assay.

4.4. SARS-CoV-2 Yield Reduction Assay

The VERO-E6 cells were incubated with and without a tested compound (at different concentrations) for 1 h, followed by SARS-CoV-2 infection at MOI 0.04 for 3 days at 37 °C in 5% CO_2. Virus yield was determined by a plaque assay in a 24-well plate. Briefly, 100 µL of the supernatant was added to VERO-E6 cell monolayer, incubated for 4 h at 37 °C in 5% CO_2 and overlaid with 3% carboxymethyl cellulose. After a 5-day incubation, the cells were fixed and stained with Naphthalene black and the plaques were counted.

4.5. Anti-TBEV Studies

TBEV strain Hypr, a representative of the European TBEV subtype, was provided by the Collection of Arboviruses, Institute of Parasitology, Biology Centre of the Czech Academy of Sciences, Ceske Budejovice, Czech Republic (http://www.arboviruscollection.cz/index.php?lang=en, accessed on 20 February 2022). Porcine kidney stable (PS) cells [26] were cultured in Leibovitz (L-15) medium and supplemented with 3% newborn calf serum, 100 U/mL penicillin, 100 µg/mL streptomycin and 1% glutamine (Sigma-Aldrich KGaA, Darmstadt, Germany). PS cells were cultivated at 37 °C under a normal atmosphere (without CO_2 supplementation).

To determine the cytotoxicity of PR673, PS cells were seeded in 96-well microtitration plates (2×10^4 cells per well) and incubated for 24 h at 37 °C. After incubation, PR673 was added to the cells (0 to 50 µM). 7-deaza-2′-CMA (Carbosynth, Compton, UK) in the same concentration range was used as a positive control. Then, the treated cells were cultivated for 48 h at 37 °C. The cytotoxicity measured in terms of cell viability was determined with Cell Counting Kit-8 (Dojindo Molecular Technologies) according to manufacturer's instructions. The respective concentrations of each compound that reduced cell viability by 50% (CC_{50} values) were determined. The experiment was performed in triplicate.

TBEV titer reduction assays were performed to determine anti-TBEV activity of PR673 in the PS cell culture. The cells were seeded in 96-well plates (2×10^4 cells per well) and incubated for 24 h at 37 °C to form a confluent monolayer. Subsequently, the cells were infected with TBEV (multiplication of infection of 0.1), simultaneously treated with PR673 at concentrations of 0 to 50 µM and incubated for 48 h at 37 °C. Following incubation, media were collected and viral titers determined by plaque assay [25] to construct dose-dependent inhibition curves and to estimate 50% effective concentration (EC_{50}) values. Similarly to the cytotoxicity assays, the experiment was performed in triplicate and the 7-deaza-2′-CMA was used as a positive control.

4.6. Protein Expression and Purification

NS5 proteins and SARS-CoV-2 nsp12, nsp8 and nsp7 were expressed with appropriate purification and folding tags, as detailed in Supplementary Table S1 and as described before [21,35,39]. Briefly, all of the proteins were expressed in bacterial cells, except for the full length nsp12 protein, which was expressed in insect cells. Other genes were expressed in *E. coli* (BL-21 CodonPlus (DE3)-RIL). Transformed cells were grown to an optimal OD_{600} in LB medium at 37 °C; then, the protein expression was induced by addition of IPTG to 0.4 mM and the cells were grown at 18 °C for 16 h. The recombinant proteins were purified using Ni^{2+} affinity chromatography followed by tag cleavage (when appropriate), and further purified using size exclusion chromatography.

4.7. Primer Extension Polymerase Activity Assay

The polymerase activity was determined in a primer extension reaction using a fluorescently labeled primer 1 (P1: 5′-Cy5-AGAACCUGUUGAACAAAAGC-3′) or primer 2 (P2: 5′-HEX-AGAACCUGUUUAACAAAAGC-3′) and an RNA template 1 (T1: 5′-AUUAUUAGCUGCUUUUGU-3′) or template 2 (T2: 5′-AUUAUUAGCUGCUUUUGUUAAACAGGUUCU-3′). All primers were synthesized by Sigma-Aldrich.

The polymerase activity assay was performed in a total volume of 10 µL of reaction mixture containing reaction buffer, NTPs, template/primer, the viral polymerase and 0.01U RNasin (New England BioLabs Int.). The exact composition of each reaction mixture was optimized for each polymerase, as detailed in Supplementary Table S2. The reactions were incubated for 1 h at 30 °C for SARS-CoV-2 RdRp or 1 h at 33 °C for flaviviral RdRp, respectively. After incubation, reactions were stopped by adding 20 µL of stop buffer (80% formamide, 50 mM EDTA), samples were denatured at 95 °C for 10 min and primer extension products were separated on a 20% denaturing polyacrylamide gel (8 M urea, 1× TBE, 20% acryl amide (19:1)). After electrophoresis, gels were scanned on Amersham Typhoon 5 Biomolecular Imager (GE Healthcare) and analyzed by ImageQuant TL8.2 (Cytiva).

4.8. In Vitro Determination of IC_{50}

IC_{50} values were determined in a similar polymerase activity assay as above but using radioactive labeling. The assay was performed in a total volume of 20 µL reaction mixture (Supplementary Table S2), but, as template, we used an RNA oligo containing a hairpin 5′-25U-HP-3′(5′-UUUUUUUUUUUUUUUUUUUUUUUUUAACAGGUUCUAGAACCUGUU-3′) and NTPs were replaced by 0.01 µCi/µL [α-^{32}P]-ATP. After incubation, 5 µL of reaction mixtures was spotted on anion exchange cellulose filter paper (Whatman^{TM} Grade DE81 DEAE cellulose paper; GE Healthcare) in triplicate. The Whatman filter was then dried, subsequently washed by 0.125 mM Na_2HPO_4, water and ethanol and dried again. Dry filter paper was then analyzed using phosphorimaging. The plate was scanned on Amersham Typhoon 5 Biomolecular Imager (GE Healthcare), the products were quantified with Image Studio Lite (LI-COR) and data were analyzed using GraphPad version 6 (GraphPad Prism version 6, GraphPad Software, San Diego, CA, USA).

Supplementary Materials: The following supporting information can be downloaded at: https://www.mdpi.com/article/10.3390/molecules27061894/s1, Figure S1: Immunofluorescence microscopy analysis of SARS-CoV-2 nucleoprotein expression after addition of 50 µM, 25 µM, and 12.5 µM of PR673; Figure S2: Synthesis of PR673 by a condensation reaction between the helquat MJB and methylbenzothiazole PR739; Table S1: Summery of viral polymerases list of polymerases used in this study; Table S2: Exact composition of each polymerase reaction mixture.

Author Contributions: E.K., K.K., L.E., J.H., M.Z., A.F. and M.J. performed the experiments and prepared figures. F.T., P.E.R.-G., D.R., J.W. and E.B. designed experiments and supervised the study. E.B. wrote the manuscript. All authors have read and agreed to the published version of the manuscript.

Funding: This project was funded by the grant number 21-25280S of the Czech Science Foundation, by the Ministry of Health of the Czech Republic (project No. NU20-05-00472) and Ministry of Education, Youth and Sports (LTAUSA18016). The Academy of Sciences of the Czech Republic (RVO: 61388963) is also acknowledged.

Institutional Review Board Statement: Not applicable.

Informed Consent Statement: Not applicable.

Data Availability Statement: Not applicable.

Conflicts of Interest: The authors declare no conflict of interests.

Sample Availability: Samples of the compounds are available from the corresponding author upon request.

References

1. Moureau, G.; Cook, S.; Lemey, P.; Nougairede, A.; Forrester, N.L.; Khasnatinov, M.; Charrel, R.N.; Firth, A.E.; Gould, E.A.; de Lamballerie, X. New Insights into Flavivirus Evolution, Taxonomy and Biogeographic History, Extended by Analysis of Canonical and Alternative Coding Sequences. *PLoS ONE* **2015**, *10*, e0117849.
2. Simmonds, P.; Becher, P.; Bukh, J.; Gould, E.A.; Meyers, G.; Monath, T.; Muerhoff, S.; Pletnev, A.; Rico-Hesse, R.; Smith, D.B.; et al. ICTV Virus Taxonomy Profile: Flaviviridae. *J. Gen. Virol.* **2017**, *98*, 2–3. [CrossRef] [PubMed]
3. Abdelaziz, O.S.; Waffa, Z. Neuropathogenic human coronaviruses: A review. *Rev. Med. Virol.* **2020**, *30*, e2118. [CrossRef] [PubMed]
4. Shchelkanov, M.Y.; Popova, A.Y.; Dedkov, V.G.; Akimkin, V.G.; Maleev, V.V. History of Investigation and Current Classification of Coronaviruses (Nidovirales: Coronaviridae). *Russ. J. Infect. Immun.* **2020**, *10*, 221–246. [CrossRef]
5. Pierson, T.C.; Diamond, M.S. The continued threat of emerging flaviviruses. *Nat. Microbiol.* **2020**, *5*, 796–812. [CrossRef] [PubMed]
6. Graham, R.L.; Donaldson, E.F.; Baric, R.S. A decade after SARS: Strategies for controlling emerging coronaviruses. *Nat. Rev. Microbiol.* **2013**, *11*, 836–848. [CrossRef] [PubMed]
7. de Wit, E.; van Doremalen, N.; Falzarano, D.; Munster, V.J. SARS and MERS: Recent insights into emerging coronaviruses. *Nat. Rev. Microbiol.* **2016**, *14*, 523–534. [CrossRef] [PubMed]
8. Paixao, E.S.; Barreto, F.; Teixeira Mda, G.; Costa Mda, C.; Rodrigues, L.C. History, Epidemiology, and Clinical Manifestations of Zika: A Systematic Review. *Am. J. Public Health* **2016**, *106*, 606–612. [CrossRef]
9. Rubin, D.; Chan-Tack, K.; Farley, J.; Sherwat, A. FDA Approval of Remdesivir—A Step in the Right Direction. *N. Engl. J. Med.* **2020**, *383*, 2598–2600. [CrossRef]
10. Fischer, W.; Eron, J.J.; Holman, W.; Cohen, M.S.; Fang, L.; Szewczyk, L.J.; Sheahan, T.P.; Baric, R.; Mollan, K.R.; Wolfe, C.R.; et al. Molnupiravir, an Oral Antiviral Treatment for COVID-19. *medRxiv* **2021**. [CrossRef]
11. Owen, D.R.; Allerton, C.M.N.; Anderson, A.S.; Aschenbrenner, L.; Avery, M.; Berritt, S.; Boras, B.; Cardin, R.D.; Carlo, A.; Coffman, K.J.; et al. An oral SARS-CoV-2 M(pro) inhibitor clinical candidate for the treatment of COVID-19. *Science* **2021**, *374*, 1586–1593. [CrossRef] [PubMed]
12. Li, P.F.; Wang, Y.N.; Lavrijsen, M.; Lamers, M.M.; de Vries, A.C.; Rottier, R.J.; Bruno, M.J.; Peppelenbosch, M.P.; Haagmans, B.L.; Pan, Q.W. SARS-CoV-2 Omicron variant is highly sensitive to molnupiravir, nirmatrelvir, and the combination. *Cell Res.* **2022**, *32*, 322–324. [CrossRef] [PubMed]
13. Frazier, M.N.; Dillard, L.B.; Krahn, J.M.; Perera, L.; Williams, J.G.; Wilson, I.M.; Stewart, Z.D.; Pillon, M.C.; Deterding, L.J.; Borgnia, M.J.; et al. Characterization of SARS2 Nsp15 nuclease activity reveals it's mad about U. *Nucleic Acids Res.* **2021**, *49*, 10136–10149. [CrossRef] [PubMed]
14. Newman, J.A.; Douangamath, A.; Yadzani, S.; Yosaatmadja, Y.; Aimon, A.; Brandao-Neto, J.; Dunnett, L.; Gorrie-stone, T.; Skyner, R.; Fearon, D.; et al. Structure, mechanism and crystallographic fragment screening of the SARS-CoV-2 NSP13 helicase. *Nat. Commun.* **2021**, *12*, 4848. [CrossRef] [PubMed]
15. Cihlova, B.; Huskova, A.; Boserle, J.; Nencka, R.; Boura, E.; Silhan, J. High-Throughput Fluorescent Assay for Inhibitor Screening of Proteases from RNA Viruses. *Molecules* **2021**, *26*, 3792. [CrossRef] [PubMed]
16. Nencka, R.; Silhan, J.; Klima, M.; Otava, T.; Kocek, H.; Krafcikova, P.; Boura, E. Coronaviral RNA-methyltransferases: Function, structure and inhibition. *Nucleic Acids Res.* **2022**, *50*, 635–650. [CrossRef] [PubMed]
17. Konkolova, E.; Klima, M.; Nencka, R.; Boura, E. Structural analysis of the putative SARS-CoV-2 primase complex. *J. Struct. Biol.* **2020**, *211*, 107548. [CrossRef] [PubMed]
18. Otava, T.; Sala, M.; Li, F.; Fanfrlik, J.; Devkota, K.; Perveen, S.; Chau, I.; Pakarian, P.; Hobza, P.; Vedadi, M.; et al. The Structure-Based Design of SARS-CoV-2 nsp14 Methyltransferase Ligands Yields Nanomolar Inhibitors. *ACS Infect. Dis.* **2021**, *7*, 2214–2220. [CrossRef]
19. Devkota, K.; Schapira, M.; Perveen, S.; Khalili Yazdi, A.; Li, F.; Chau, I.; Ghiabi, P.; Hajian, T.; Loppnau, P.; Bolotokova, A.; et al. Probing the SAM Binding Site of SARS-CoV-2 Nsp14 In Vitro Using SAM Competitive Inhibitors Guides Developing Selective Bisubstrate Inhibitors. *SLAS Discov.* **2021**, *26*, 1200–1211. [CrossRef]
20. Perveen, S.; Khalili Yazdi, A.; Devkota, K.; Li, F.; Ghiabi, P.; Hajian, T.; Loppnau, P.; Bolotokova, A.; Vedadi, M. A High-Throughput RNA Displacement Assay for Screening SARS-CoV-2 nsp10-nsp16 Complex toward Developing Therapeutics for COVID-19. *SLAS Discov.* **2021**, *26*, 620–627. [CrossRef] [PubMed]
21. Dejmek, M.; Konkolova, E.; Eyer, L.; Strakova, P.; Svoboda, P.; Sala, M.; Krejcova, K.; Ruzek, D.; Boura, E.; Nencka, R. Non-Nucleotide RNA-Dependent RNA Polymerase Inhibitor That Blocks SARS-CoV-2 Replication. *Viruses* **2021**, *13*, 1585. [CrossRef] [PubMed]
22. Eggleton, J.S.; Nagalli, S. *Highly Active Antiretroviral Therapy (HAART)*; StatPearls: Treasure Island, FL, USA, 2022.
23. Tykvart, J.; Navratil, V.; Kugler, M.; Sacha, P.; Schimer, J.; Hlavackova, A.; Tenora, L.; Zemanova, J.; Dejmek, M.; Kral, V.; et al. Identification of Novel Carbonic Anhydrase IX Inhibitors Using High-Throughput Screening of Pooled Compound Libraries by DNA-Linked Inhibitor Antibody Assay (DIANA). *SLAS Discov.* **2020**, *25*, 1026–1037. [CrossRef] [PubMed]
24. Eyer, L.; Smidkova, M.; Nencka, R.; Neca, J.; Kastl, T.; Palus, M.; De Clercq, E.; Ruzek, D. Structure-activity relationships of nucleoside analogues for inhibition of tick-borne encephalitis virus. *Antivir. Res.* **2016**, *133*, 119–129. [CrossRef] [PubMed]
25. Eyer, L.; Valdes, J.J.; Gil, V.A.; Nencka, R.; Hrebabecky, H.; Sala, M.; Salat, J.; Cerny, J.; Palus, M.; De Clercq, E.; et al. Nucleoside inhibitors of tick-borne encephalitis virus. *Antimicrob. Agents Chemother.* **2015**, *59*, 5483–5493. [CrossRef] [PubMed]

viruses

MDPI

Brief Report

Non-Nucleotide RNA-Dependent RNA Polymerase Inhibitor That Blocks SARS-CoV-2 Replication

Milan Dejmek [1,†], Eva Konkoľová [1,†], Luděk Eyer [2,3], Petra Straková [2,3], Pavel Svoboda [2,3,4], Michal Šála [1], Kateřina Krejčová [1], Daniel Růžek [2,3,*], Evzen Boura [1,*] and Radim Nencka [1,*]

1 Institute of Organic Chemistry and Biochemistry, Czech Academy of Sciences, Flemingovo náměstí 542/2, 160 00 Praha, Czech Republic; dejmek@uochb.cas.cz (M.D.); eva.konkolova@uochb.cas.cz (E.K.); sala@uochb.cas.cz (M.Š.); katerina.krejcova@uochb.cas.cz (K.K.)
2 Veterinary Research Institute, Emerging Viral Diseases, Hudcova 296/70, 621 00 Brno, Czech Republic; eyer@vri.cz (L.E.); strakova.p@centrum.cz (P.S.); svoboda@vri.cz (P.S.)
3 Institute of Parasitology, Biology Centre of the Czech Academy of Sciences, Branišovská 1160/31, 370 05 České Budějovice, Czech Republic
4 Department of Pharmacology and Pharmacy, Faculty of Veterinary Medicine, University of Veterinary Sciences Brno, Palackého tř. 1946/1, 612 42 Brno, Czech Republic
* Correspondence: ruzekd@paru.cas.cz (D.R.); boura@uochb.cas.cz (E.B.); nencka@uochb.cas.cz (R.N.)
† These authors contributed equally.

Abstract: SARS-CoV-2 has caused an extensive pandemic of COVID-19 all around the world. Key viral enzymes are suitable molecular targets for the development of new antivirals against SARS-CoV-2 which could represent potential treatments of the corresponding disease. With respect to its essential role in the replication of viral RNA, RNA-dependent RNA polymerase (RdRp) is one of the prime targets. HeE1-2Tyr and related derivatives were originally discovered as inhibitors of the RdRp of flaviviruses. Here, we present that these pyridobenzothiazole derivatives also significantly inhibit SARS-CoV-2 RdRp, as demonstrated using both polymerase- and cell-based antiviral assays.

Keywords: non-nucleotide inhibitor; RNA-dependent RNA polymerase; SAR-CoV-2; COVID-19; antiviral agents

Citation: Dejmek, M.; Konkoľová, E.; Eyer, L.; Straková, P.; Svoboda, P.; Šála, M.; Krejčová, K.; Růžek, D.; Boura, E.; Nencka, R. Non-Nucleotide RNA-Dependent RNA Polymerase Inhibitor That Blocks SARS-CoV-2 Replication. *Viruses* **2021**, *13*, 1585. https://doi.org/10.3390/v13081585

Academic Editor: Tomas Ruml

Received: 4 July 2021
Accepted: 9 August 2021
Published: 11 August 2021

1. Introduction

Coronaviruses are positive-sense RNA viruses that cause numerous important human and animal diseases. These viruses are classified into four genera including *Alphacoronavirus* and *Deltacoronavirus* [1]. While infectivity of gammacoronaviruses and deltacoronaviruses is limited to animals, mostly birds [2], alphacoronaviruses and betacoronaviruses comprise numerous mammalian and human pathogens [3,4]. Important alphacoronaviruses are Human coronaviruses (HCoVs) 229E and NL63, as well as Feline coronavirus (FIPV) and Porcine epidemic diarrhea virus (PEDV). Betacoronaviruses include the rest of human coronaviruses (HCoV-OC43, HCoV-HKU1, Severe acute respiratory syndrome coronavirus (SARS-CoV and SARS-CoV-2), Middle East respiratory syndrome coronavirus (MERS-CoV)) and a number of other animal pathogens. While coronaviruses that have persisted in the human population for a long time (HCoV-229E, HCoV-NL63, HCoV-OC43, and HCoV-HKU1) cause milder upper respiratory illnesses, SARS-CoV, SARS-CoV-2, and MERS-CoV are highly pathogenic viruses causing severe lower respiratory illness that can progress to life-threatening pneumonia with significant mortality rates [5,6].

SARS-CoV-2 is responsible for the largest pandemic of acute viral disease that our world has faced since the Spanish flu [7]. Although the mortality of this disease is not as high as in that of SARS-CoV or MERS-CoV infections, the disease caused by this virus (COVID-19) has significantly changed the world in which we live [8]. In particular, mortality in older age groups is alarming [9], and although we already have vaccines [10] as well as several drugs based on both monoclonal antibodies and small molecules, the

effectiveness of these treatments is limited by several factors, including the high mutation rate of this virus [11]. Therefore, it is essential that pharmaceutical research focuses on the widest possible range of molecular targets and that we seek to find substances that we can use in combination with already known drugs to reduce the risk of the development of resistance. One of the main molecular targets in viruses is their polymerase, which is responsible for the replication of their genetic information. The example of HIV has shown that a combination of nucleoside and non-nucleoside reverse transcriptase inhibitors can lead to a very effective therapy for this serious disease [12]. Therapies for diseases caused by other viral pathogens, such as hepatitis B and C viruses (HBV and HCV), also rely largely on polymerase inhibitors [13,14]. Therefore, it is not surprising that the main approach for the development of new antivirals against SARS-CoV-2, as well as other coronaviruses, is based on targeting the RNA-dependent RNA polymerase (RdRp) as a central replication enzyme of the virus [15]. RdRp is part of the large coronaviral replication complex that also includes RNA methyltransferases, helicase, nsp9, and probably the N protein [16]. The coronaviral RdRp is a highly conserved heterotrimeric protein complex that is composed of two accessory but essential proteins (nsp7 and nsp8) and the catalytic subunit nsp12 [17]. While the first nucleoside-based RdRp inhibitor has already been approved by the relevant authorities around the world [18], information on potent non-nucleoside inhibitors of this key enzyme is rather scarce. Recently, suramin was reported as a potent non-nucleoside inhibitor of SARS-CoV-2 RdRp, and its mode of action was supported by a cryo-EM structure [19]. Also, several natural products including corilagin [20] and lycorine [21] exert inhibition potency against SARS-CoV-2 RdRp. Although efforts have been made to identify new non-nucleoside inhibitors of this enzyme by in silico methods since the beginning of the pandemic, the results of these studies are unfortunately rarely supported by experimental data [22].

HeE1-2Tyr (compound **16**) was initially identified by Tarantino et al. as a potent inhibitor of RdRp from Dengue virus (DENV), West Nile virus, and Yellow fever virus, all members of genus *Flavivirus* [23–26]. This compound was crystalized in complex with the RdRp from DENV 3. It was shown that the drug binds on the thumb side of the RNA-binding site, with significant movement of the priming loop. The authors also suggested that there is another possible binding site of the compound that is hidden by the priming loop. This hypothesis has been supported by point mutation experiments [23].

Here, we report on the identification of HeE1-2Tyr (**16**) and its derivatives as potential inhibitors of SARS-CoV-2 RdRp. The drugs exert activity not only against SARS-CoV-2 but also against FIPV. Our study started with the screening of our small collection of various nucleoside triphosphate and non-nucleoside inhibitors of polymerases from different viruses against SARS-CoV-2 RdRp and, in parallel, a screening of our complementary nucleoside, nucleotide prodrug, and non-nucleoside derivative library against SARS-CoV-2 in cell-based assays. To our surprise, we identified HeE1-2Tyr (**16**), which we prepared as a standard for our studies on flavivirus RdRps, as an effective inhibitor of SARS-CoV-2 RdRp that also exerted significant activity against the virus in cell cultures.

2. Material and Methods

2.1. Protein Expression and Purification

SARS-CoV-2 nsp7 (GeneBank: YP_009725303), nsp8 (GeneBank: YP_009725304,) and nsp12 (GeneBank: YP_009725307) genes were commercially synthesized as codon-optimized for *E. coli* (Invitrogen). The gene for nsp7 was cloned into a modified pRSF-Duet vector containing an N-terminal 6×His tag, followed by a GB1 solubility tag, a 10×Asp spacer sequence, and a tobacco etch virus (TEV) protease cleavage site in cloning site 1. The nsp8 gene was subsequently cloned into cloning site 2 without any tag. The gene for nsp12 was cloned into the pAceBac vector with cleavable 6×His on the C-terminus. The nsp7/nsp8 protein complex was expressed and purified as described previously for truncated nsp7/nsp8 in *E. coli* [27]. The SARS-CoV-2 nsp12 plasmid was used to prepare recombinant baculovirus Sf9 insect cells that were infected at 1–2 $\times$ 10^6 cell/mL with the

tertiary recombinant baculovirus. After 68 h, the cells were collected by centrifugation, resuspended in lysis buffer (50 mM HEPES 7.4, 300 mM NaCl, 20 mM imidazole, 3 mM $MgCl_2$, 10% (*v/v*) glycerol, and 3 mM β-mercaptoethanol) and sonicated (Q700 Sonicator, QSonica). The lysate was subsequently cleared by centrifugation, and the supernatant was incubated with Ni-NTA agarose (Thermo Scientific) and washed with lysis buffer; finally, the protein was eluted with lysis buffer supplemented with 300 mM imidazole. Nsp12 protein was further purified by size-exclusion chromatography using Superdex 200 16/600 (GE Healthcare) in size-exclusion buffer (20 mM HEPES 7.4, 300 mM NaCl, 1 mM $MgCl_2$, 10% (*v/v*) glycerol, and 3 mM β-mercaptoethanol). Fractions containing the pure nsp12 protein were concentrated to 5 mg/mL, flash-frozen, and stored at −80 °C until needed.

2.2. Fluorescence-Based Primer Extension Polymerase Assay

The polymerase activity was determined in a primer extension reaction using a fluorescently labeled primer (HEX-5′-AGAACCUGUUGAACAAAAGC-3′) and an RNA template (5′- AUUAUUAGCUGCUUUUGUUCAACAGGUUCU-3′). The polymerase activity assay was performed in a total volume of 10 µL containing the reaction buffer (10 mM Tris pH 8.0, 2 mM $MgCl_2$, 10 mM KCl, 1 mM β-mercaptoethanol), 10 µM NTPs, 0.5 µM T/P complex, 1 µM nsp12 polymerase, and 3 µM nsp7/nsp8 complex. The reactions were incubated for 1 h with various concentrations of the inhibitors tested at 30 °C and stopped by adding 20 µL of the stop buffer (80% formamide, 50 mM EDTA). The samples were denatured at 95 °C for 10 min, and primer extension products were separated on a 20% denaturing polyacrylamide gel (8 M urea, 1× TBE, 20% acrylamide (19:1)) and scanned on a Typhoon 5 Biomolecular Imager (GE Healthcare).

2.3. Radioactivity-Based Primer Extension Polymerase Assay

The assay was performed as above, except that the reaction mixture contained 0.5 µM T/P complex (P-5′-AGAACCUGUUGAACAAAAGC-3′, T-5′-U25-GCUUUUGUUCAACA GGUUCU-3′) and 0.01µCi/µL [α-32P]-ATP. After incubation, 5 µL of the reaction mixtures was spotted on an anion-exchange cellulose filter paper (WhatmanTM Grade DE81 DEAE cellulose paper; GE Healthcare) in triplicates. The Whatman filter was then dried, subsequently washed with 0.125 mM Na_2HPO_4, water, and ethanol, and dried again. The dry filter paper was then analyzed using phosphorimaging, the plate was scanned on Amersham Typhoon 5 Biomolecular Imager (GE Healthcare), products were quantified with Image Studio Lite (LI-COR), and the data were processed using GraphPad version 6 (GraphPad Prism version 6, GraphPad Software, San Diego, CA, USA).

2.4. Viruses and Cell Lines

Two representatives of the *Coronaviridae* family, i.e., SARS-CoV-2 (strain SARS-CoV-2/human/Czech Republic/951/2020 isolated from a clinical sample at the National Institute of Health, Prague, Czech Republic, and kindly provided by Dr. Jan Weber, Institute of Organic Chemistry and Biochemistry, Prague, Czech Republic) and feline infectious peritonitis virus (FIPV, ATCC VR990, a pathogen of domestic cats and other felines), were used for our antiviral cell-based studies. The experiments with the live coronaviruses were performed in our BSL3 facility.

Vero cells (ATCC CCL-81, African Green Monkey, adult kidney, epithelial) and Vero E6 cells (ATCC CRL-1586) were cultured in Dulbecco's modified Eagle's medium (DMEM) supplemented with 10% newborn calf serum, 100 U/mL penicillin, 100 µg/mL streptomycin, and 1% glutamine (Sigma-Aldrich, Prague, Czech Republic) at 37 °C and 5% CO_2. Colorectal adenocarcinoma cells (CaCo-2, ATCC HTB-37) were grown in DMEM medium, containing, 20% newborn calf serum with 100 U/mL penicillin, 100 µg/mL streptomycin, and 1% L-glutamine (Sigma-Aldrich, Prague, Czech Republic) at 37 °C and 5% CO_2. *Felis catus* kidney cortex cells (CRFK, ATCC CCL-94) were grown in DMEM supplemented with 10% newborn calf serum, 100 U/mL penicillin, 100 µg/mL streptomycin, and 1% glutamine (Sigma-Aldrich, Prague, Czech Republic) at 37 °C and 5% CO_2. Vero (ATCC

CCL-81), CaCo-2 (ATCC HTB-37), and CRFK (ATCC CCL-94) cells were used for antiviral and cytotoxicity assays, and Vero E6 cells (ATCC CRL-1586) were used to perform plaque assays.

2.5. Cytotoxicity Studies

Vero (ATCC CCL-81), CaCo-2 (ATCC HTB-37), and CRFK (ATCC CCL-94) cells were seeded into each well of 96-well microtitrate plates (approx. 2×10^4 cells per a well) and were incubated for 24 h at 37 °C and 5% CO_2. Cell monolayers in 96-well plates were treated with the compounds remdesivir, HeE1-2Tyr (**16**), **17**, or **18** at the concentration of 50 μM or with 1% DMSO (*w*/*w*) (for the initial screening; Vero and CRFK cell lines) or with the compounds remdesivir, HeE1-2Tyr (**16**) and **17** in concentration ranges from 0 to 50 μM (for dose–response studies; 2-fold dilutions, three wells per concentration; Vero, CaCo-2, and CRFK cell lines) and cultured for 48 h. The cytotoxic activity of the compounds was determined in terms of cell viability using a Cell Counting Kit-8 (Dojindo Molecular Technologies, Munich, Germany) following the manufacturer's instructions. The assay is based on the quantitative reduction of WST-8 tetrazolium salt to yellow formazan by cellular dehydrogenases. Cell viability was estimated as the percentage of colorimetric absorbance at 450 nm of the compound-treated cells relative to the absorbance of mock-treated cells. The concentration of compound that reduced cell viability by 50% was considered the 50% cytotoxic concentration (CC_{50}).

2.6. Antiviral Efficacy of the Studied Compounds in Cell-Based Assays

To study the antiviral effects of compounds HeE1-2Tyr (**16**), **17**, and **18**, we used a viral titer reduction assay. Vero (ATCC CCL-81), CaCo-2 (ATCC HTB-37), and CRFK (ATCC CCL-94) cells were seeded into each well of 96-well microtitrate plates (approx. 2×10^4 cells per a well) and incubated for 24 h at 37 °C and 5% CO_2. Then, the medium was aspirated, replaced with 200 μL of fresh medium containing compounds HeE1-2Tyr (**16**), **17**, or **18** at the concentration of 50 μM (for the initial screening) or with compounds HeE1-2Tyr (**16**) or **17** in the concentration range of 0 to 50 μM (for dose–response antiviral studies; 2-fold dilution, three wells per compound). The treated cells were simultaneously inoculated with SARS-CoV-2 (for Vero and CaCo-2 cells) or FIPV (for CRFK cells) at an MOI of 0.1 and incubated for an additional 48 h. Virus-infected cells treated with remdesivir (at the same concentrations) or DMSO (1% *w*/*w*) were used as positive and negative controls, respectively. Viral titers were determined from the collected supernatant media by a plaque assay and used to construct dose–response curves (dependence of the viral titers [PFU/mL] on the compound concentration [μM]) and inhibition curves (dependence of the inhibition percentage on the compound concentration [μM]) and for calculation of the 50% effective concentrations (EC_{50}; the concentration of compound required to inhibit the viral titer by 50% compared to the control value).

2.7. Plaque Assay

Plaque assays were performed using Vero E6 cells (ATCC CRL-1586) as described previously [28,29]. Briefly, 10-fold dilutions of SARS-CoV-2 or FIPV were prepared in 24-well tissue culture plates, and the cells were added to each well ($0.6–1.5 \times 10^5$ cells per well). After a 4 h incubation at 37 °C and 5% CO_2, the suspension was overlaid with 1.5% (*w*/*v*) carboxymethylcellulose in a two-fold concentrated DMEM medium. Following a 5-day incubation at 37 °C and 5% CO_2, the infected plates were washed with phosphate-buffered saline, and the cell monolayers were stained with naphthalene black. The virus titer was expressed as plaque-forming units (PFU)/mL.

3. Results and Discussion

Although the synthesis of HeE1-2Tyr (**16**) and its derivatives has been well documented by work of Tarantino et al., we devised a modified approach in order to have easier access to a broader range of substituents in the 8-OH position of the benzothiazolo

pyridinone (Scheme 1). To achieve this goal, we decided to protect the 5-OH group of the benzothiazole throughout the stages of central core construction. This way, the alkyl substituent could be introduced by the Mitsunobu reaction just prior to the introduction of the amino acid residue. After initial experiments with a TBDMS, which proved difficult to install and not very stable, we decided to use benzyl for this purpose. The 2-methyl group was then converted to an ethyl acetate by a reaction of an appropriate salt with ethyl carbonate. By using LiHMDS we achieved a very good yield in a short reaction time compared to methods using sodium hydride. A dimethylaminomethylene group was then introduced by the Vilsmeier–Haack reaction, and the pyridinone ring was subsequently closed by heating compound **4** with a neat acyl anhydride—acetic or phenylacetic. The benzyl group was comfortably cleaved using methansulfonic acid, providing compounds suitable for the Mitsunobu reaction, which afforded products **9** and **11**, respectively. Workup of compounds **5**–**8** proved to be very easy, as these compounds are very poorly soluble, and reaction conversions are high. The rest of the synthesis was performed in a similar way as reported by Tarantino et al. An ethyl ester function was saponified, and *L*-Tyrosine and *L*-Phenylalanine methylesters, respectively, were connected to the free carboxylic acid by EDC-HOBt peptide coupling. This set of conditions proved to provide the best yields in the short optimization we performed. This procedure gave HeE1-2Tyr (**16**), as well two novel analogues **17** and **18**, in excellent yields. Detailed descriptions of the synthesis is provided in the Supplementary File.

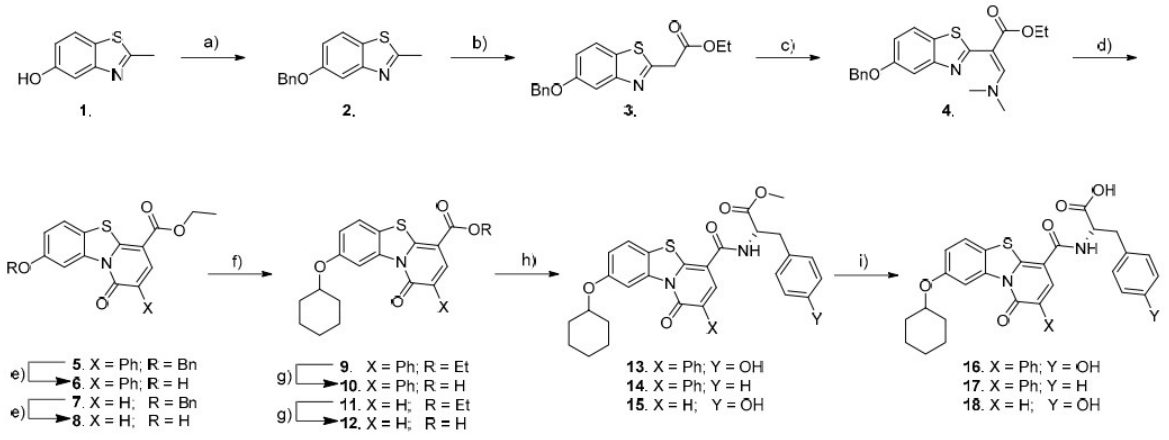

a) BnOH, PPh_3, DIAD, dioxane, RT, 48 h, 96 %; b) LiHMDS, $(E{:}O)_2CO$, THF, -78°C to RT, 30 min, 82 %; c) $POCl_3$, DMF, 90°C, 30 min, 81 %; d) Respective anhydride, 100°C, 5 h, 99 % for **5**, 94 % for **7**; e) CH_3SO_3H, DCM, RT, 3 h, 76 % for **6**, 82 % for **8**: f) Cyclohexanol, PPh_3, DIAD, dioxane, RT, 48 h, 89 % for **9**, 87 % for **11**; g) NaOH, MeOH-H_2O, reflux, 3 h, 84 % for **10**, 94 % for **12**: h) TyrOMe.HCl or PheOMe.HCl, EDC, HOBt, TEA, DCM. DMF, RT, 12h, 92 % for **13**, 91 % for **14**, 92 % for **15**; i) LiOH, THF-H_2O, 30 min, 88 % for **16**; 90 % for **17**, 88 % for **18**.

Scheme 1. Synthetic pathway to HeE1-2Tyr (**16**) and its derivatives.

Our in vitro RdRp assay confirmed the inhibitory effect of compounds HeE1-2Tyr (**16**), **17**, and **18** against SARS-CoV-2 polymerase. The compounds were initially tested at one concentration (100 μM), which confirmed that compounds HeE1-2Tyr (**16**), **17,** and **18** inhibit SARS-CoV-2 RdRp. Subsequently, the RdRp assay was used to determine the IC_{50} values. Surprisingly, compound HeE1-2Tyr (**16**) was found to be the best inhibitor, with IC_{50} of 27.6 ± 2.1 μM, while the inhibition effect of compound **18** was rather weak (IC_{50} = 85.5 ± 2.0 μM, Figure 1).

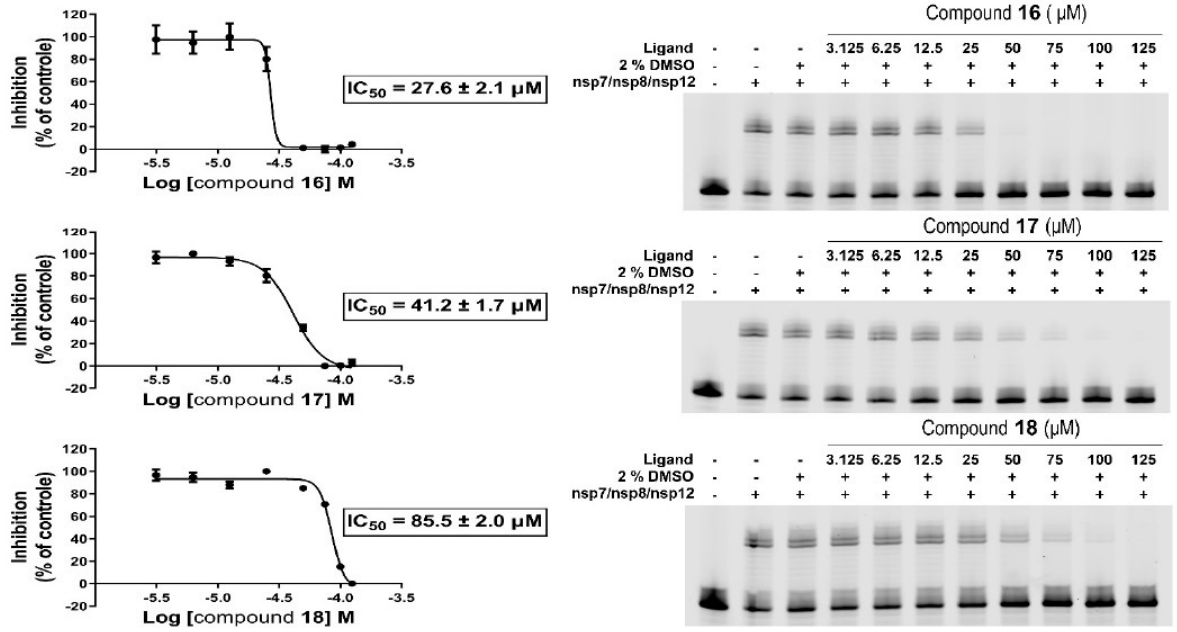

Figure 1. Inhibitions of SARS-CoV-2 RdRp by compounds **16**, **17**, and **18**. (**left**) IC_{50} values were established for each tested compound using a radioactive primer extension assay. Error bars represent the standard error of the mean ($n = 3$). (**right**) A fluorescence-based primer extension assay. Formation of the 40-nt product decreases with increasing concentration of the compound.

Based on our findings that the compounds showed inhibitory activities in SARS-CoV-2 RdRp assays, we next evaluated cytotoxicity and antiviral activity of HeE1-2Tyr (**16**), **17**, and **18** in cell-based systems. The compounds were initially tested at one single concentration of 50 µM against SARS-CoV-2 and FIPV in Vero and CRFK cells, respectively. This initial screening revealed that all compounds at 50 µM were not cytotoxic for both cell lines (Figure 2A). Moreover, compounds HeE1-2Tyr (**16**) and **17** were found to completely inhibit the replication of both coronaviruses (Figure 2B). Surprisingly, compound **18** was found to be inactive against SARS-CoV-2 and FIPV in both cell-based systems tested (EC_{50} > 50 µM) (Figure 2B). The inactivity could be explained by its poor cellular uptake or extensive degradation by cellular catabolic enzymes. Therefore, compound **18** was excluded from further testing.

The cytotoxicity of compounds HeE1-2Tyr (**16**) and **17** was studied in detail using Vero, CaCo-2, and CRFK cells in a concentration range from 0 to 50 µM. Both compounds showed good cytotoxicity profiles for the studied cell lines and were characterized by CC_{50} values >50 µM (Figure 2C–E; Tables 1–3). Interestingly, compound **17** caused a moderate increase in cell viability in Vero and CaCo-2 cells (to approx. 125% of untreated cells) but was slightly cytotoxic for CRFK cells (cell viability of approx. 60%) at the highest concentration tested (50 µM) (Figure 2C–E). The observed changes in the viability of cells treated by compound **17**, however, did not affect the CC_{50} values, which were calculated to be >50 µM for all the cell lines tested.

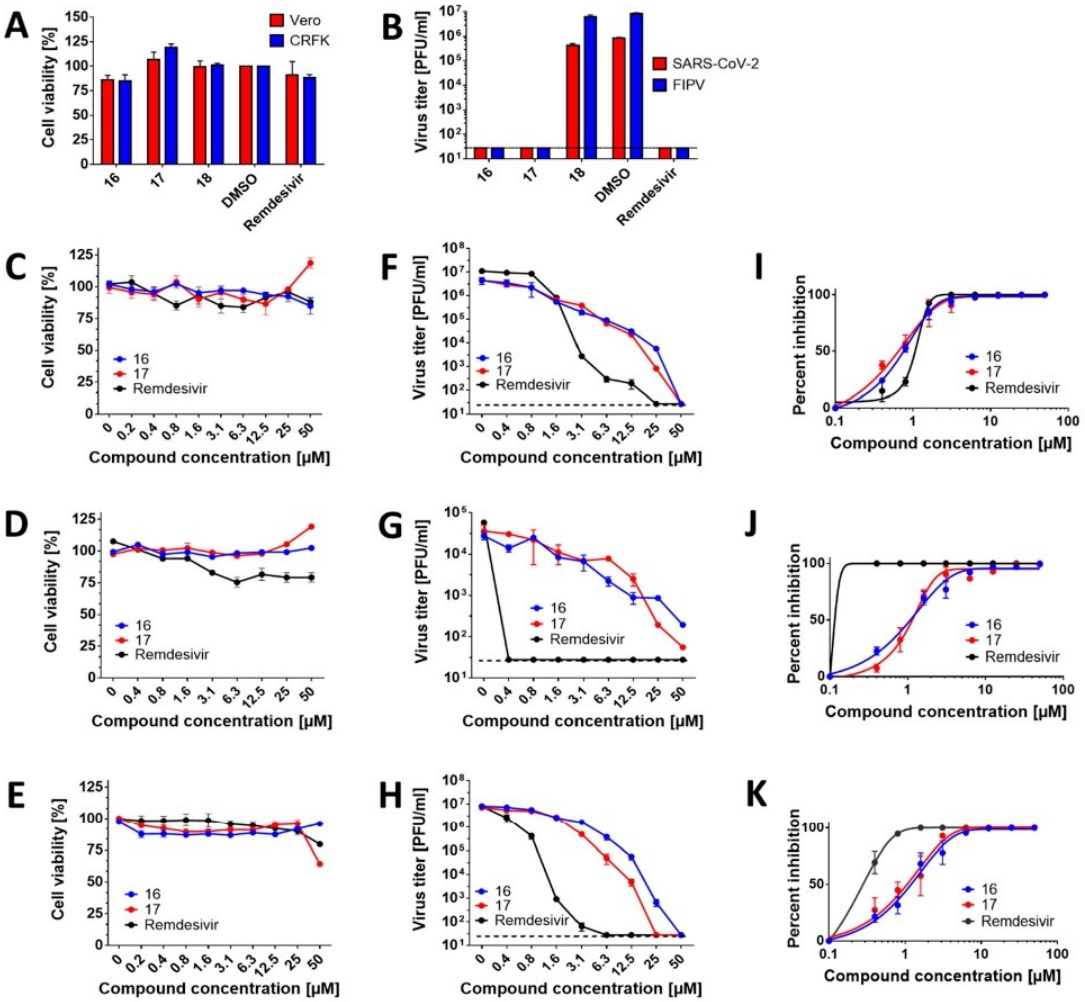

Figure 2. Antiviral efficacy and cytotoxicity of the studied RdRp inhibitors in cell-based assays. (**A**) Cytotoxicity of the indicated compounds in Vero and CRFK cells. The cell monolayers were treated with the compounds (50 μM) and incubated for 48 h. The cell-mediated conversion of tetrazolium salt WST-8 to formazan was monitored by absorbance measurement (450 nm). Cytotoxicity was expressed in terms of cell viability percentage. (**B**) Anti-SARS-CoV-2 and anti-FIPV efficacies of the indicated compounds in Vero and CRFK cells, respectively. The cell monolayers were treated with the compounds (50 μM), infected with the respective virus at a MOI of 0.1, and incubated for 48 h. The supernatant media were collected, and viral titers were determined by plaque assays. (**C**–**E**) Dose-dependent cytotoxic effects of the compounds in Vero (**C**), CaCo-2 (**D**), and CRFK (**E**) cells. The cell monolayers were treated with the compounds in the concentration range from 0 to 50 μM and incubated for 48 h. Cytotoxicity was determined, as described for (A). (**F**,**G**) Dose-dependent anti-SARS-CoV-2 activity of the compounds in Vero (**F**) and CaCo-2 (**G**) cells. The cell monolayers were treated with the compounds in the concentration range 0–50 μM and simultaneously infected with SARS-CoV-2 at a MOI of 0.1. The infected cells were incubated with the compounds for 48 h p.i., and viral titers were determined using the plaque assay. (**H**) Dose-dependent anti-FIPV activity of the compounds in CRFK cells. The protocol was the same as described for (**F**,**G**). (**I**–**K**) Inhibitory curves for the indicated compounds in Vero (**I**), CaCo-2 (**J**), and CRFK (**K**) cells. The mean titers from three biological replicates are shown, and error bars indicate standard errors of the mean ($n = 3$). The horizontal dashed line indicates the minimum detectable threshold of 1.44 $\log_{10}$ PFU/mL.

Table 1. Anti-SARS-CoV-2 activity and cytotoxicity of the tested compounds in Vero cells.

Compound	EC_{50} (μM) (95% CI) [a,b]	CC_{50} (μM) [a]	SI [c]
16	0.6535 (0.4376–0.9760)	>50	>76.5
17	0.5273 (0.4423–0.6286)	>50	>94.8
18	>50	>50	>1
Remdesivir	0.9012 (0.7997–1.016)	>50	>55.5

[a] Determined from three independent experiments. [b] Expressed as a 50% reduction in viral titers and calculated as inflection points of sigmoidal inhibitory curves which were obtained by a nonlinear fit of transformed inhibitor concentrations versus normalized response using GraphPad Prism 7.04 (GraphPad Software, Inc., USA). [c] CC_{50}/EC_{50}.

Table 2. Anti-SARS-CoV-2 activity and cytotoxicity of the tested compounds in CaCo-2 cells.

Compound	EC_{50} (μM) (95% CI) [a,b]	CC_{50} (μM) [a]	SI [c]
16	0.9493 (0.5131–1.756)	>50	>52.7
17	0.9959 (0.5427–1.827)	>50	>50.2
18	>25	>50	>2
Remdesivir	<0.3	>50	>216.9

For [a–c] see Table 1.

Table 3. Anti-FIPV activity and cytotoxicity of the tested compounds in CRFK cells.

Compound	EC_{50} (μM) (95% CI) [a,b]	CC_{50} (μM) [a]	SI [c]
16	1.062 (0.8188–1.377)	>50	>47.1
17	0.9989 (0.8274–1.206)	>50	>50.1
18	>50	>50	>1
Remdesivir	0.2230 (0.1694–0.2937)	>50	>224.2

For [a–c] see Table 1.

We further evaluated the dose-dependent, anti-coronaviral activities of compounds HeE1-2Tyr (**16**) and **17**. Anti-SARS-CoV-2 potency of both compounds in Vero cells reached sub-micro molar concentrations, with EC_{50} values of 653.5 nM (for **16**) and 527.3 nM (for **17**). These values were similar or even better than those of remdesivir (EC_{50} = 901.2 nM) (Figure 2F,I, Table 1). Although the EC_{50} values for HeE1-2Tyr (**16**) and **17** were slightly lower compared with those for remdesivir, the growth inhibition curve slopes for remdesivir were substantially steeper than those for HeE1-2Tyr (**16**) and **17**, indicating that remdesivir had a superior inhibitory profile over HeE1-2Tyr (**16**) and **17**. In CaCo-2 cells, compounds HeE1-2Tyr (**16**) and **17** showed EC_{50} values close to 1 μM (949.3 and 995.9 nM, respectively) and had somewhat lower antiviral potencies compared with remdesivir (EC_{50} < 300 nM) (Figure 2G,J, Table 2). Because of their low cytotoxicity, both compounds were characterized by relatively high selectivity indexes (>70 in Vero cells and >50 in CaCo-2 cells) (Tables 1 and 2). In vitro replication of FIPV, another member of the *Coronaviridae* family used in our antiviral study, was also strongly suppressed with compounds HeE1-2Tyr (**16**) and **17**. The anti-FIPV activity of these compounds was characterized by EC_{50} values of about 1 μM, was approx. 5-fold lower compared with remdesivir (EC_{50} = 223 nM), and showed selectivity indexes exceeding 40 (Figure 2H,K, Table 3).

In conclusion, HeE1-2Tyr (**16**) and its derivatives are potent non-nucleoside inhibitors of coronaviral RdRp that probably act as competitive inhibitors interacting via RNA template tunnel in contrast to chain terminator inhibitors such as remdesivir. These compounds represent suitable candidates for the preparation of clinically usable compounds against SAR-CoV-2 and other coronaviruses, as we have shown with an FIPV example. Compounds HeE1-2Tyr (**16**) and **17** showed significant activity against these coronaviruses in cell cultures. We have also unveiled that one of the mechanisms of action of these compounds is the inhibition of RdRp SARS-CoV-2. This key virus enzyme was inhibited by these compounds, with HeE1-2Tyr (**16**) and **17** showing significantly higher activity compared to **18**. This suggests that the phenyl substituent on the pyridinone portion of the

backbone may significantly affect the activity of these derivatives, both in the polymerase assay and in the cell lines. Clearly, further chemical modification and optimization to enhance potency and physicochemical properties will be required for the eventual use of this type of compounds in clinical practice; however, the derivatives of HeE1-2Tyr (**16**) may be one of the rare non-nucleoside inhibitors of coronavirus replication that interfere with RdRp, a key enzyme of these viruses. Although remdesivir is the only RdRp-targeting inhibitor approved by the FDA and EMA for clinical use, some studies suggest that its in vivo effects are suboptimal. Experience with other viral diseases suggests that combinations with other polymerase inhibitors can provide a significant synergistic effect and prevent the evolution of drug-resistant virus mutants; therefore, the introduction of new types of inhibitors may have a significant impact on improving the clinical outcome for patients.

Supplementary Materials: The following are available online at https://www.mdpi.com/article/10.3390/v13081585/s1, Supplementary File S1: chemical synthesis of the compounds and NMR spectra.

Author Contributions: M.D. and E.K. contributed equally; conceptualization, M.D., D.R., E.B. and R.N.; synthesis M.D. and M.Š.; methodology, E.K., L.E., P.S. (Petra Straková), P.S. (Pavel Svoboda), K.K.; writing—original draft preparation, M.D., E.K., L.E., D.R., E.B. and R.N.; supervision and funding acquisition, L.E., D.R., E.B. and R.N. All authors have read and agreed to the published version of the manuscript.

Funding: The work was supported by the European Regional Development Fund; OP RDE; Project: "Chemical Biology for Drugging Undruggable Targets (ChemBioDrug)" (No. CZ.02.1.01/0.0/0.0/16_019/0000729), Ministry of Health of the Czech Republic (grant NU20-05-00472), the Czech Academy of Sciences (RVO: 61388963), and Gilead Sciences Inc. This study was also supported by a grant from the Ministry of Education, Youth, and Sports of the Czech Republic (grant LTAUSA18016) (to L.E. and R.N.).

Institutional Review Board Statement: Not applicable.

Informed Consent Statement: Not applicable.

Data Availability Statement: Not applicable.

Conflicts of Interest: The research was partially sponsored by Gilead Sciences Inc., Foster City, CA, USA.

References

1. Cui, J.; Li, F.; Shi, Z.L. Origin and evolution of pathogenic coronaviruses. *Nat. Rev. Microbiol.* **2019**, *17*, 181–192. [CrossRef]
2. De Wit, J.J.; Cook, J.K.A. Spotlight on avian coronaviruses. *Avian Pathol.* **2020**, *49*, 313–316. [CrossRef]
3. Monchatre-Leroy, E.; Boue, F.; Boucher, J.M.; Renault, C.; Moutou, F.; Gouilh, M.A.; Umhang, G. Identification of Alpha and Beta Coronavirus in Wildlife Species in France: Bats, Rodents, Rabbits, and Hedgehogs. *Viruses* **2017**, *9*, 364. [CrossRef]
4. Chen, Y.; Liu, Q.Y.; Guo, D.Y. Emerging coronaviruses: Genome structure, replication, and pathogenesis. *J. Med. Virol.* **2020**, *92*, 418–423. [CrossRef]
5. De Wit, E.; Van Doremalen, N.; Falzarano, D.; Munster, V.J. SARS and MERS: Recent insights into emerging coronaviruses. *Nat. Rev. Microbiol.* **2016**, *14*, 523–534. [CrossRef]
6. Zumla, A.; Chan, J.F.W.; Azhar, E.I.; Hui, D.S.C.; Yuen, K.-Y. Coronaviruses—Drug discovery and therapeutic options. *Nat. Rev. Drug Discov.* **2016**, *15*, 327–347. [CrossRef]
7. Gorbalenya, A.E.; Baker, S.C.; Baric, R.S.; De Groot, R.J.; Drosten, C.; Gulyaeva, A.A.; Haagmans, B.L.; Lauber, C.; Leontovich, A.M.; Neuman, B.W.; et al. The species Severe acute respiratory syndrome-related coronavirus: Classifying 2019-nCoV and naming it SARS-CoV-2. *Nat. Microbiol.* **2020**, *5*, 536–544. [CrossRef]
8. Lu, L.; Zhong, W.Y.; Bian, Z.W.; Li, Z.M.; Zhang, K.; Liang, B.X.; Zhong, Y.Z.; Hu, M.J.; Lin, L.; Liu, J.; et al. A comparison of mortality-related risk factors of COVID-19, SARS, and MERS: A systematic review and meta-analysis. *J. Infect.* **2020**, *81*, E18–E25. [CrossRef]
9. Finelli, L.; Gupta, V.; Petigara, T.; Yu, K.; Bauer, K.A.; Puzniak, L.A. Mortality Among US Patients Hospitalized With SARS-CoV-2 Infection in 2020. *JAMA Netw. Open* **2021**, *4*, e216556. [CrossRef]
10. Tumban, E. Lead SARS-CoV-2 Candidate Vaccines: Expectations from Phase III Trials and Recommendations Post-Vaccine Approval. *Viruses* **2021**, *13*, 54. [CrossRef]
11. Wu, D.; Koganti, R.; Lambe, U.P.; Yadavalli, T.; Nandi, S.S.; Shukla, D. Vaccines and Therapies in Development for SARS-CoV-2 Infections. *J. Clin. Med.* **2020**, *9*, 1885. [CrossRef]

12. Pedersen, O.S.; Pedersen, E.B. Non-nucleoside reverse transcriptase inhibitors: The NNRTI boom. *Antivir. Chem. Chemother.* **1999**, *10*, 285–314. [CrossRef]
13. Dayal, V.; Kumar, A.; Jha, S.K.; Sharan, A.; Kumar, U.; Shahi, S.K. Viral Hepatitis (plus Antiviral Therapy) Combination therapy of lamivudine and adefovir in patients of HBeAg positive chronic hepatitis B. *J. Gastroenterol. Hepatol.* **2013**, *28*, 419.
14. Das, D.; Pandya, M. Recent Advancement of Direct-acting Antiviral Agents (DAAs) in Hepatitis C Therapy. *Mini-Rev. Med. Chem.* **2018**, *18*, 584–596. [CrossRef]
15. Vicenti, I.; Zazzi, M.; Saladini, F. SARS-CoV-2 RNA-dependent RNA polymerase as a therapeutic target for COVID-19. *Expert Opin. Ther. Pat.* **2021**, *31*, 325–337. [CrossRef]
16. Perry, J.K.; Appleby, T.C.; Bilello, J.P.; Feng, J.Y.; Schmitz, U.; Campbell, E.A. An atomistic model of the coronavirus replication-transcription complex as a hexamer assembled around nsp15. *bioRxiv* **2021**. [CrossRef]
17. Hillen, H.S.; Kokic, G.; Farnung, L.; Dienemann, C.; Tegunov, D.; Cramer, P. Structure of replicating SARS-CoV-2 polymerase. *Nature* **2020**, *584*, 154–156. [CrossRef]
18. Pruijssers, A.J.; George, A.S.; Schafer, A.; Leist, S.R.; Gralinksi, L.E.; Dinnon, K.H.; Yount, B.L.; Agostini, M.L.; Stevens, L.J.; Chappell, J.D.; et al. Remdesivir Inhibits SARS-CoV-2 in Human Lung Cells and Chimeric SARS-CoV Expressing the SARS-CoV-2 RNA Polymerase in Mice. *Cell Rep.* **2020**, *32*, 107940. [CrossRef]
19. Yin, W.C.; Luan, X.D.; Li, Z.H.; Zhou, Z.W.; Wang, Q.X.; Gao, M.Q.; Wang, X.X.; Zhou, F.L.; Shi, J.J.; You, E.R.; et al. Structural basis for inhibition of the SARS-CoV-2 RNA polymerase by suramin. *Nat. Struct. Mol. Biol.* **2021**, *28*, 319–325. [CrossRef]
20. Li, Q.; Yi, D.; Lei, X.; Zhao, J.; Zhang, Y.; Cui, X.; Xiao, X.; Jiao, T.; Dong, X.; Zhao, X.; et al. Corilagin inhibits SARS-CoV-2 replication by targeting viral RNA-dependent RNA polymerase. *Acta Pharm. Sin. B* **2021**, *11*, 1555–1567. [CrossRef]
21. Jin, Y.H.; Min, J.S.; Jeon, S.; Lee, J.; Kim, S.; Park, T.; Park, D.; Jang, M.S.; Park, C.M.; Song, J.H.; et al. Lycorine, a non-nucleoside RNA dependent RNA polymerase inhibitor, as potential treatment for emerging coronavirus infections. *Phytomedicine* **2021**, *86*, 153440. [CrossRef]
22. Agrawal, N.; Goyal, A. Potential Candidates against COVID-19 Targeting RNA-Dependent RNA Polymerase: A Comprehensive Review. *Curr. Pharm. Biotechnol.* **2021**. [CrossRef]
23. Tarantino, D.; Cannalire, R.; Mastrangelo, E.; Croci, R.; Querat, G.; Barreca, M.L.; Bolognesi, M.; Manfroni, G.; Cecchetti, V.; Milani, M. Targeting flavivirus RNA dependent RNA polymerase through a pyridobenzothiazole inhibitor. *Antivir. Res.* **2016**, *134*, 226–235. [CrossRef]
24. Cannalire, R.; Tarantino, D.; Piorkowski, G.; Carletti, T.; Massari, S.; Felicetti, T.; Barreca, M.L.; Sabatini, S.; Tabarrini, O.; Marcello, A.; et al. Broad spectrum anti-flavivirus pyridobenzothiazolones leading to less infective virions. *Antivir. Res.* **2019**, *167*, 6–12. [CrossRef]
25. Cannalire, R.; Chan, K.W.K.; Burali, M.S.; Gwee, C.P.; Wang, S.; Astolfi, A.; Massari, S.; Sabatini, S.; Tabarrini, O.; Mastrangelo, E.; et al. Pyridobenzothiazolones Exert Potent Anti-Dengue Activity by Hampering Multiple Functions of NS5 Polymerase. *ACS Med. Chem. Lett.* **2020**, *11*, 773–782. [CrossRef] [PubMed]
26. Felicetti, T.; Burali, M.S.; Gwee, C.P.; Chan, K.W.K.; Alonso, S.; Massari, S.; Sabatini, S.; Tabarrini, O.; Barreca, M.L.; Cecchetti, V.; et al. Sustainable, three-component, one-pot procedure to obtain active anti-flavivirus agents. *Eur. J. Med. Chem.* **2021**, *210*, 112992. [CrossRef]
27. Konkolova, E.; Dejmek, M.; Hrebabecky, H.; Sala, M.; Boserle, J.; Nencka, R.; Boura, E. Remdesivir triphosphate can efficiently inhibit the RNA-dependent RNA polymerase from various flaviviruses. *Antivir. Res.* **2020**, *182*, 104899. [CrossRef] [PubMed]
28. De Madrid, A.T.; Porterfield, J.S. A simple micro-culture method for the study of group B arboviruses. *Bull. World Health Organ.* **1969**, *40*, 113–121. [PubMed]
29. Eyer, L.; Valdes, J.J.; Gil, V.A.; Nencka, R.; Hrebabecky, H.; Sala, M.; Salat, J.; Cerny, J.; Palus, M.; De Clercq, E.; et al. Nucleoside Inhibitors of Tick-Borne Encephalitis Virus. *Antimicrob. Agents Chemother.* **2015**, *59*, 5483–5493. [CrossRef]